

Discovery and characterization of novel biofilm-associated proteins in
Pseudoalteromonas tunicata

by

Sura Ali

A thesis

presented to the University of Waterloo

in fulfillment of the

thesis requirement for the degree of

Doctor of Philosophy

in

Biology

Waterloo, Ontario, Canada, 2025

© Sura Ali 2025

Examining Committee Membership

The following served on the Examining Committee for this thesis. The decision of the Examining Committee is by majority vote.

External Examiner	Dr. Cezar Khursigara Professor, Department of Molecular and Cellular Biology University of Guelph
Supervisor	Dr. Andrew Doxey Associate Professor, Department of Biology University of Waterloo
Internal Member	Dr. Trevor Charles Professor, Department of Biology University of Waterloo
Internal Member	Dr. Josh D. Neufeld Professor, Department of Biology University of Waterloo
Internal-external Member	Dr. Matthew Scott Associate Professor, Department of Applied Mathematics University of Waterloo

Author's Declaration

I hereby declare that this thesis consists of material all of which I authored or co-authored: see Statement of Contributions included in the thesis. This is a true copy of the thesis, including any required final revisions, as accepted by my examiners.

I understand that my thesis may be made electronically available to the public.

Statement of Contributions

Authors Contributions in Chapter 2

Ali, S. performed experiments and data analysis.

Jenkins, B. prepared some samples for shotgun proteomic analysis.

Cheng, J. produced *Pseudoalteromonas tunicata* EAR28894 (Slr4) mutant strain.

Wei, X used AnnoView gene to investigate the neighborhoods surrounding Slr4.

Lobb, B. performed metagenomic and phylogenetic analysis.

McConkey, B. created the hypothetical model of Slr4 S-layer lattice assembly.

Egan, S. provided *P. tunicata* strain and helped with data analysis.

Charles, T. C. and Austin, J. helped with data analysis.

Andrew C. Doxey performed data analysis and conceived and supervised the study.

All authors interpreted findings and helped with manuscript preparation.

Authors Contributions Chapter 3

Sura Ali performed experiments and data analysis.

Geoffrey Che used AlphaFold and FoldSeek to investigate the top structural matches to uncharacterized domains.

Suhelen Egan, Josh D. Neufeld, Ulrich Eckhard, and Trevor Charles helped with data analysis.

Andrew C. Doxey performed data analysis and conceived and supervised the study.

All authors interpreted findings and helped with manuscript preparation.

Authors Contributions Chapter 4

Sura Ali performed experiments and data analysis.

Alexander Stavropoulos worked on crystal violet biofilm assays with Sura Ali.

Sadie Graves worked on confocal imaging with Sura Ali.

Geoffrey Che used AlphaFold and FoldSeek to investigate the top structural matches to uncharacterized domains.

Jiujun Cheng produced *Pseudoalteromonas tunicata* EAR30327 (BapP) mutant and rescue strains.

Huagang Tan and Xin Wei contributed to gene neighborhood analysis and visualization.

Suhelen Egan, Josh D. Neufeld, Ulrich Eckhard, Trevor Charles, and Benjamin Jenkins helped with data analysis.

Andrew C. Doxey performed data analysis and conceived and supervised the study.

All authors interpreted findings and helped with manuscript preparation.

Abstract

Pseudoalteromonas tunicata is a marine bacterium that is a useful model for studying mechanisms of biofilm development due to its ability to form, colonize, and inhibit growth of other microorganisms in marine and eukaryotic host-associated biofilms. However, the pathways responsible for *P. tunicata* biofilm formation are still incompletely understood, in part due to a lack of functional information for a large proportion of its proteome. In this thesis, I use comparative shotgun proteomics to explore *P. tunicata* biofilm development from the planktonic phase to three stages (early, middle, late) of biofilm development. Proteomic analysis identified 232 proteins that were up regulated during different stages of biofilm development, including proteins known to be important for *P. tunicata* biofilm development (e.g., autocidal enzyme AlpP, violacein proteins, and various pili proteins) as well as many hypothetical proteins of unknown function. I then characterized two novel, biofilm-associated hypothetical proteins, labeled EAR28894 and EAR30327.

Functional characterization of EAR28894 revealed that it is the major S-layer protein of *P. tunicata*. Bioinformatic methods predicted a beta-helical structure for EAR28894 similar to the *Caulobacter* S-layer protein, RsaA, despite sharing less than 20% sequence identity. Transmission electron microscopy revealed that purified EAR28894 protein assembled into paracrystalline sheets with a unique square lattice symmetry and a unit cell spacing of ~9.1 nm. An S-layer was found surrounding the outer membrane in wild-type cells and completely removed from cells in an EAR28894 deletion mutant. S-layer material also appeared to be “shed” from wild-type cells and was highly abundant in the extracellular matrix where it is associated with outer membrane vesicles and other matrix components. EAR28894 and its homologs form a new family of S-layer proteins that are widely distributed in Gammaproteobacteria including species of *Pseudoalteromonas* and *Vibrio* and found exclusively in marine metagenomes. This novel protein family was given the name Slr4.

Functional investigation of the uncharacterized protein, EAR30327, revealed its function as a novel biofilm adhesin. This protein, which I designated as BapP, was the top identified biofilm-associated protein by proteomic analysis. BapP showed partial homology to outer membrane adhesins containing repeats of bacterial cadherin-like and immunoglobulin (Ig) domains. A $\Delta bapP$ mutant strain was unable to form proper pellicle biofilms in liquid media. The $\Delta bapP$ mutant also had a significantly reduced ability to form biofilms in crystal violet assays, which was rescued by re-insertion of the *bapP* gene into the genome. As predicted by the identification of putative Ca^{2+} -binding motifs in BapP, biofilm formation in the wild-type strain was demonstrated to be Ca^{2+} -dependent, which was significantly reduced in the $\Delta bapP$ mutant. This study provides a unique proteomic dataset of biofilm development and identifies BapP as a Ca^{2+} -dependent adhesin responsible for biofilm formation in *P. tunicata*. The occurrence of BapP-related homologs in other species suggests that this protein family represents a broadly conserved mechanism for biofilm adhesion in marine Gammaproteobacteria species.

This thesis research establishes a proteomics-based pipeline for biofilm protein discovery and new directions for biofilm research in *P. tunicata* and related bacteria, and offers insights into potential targets for biofilm management and control.

Acknowledgements

I would like to express my deepest gratitude to my supervisor and mentor, Dr. Andrew Doxey, for his kindness, unwavering support, and belief in me. Your guidance and encouragement have shaped my journey throughout my PhD, and I will always be grateful for the knowledge you imparted and the opportunities you opened for me.

To my committee members, Dr. Trevor Charles and Dr. Josh Neufeld, thank you for your insightful feedback and for encouraging me to look at science from different perspectives. Your input has been critical in shaping this work, and I am grateful for the ways you have transformed my approach to research and scientific inquiry.

I also wish to thank Dr. Brendan McConkey for his constant belief in me, and for providing countless opportunities that have enriched my academic experience and helped me grow professionally. Your support was invaluable. A special acknowledgment goes to Dr. JiuJun Cheng for his dedication to this research. I also extend my thanks to Dr. Barbara Moffatt for allowing me to use her laboratory for culturing biofilms, and to Dr. Jozef Nissimov for providing his lab sonicator. Thank you once again to Dr. Trevor Charles and Dr. Josh Neufeld for granting me access to their labs when needed, and to Mishi Groh for her technical assistance with TEM. I would also like to express my appreciation to Mr. Tim Ireland, the Librarian, for his invaluable help with Zotero reference manager.

I am indebted to our collaborators, John Austin, Ulrich Eckhard, and Suhelen Egan, for their essential contributions and input. Special thanks to Benjamin Jenkins, my lab mate, for sharing in the excitement of exploring *Pseudoalteromonas tunicata*; your enthusiasm has been infectious. To all the graduate and undergraduate students who joined the Doxey lab and contributed to this project, including Alexander Stavropoulos, Geoffrey Che, and Sadie Graves thank you for your hard work and dedication. I would also like to extend my gratitude to Yiming Xiao from Bioinformatics Solutions and Dyanne Brewer from the mass spectrometry facility at the University of Guelph for their technical expertise and assistance.

I gratefully acknowledge the financial support provided by the Ontario Graduate Scholarship and the University of Waterloo. Without this funding, my research would not have been possible.

On a personal note, my deepest thanks go to my husband, Hassan Hassan, for working tirelessly and going above and beyond to support our family during my PhD journey. To my children, Manar, Mustafa, and Mena, thank you for your patience and understanding during the many times I had to focus on my work instead of spending time with you. To my mother, whose constant prayers and encouragement have been a source of strength through difficult times, and to my father, who has been a role model and instilled in me a love for learning and teaching. Thank you for believing in me and for your love.

This work is the result of collective efforts, and I am deeply grateful to everyone who has been a part of it.

Dedication

To my beloved husband, whose unwavering support has been my anchor throughout this journey. Your encouragement, patience, and faith in me made every challenge feel surmountable.

To my incredible children, who have grown into remarkable individuals, bringing wisdom, strength, and love into my life. Your understanding and support during my journey have been a source of strength. You have each, in your own way, taught me invaluable lessons in resilience, patience, and perspective. I am deeply proud of you all.

To my mother and father, whose unwavering dedication to my dreams and tireless sacrifices have been the foundation upon which I stand today. You showed me the meaning of hard work, love, and perseverance, and for that, I am forever in your debt.

And to all the cherished souls - family, friends, mentors - who walked beside me, offering wisdom, support, and love, this journey has been enriched by your presence. I carry your kindness and belief with me, always.

This achievement is as much yours as it is mine.

Table of Contents

Examining Committee Membership.....	ii
Author’s Declaration	iii
Statement of Contributions.....	iv
Authors Contributions in Chapter 2	iv
Authors Contributions Chapter 3.....	iv
Authors Contributions Chapter 4.....	v
Abstract	vi
Acknowledgements	viii
Dedication	ix
List of Figures	xiv
List of Tables.....	xvii
List of Abbreviations.....	xviii
Chapter 1 General Introduction.....	1
1.1 Bacterial biofilms	1
1.2 Initial adhesion to surfaces through adhesins and cell appendages.....	3
1.3 Surface sensing, quorum sensing, and initiation of the biofilm developmental program	6
1.4 Components of the extracellular biofilm matrix.....	9
1.5 Dispersal mechanisms	11
1.6 Biology of <i>Pseudoalteromonas tunicata</i>	14
1.6.1 <i>P. tunicata</i> as a model organism for studying biofilm development.....	14
1.6.2 Mechanisms of biofilm development in <i>Pseudoalteromonas tunicata</i>	16
1.7 Research Objectives and Hypothesis.....	18

Chapter 2 Proteomic investigation of biofilm development in <i>Pseudoalteromonas tunicata</i>	20
2.1 Introduction	20
2.2 Methods	22
2.2.1 Culturing of <i>P. tunicata</i> samples throughout planktonic to biofilm development	22
2.2.1 Shotgun proteomics	25
2.2.2 Proteomics	26
2.3 Results	28
2.3.1 Proteomic analysis of planktonic and biofilm proteins in <i>Pseudoalteromonas tunicata</i>	28
2.4 Discussion	40
Chapter 3 Slr4, a newly identified S-layer protein from marine Gammaproteobacteria, is a major biofilm matrix component	43
3.1 Background information on S-layer proteins	43
3.2 Study objectives	46
3.3 Experimental Procedures	46
3.3.1 Purification of S-layer protein	46
3.3.2 Construction of mutant strain	47
3.3.3 Negative staining and image analysis	49
3.3.4 Analysis of Slr4 phylogenomic and metagenomic distribution	49
3.4 Results	50
3.4.1 Identification of an abundant protein in cultures of <i>Pseudoalteromonas tunicata</i>	50
3.4.2 Protein structure prediction suggests EAR28894 is an S-layer protein	54
3.4.3 Confirmation of EAR28894 as an S-layer protein using TEM and knockout studies	56
3.4.4 S-layer is shed from cells and is a major component of the biofilm matrix	65
3.4.5 The Slr4 protein family is widespread in marine bacterial genomes and metagenomes	69

3.5 Discussion	73
3.5.1 Sequence-to-structure relationship	74
3.5.2 A putative role for Slr4 in marine biofilms	75
Chapter 4 Comparative proteomics identifies a Ca ²⁺ -dependent adhesin required for biofilm formation in <i>Pseudoalteromonas tunicata</i>	78
4.1 Introduction	78
4.2 Methods	80
4.2.1 Bioinformatic analysis of EAR30327.....	80
4.2.2 Construction of EAR30327 (BapP) deletion and rescue plasmids	81
4.2.3 Crystal Violet Biofilm Assays.....	85
4.2.4 Confocal Laser Scanning Microscopy.....	86
4.2.5 SDS-PAGE.....	86
4.3 Results	87
4.3.1 EAR30327 is the top biofilm-associated protein in <i>P. tunicata</i>	87
4.3.2 EAR30327 (“BapP”) predicted as a Ca ²⁺ -dependent outer membrane adhesin	88
4.3.3 EAR30327 (“BapP”) required for proper biofilm formation and surface adhesion	92
4.3.4 Ca ²⁺ -dependent BapP-mediated biofilm formation	98
4.3.5 Phylogenomic analysis and distribution of the <i>Pseudoalteromonas</i> BapP adhesin family.....	101
4.4 Discussion	110
Chapter 5	114
5.1 Summary	114
5.2 Additional biofilm-associated proteins during biofilm formation in <i>Pseudoalteromonas tunicata</i>	115
5.3 BapP: insights and future questions	118

5.4 Slr4: insights and future questions	119
5.5 Concluding Remarks	120
References	123
Appendix A	158
Protein Sequences.....	158
>EAR28894.1 hypothetical protein PTD2_07619	158
>EAR30327.1 hypothetical protein PTD2_02121	1589
Appendix B.....	160
Media composition	160
Complex media (CM1).....	160
Difco Marine agar 2216.....	160
Difco Marine broth 2216.....	1601
Appendix C.....	162
Proteomics LC-MS/MS protein.....	162
C.1. Proteomics LC-MS/MS protein abundance across all samples data. All detected <i>P. tunicata</i> proteins and supplementary information	162
C.2. The supplementary material and data that supports the findings of Ali et al., (2020) article	162
Appendix D	163
D.1. The top thirty supporting peptides for EAR28894 identification by LC-MS/MS.....	163
D.2. Niche analysis of Slr4-containing species	185

List of Figures

Figure 1.1. Stages of biofilm development.	2
Figure 1.2. The Lap system and mechanism for controlling biofilm formation and dispersal.....	13
Figure 2.1. Biofilm sample collection tool.....	23
Figure 2.2. Overview of protocol for sampling of <i>Pseudoalteromonas tunicata</i> pellicle biofilms and planktonic cultures.	26
Figure 2.3. Comparative proteomic analysis of <i>Pseudoalteromonas tunicata</i> throughout biofilm development.	30
Figure 2.4. Principal component analysis (PCA) plot of samples based on their proteomic profiles. .	31
Figure 2.5. Volcano plot depicting differentially abundant proteins in biofilm samples (N = 18) versus planktonic (N = 3) samples.	32
Figure 2.6. Identified <i>Pseudoalteromonas tunicata</i> proteins by LC-MS/MS analysis of planktonic and biofilm cultures.....	33
Figure 2.7. Relative abundance of selected proteins across planktonic, biofilm, and media samples based on LC-MS/MS proteomic analysis.....	37
Figure 3.1. Identification of an abundant hypothetical protein in the <i>Pseudoalteromonas tunicata</i> proteome.....	51
Figure 3.2. LC-MS/MS coverage of the EAR28894 protein.....	53
Figure 3.3. Ratio of semi-tryptic to tryptic peptides across all proteins in LC-MS/MS data.	54
Figure 3.4. Bioinformatic analysis predicts <i>Pseudoalteromonas tunicata</i> EAR28894 hypothetical protein as an S-layer protein.....	55
Figure 3.5. Genomic context surrounding the EAR28894 gene in <i>Pseudoalteromonas tunicata</i> D2 and related genes in other genomes predicts <i>P. tunicata</i> EAR28894 hypothetical protein as an S-layer protein.....	56
Figure 3.6. Purification of EAR28894 by ultracentrifugation (L1) followed by detergent washes (L2).	57

Figure 3.7. TEM imaging of purified EAR28894 reveals a paracrystalline lattice with square (p4) symmetry.....	58
Figure 3.8. Hypothetical model of Slr4 S-layer lattice assembly (right) compared to RsaA S-layer assembly (left).....	59
Figure 3.9. Verification of Δ slr4 (EAR28894 gene deletion) mutant in <i>Pseudoalteromonas tunicata</i> PnAD3.....	60
Figure 3.10. SDS-PAGE analysis of whole cell extract of WT versus Δ slr4 <i>Pseudoalteromonas tunicata</i> strains.....	61
Figure 3.11. Pellicle biofilms formed by the WT vs Δ slr4 mutant strain.....	62
Figure 3.12. TEM micrograph of a <i>Pseudoalteromonas tunicata</i> cell revealing the presence of a putative outermost capsular layer.....	63
Figure 3.13. Electron micrographs of <i>Pseudoalteromonas tunicata</i> revealing presence/absence of a square grid S-layer in WT and Δ slr4 cells, respectively.....	64
Figure 3.14. S-layer is present in the <i>Pseudoalteromonas tunicata</i> extracellular environment and biofilm matrix.....	66
Figure 3.15. TEM micrographs of 48-hr pellicle biofilms (WT versus Δ slr4 mutant strain).....	68
Figure 3.16. Taxonomic distribution of Slr4 homologs.....	70
Figure 3.17. Phylogeny of Slr4 homologs.....	71
Figure 3.18. Metagenomic occurrence of Slr4 homologs.....	73
Figure 4.1. PCR primer binding regions in <i>Pseudoalteromonas tunicata</i> genomes.....	83
Figure 4.2. Abundance of the EAR30327 protein across samples based on LC-MS/MS shotgun proteomic data.....	87
Figure 4.3. Sequence and structural analysis predicts EAR30327 (“BapP”) as a Ca ²⁺ -dependent outer membrane adhesin.....	89
Figure 4.4. Partial sequence homology between a putative binding region in BapP and binding domains from other biofilm adhesins.....	91

Figure 4.5. Verification of <i>Pseudoalteromonas tunicata</i> strains by PCR amplification.	92
Figure 4.6. SDS-PAGE gel of supernatant protein collected from the WT, $\Delta bapP$, and $\Delta bapP+$ strains.....	94
Figure 4.7. Loss of BapP reduces biofilm formation and surface adhesion.	95
Figure 4.8. Loss of BapP reduces biofilm formation and surface adhesion.	96
Figure 4.9. Loss of BapP reduces biofilm formation and surface adhesion.	97
Figure 4.10. Quantification of the effect of Ca^{2+} addition on biofilm formation.	99
Figure 4.11. Quantification of the effect of Ca^{2+} addition on biofilm formation.	100
Figure 4.12. Line graphs depicting biofilm growth, quantified via 550 nm absorbance, and total cell growth, quantified via 600 nm absorbance, against added $CaCl_2$	101
Figure 4.13. Phylogenomic distribution of <i>Pseudoalteromonas tunicata</i> BapP homologs available metagenomes.	102
Figure 4.14. Occurrence of BapP of <i>Pseudoalteromonas tunicata</i> available metagenomes.	103
Figure 4.15. BLAST alignment dot plot depicting regions of similarity between BapP (x-axis) and a related <i>Pseudoalteromonas tunicata</i> protein (EAR26681).....	105
Figure 4.16. Phylogenetic tree of <i>Pseudoalteromonas tunicata</i> BapP along with its the top six identified homologs (all with coverage exceeding 50%).	107
Figure 4.17. Categories of metagenomic datasets containing <i>Pseudoalteromonas tunicata</i> BapP genes identified using PebbleScout.	110

List of Tables

Table 2.1. The top 15 detected biofilm-associated proteins. The full table is found in Appendix C (C.1).....	34
Table 2.2. Proteins with increased abundance in planktonic conditions.	35
Table 2.3. Top detected media-enriched proteins.....	38
Table 3.1. Oligos used for plasmid construction.	48
Table 3.2. Top proteins identified by LC-MS/MS.	52
Table 4.1. Bacterial strains and plasmids were used in this work.	82
Table 4.2. Sequences of primers used in this work.	84
Table 4.3. Identified peptides for top-matching <i>P. tunicata</i> proteins by LC-MS/MS.....	95
Table 4.4. Pebblescout results for Sequence Read Archive datasets of the top 30 results containing matches to the <i>P. tunicata</i> BapP protein.	108

List of Abbreviations

Abbreviation	Full name
ABC	ATP-Binding Cassette Transporters
AHL	N-acyl homoserine lactones
AMP	Adenosine monophosphate
ATP	Adenosine Triphosphate
BH	Biohydrogen
BIG	Bacterial Isolate Genome
BLAST	Basic Local Alignment Search Tool
BLU	Bacterial Luciferase Unit (bioluminescence)
C18	C18 reversed-phase column (used in HPLC)
CCM	Carbon Concentrating Mechanism
CDD	Conserved Domain Database
CDHL	Cadherin-Like Domain
CHDL	Carbapenem-Hydrolyzing Class D β -Lactamase
CLSM	Confocal Laser Scanning Microscopy
CM1	Complex Media
CMR	Complete Microbial Resource
DIC	Differential Interference Contrast (microscopy)
DNA	Deoxyribonucleic acid
EBI	European Bioinformatics Institute
ECM	Extracellular Matrix
EDTA	Ethylenediaminetetraacetic Acid
EMBO	European Molecular Biology Organization
EPS	Extracellular polymeric substances
FA	Fatty Acid
FEMS	Federation of European Microbiological Societies
FKBP	FK506-Binding Protein (immunophilin)
FM4	FM4-64 (fluorescent dye for cell membranes)
GMP	Guanosine monophosphate
GTDB	Genome Taxonomy Database
HC	Heavy Chain (in antibodies)
HRCR	Highly Repetitive CRISPR Region
ITOL	Interactive Tree Of Life
JB	Journal of Bacteriology
KD	Knockdown (gene silencing)

Abbreviation	Full name
L32	Ribosomal Protein L32
LB	Lysogeny Broth (bacterial growth media)
LC-MS/MS	Liquid Chromatography with tandem mass spectrometry
LG	Linkage Group or <i>Lactococcus garvieae</i>
LRT	Likelihood Ratio Test (statistical test)
LSM	Laser Scanning Microscopy
MG	Magnesium or <i>Mycoplasma genitalium</i>
M	Molar (concentration)
ML	Machine Learning or Maximum Likelihood
MMBR	Microbiology and Molecular Biology Reviews
MMG024	Specific gene or protein ID
MSCRAMM	Microbial Surface Components Recognizing Adhesive Matrix Molecules
MSHA	Mannose-Sensitive Hemagglutinin
MUSCLE	MULTiple Sequence Comparison by Log-Expectation
MW	Molecular Weight
NADH	Nicotinamide Adenine Dinucleotide (Reduced Form)
NCBI	National Center for Biotechnology Information
NEB	New England Biolabs
NP	Nanoparticle or Nucleoprotein
OD600	Optical Density at 600 nm (measures bacterial growth)
OMV	Outer Membrane Vesicles
ORF	Open Reading Frame
PAL	Phenylalanine Ammonia-Lyase
PAO1	<i>Pseudomonas aeruginosa</i> PAO1 strain
PASEF	Parallel Accumulation Serial Fragmentation (mass spectrometry)
PBS	Phosphate-Buffered Saline
PCA	Principal component analysis
PCR	Polymerase Chain Reaction
PDB	Protein Data Bank
PEAKS	PEAKS Software (de novo peptide sequencing and protein analysis)
PKD	Polycystic Kidney Disease or Protein Kinase Domain
PKD	Polycystic Kidney Disease (repeated)
PL	Phospholipase
PLOS ONE	Public Library of Science ONE (journal)
PnAD3	<i>Pseudomonas tunicata</i> Andrew Doxey strain collection No.3

Abbreviation	Full name
PPR	Pentatricopeptide Repeat (protein motif)
PTFE	Polytetrafluoroethylene (Teflon material)
PTM	Post-Translational Modification
QQ	Quorum Quenching
QS	Quorum Sensing
QSI	Quorum Sensing Inhibitors
RIPA	Radioimmunoprecipitation Assay (lysis buffer)
RK600	Bacterial strain or plasmid
RNA	Ribonucleic acid
RND	Resistance-Nodulation-Cell Division Efflux Pump
RTX	Repeats in Toxin
S46	Serine Protease S46 Family
SAAT	Self-associating autotransporters
SDS-PAGE	Sodium Dodecyl Sulphate-Polyacrylamide Gel Electrophoresis
SEP	Separation (chromatography)
SH	Sulfhydryl Group (-SH in biochemistry)
SLH	Surface Layer Homology Domain
Slr4	Surface Layer type 4
SPI	Salmonella Pathogenicity Island
SRR12112860	Sequence Read Archive ID (NCBI dataset)
TEM	Transmission Electron Microscopy
T0	Time point 0
T24	Time point 24 hours
T48	Time point 48 hours
T72	Time point 72 hours
2FC	Two-Fold Change (gene expression analysis)
T4P	Type IV pili
T1SS	Type I secretion systems
TASSER	Threading/ASSEMBLY/Refinement (protein structure prediction method)
3-oxo-C6-HSL	N-(3-oxo-hexanoyl)-l-homoserine lactone
TFA	Trifluoroacetic Acid
TIMS	Trapped Ion Mobility Spectrometry
TOF	Time-of-Flight (mass spectrometry)
TOL4	Related to <i>TOL</i> plasmid components
UP000006201	UniProt ID for <i>Escherichia coli</i> K-12 reference proteome
V8	V8 protease (<i>Staphylococcus aureus</i> serine endoprotease)

Abbreviation	Full name
VCBS	<i>Vibrio</i> , <i>Colwellia</i> , <i>Bradyrhizobium</i> , and <i>Shewanella</i> contain long protein copies.
WT	Wild Type
YEG	YEG protein family (bacterial ABC transporters)

Chapter 1

General Introduction

1.1 Bacterial biofilms

Organisms in most environments exist not in isolation, but rather in dense, complex multicellular communities called biofilms. Biofilms are multicellular communities of bacterial cells that adhere to surfaces and to each other by slimy extracellular polymeric substances (EPSs), and engage in collective sharing of resources, metabolism, and protection from external stressors. Biofilm EPSs are composed of proteins, extracellular polysaccharides, lipids, and DNA (Flemming et al., 2016; Hall-Stoodley et al., 2004; Munoz-Lopez & Garcia-Perez, 2010).

Harmful bacterial biofilms can have a massive impact in industrial, agricultural, food, as well as biomedical settings. These unwanted biofilms can form on plants (Srey et al., 2013), medical devices, industrial pipes, aquaculture equipment, and much more (Braithwaite & McEvoy, 2004). Biofilms are also implicated in up to 80% of human bacterial infections (Mirzaei et al., 2020). For example, *Pseudomonas aeruginosa* is the major pathogen in the lungs of cystic fibrosis patients, and forms biofilms that complicate treatment (Davies, 2002). In general, biofilms display enhanced resistance to antibiotics and other disinfectants, which makes them particularly hard to treat and control (Del Pozo et al., 2008; Kim et al., 2015; Lazar, 2011). Biofilms also have enhanced protection to other environmental, physical, and chemical factors (Davey & O'toole, 2000).

Despite the problems associated with unwanted biofilms, biofilms are fundamental to microbial biology in virtually all natural environments (Boltz et al., 2017; Jain et al., 2007). It has been estimated that 40-80% of all cells (bacteria and archaea) reside in biofilms, making them critical for all biogeochemical cycles (Flemming & Wuertz, 2019). Environments harboring microbial biofilms include the deep oceanic biosphere, deep continental

subsurface, upper ocean sediments, soil, oceans, host-associated microbial communities, and even the atmosphere (Flemming & Wuertz, 2019). The metabolic capacities of biofilms can also be harnessed by humans. For example, biofilms play important roles in wastewater treatment plants, as they are used in secondary treatment to extract and digest organic compounds (Di Biase et al., 2019; T. Ibrahim et al., 2012).

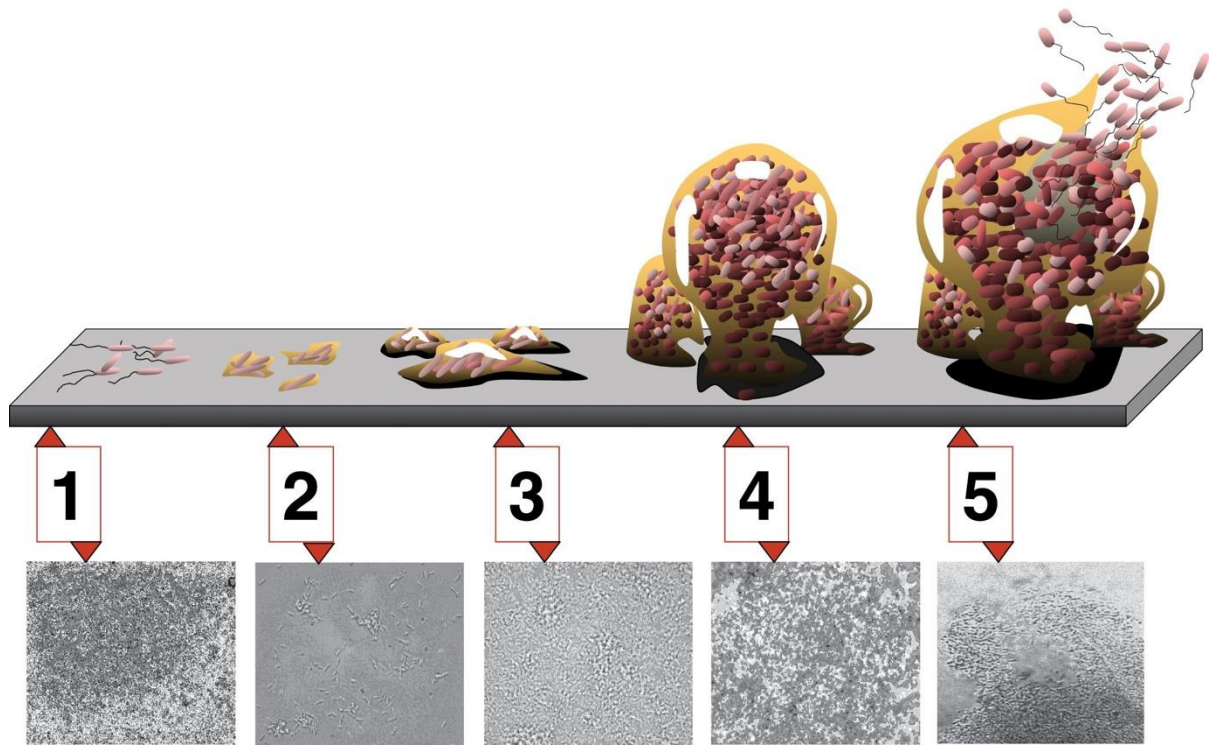


Figure 1.1. Stages of biofilm development. (1) Initial attachment, (2) Irreversible attachment, (3) Maturation I, (4) Maturation II, and (5) Dispersion. The diagram pairs each developmental stage with a corresponding photomicrograph of a developing *P. aeruginosa* biofilm, all displayed at the same scale (Monroe, 2007).

The biofilm development cycle typically involves four stages: initial attachment of microorganisms to a surface or each other, formation of microcolonies, maturation of the biofilm, and dispersal (Sauer et al., 2002). Each stage of biofilm development is

characterized by specific bacterial physiological and phenotypic changes that suggest the presence of a unique biofilm biology, distinct from that of planktonic bacteria (Tolker-Nielsen, 2015). Transitioning from a solitary planktonic lifestyle to a communal biofilm lifestyle requires bacteria to undergo significant changes, including changes in levels of key regulatory molecules such as cyclic-3'5'-diguanylic acid (c-di-GMP), and the production of adhesins and extracellular biofilm matrix compounds that interconnect cells and provide mechanical stability. This matrix is involved in various processes, such as cell attachment, cell-to-cell interactions, and antimicrobial tolerance (Friedman & Kolter, 2004; Jackson et al., 2004; S. Yang et al., 2009).

The molecular mechanisms underlying biofilm development are complex and involve sophisticated regulatory networks that control the transition from planktonic to a surface-associated lifestyle. Each step of the biofilm developmental process, from initial adhesion to maturation to dispersal, is governed by specific proteins and regulatory mechanisms (Schembri et al., 2003), which I discuss in more detail below.

1.2 Initial adhesion to surfaces through adhesins and cell appendages

The first step in biofilm formation is the adhesion of one or more bacterial cells to a surface, which can be biotic or abiotic depending on the bacterial species and its environmental context. For flagellated bacteria, flagella will power the motility of planktonic cells until they encounter a surface, through binding interactions that may involve numerous types of adhesins and surface structures (Belas, 2014; Tolker-Nielsen, 2015).

Primary adhesion or the initial “docking phase” is typically reversible and dependent on surface conditioning and chemistry (Dunne, 2002; Shinde et al., 2021). Through the action of adhesive structures such as pili, fimbriae, flagella, and other adhesin proteins, the cell can anchor itself to the surface. Homophilic interactions between cells also occur where

cells adhere to each other and form clusters or aggregates. The presence of surface-attached cells can also promote further aggregation by other cells.

Adhesins associated with initial biofilm development include a wide variety of proteins and systems including pili and fimbrial adhesins, non-fimbrial adhesins, and polysaccharide adhesins (Berne et al., 2015). Gram-negative fimbrial adhesins include Type IV pili, Tad pili, and amyloid-like curli fibers found in *Escherichia coli* and other species. Non-fimbrial adhesins include a wide diversity of adhesins secreted through different secretion mechanisms, including the Bap proteins (biofilm-associated proteins), autotransporter adhesins, and hemagglutinin-like adhesins. Bap proteins promote adhesion to biotic and abiotic surfaces (Latasa et al., 2006) and are important determinants of biofilm formation. Baps are secreted by the T1SS and are typically large proteins of up to almost 10,000 residues in length (Berne et al., 2015). The *Staphylococcus aureus* Bap protein promotes biofilm formation by reinforcing the biofilm matrix and facilitating cell-to-cell adhesion. *S. aureus* Bap is characterized by its large size (2,276 aa in length) and structure which consists of 13 nearly identical tandem repeats, which are essential for biofilm formation and adhesion (Berne et al., 2015). Bap-related proteins are particularly important in bacterial infectious processes, playing a significant role in chronic and persistent infections, such as mastitis and implant-associated infections, where biofilms protect bacteria from host defenses (Lasa & Penadés, 2006).

Another well-studied Bap is the RTX adhesin LapA found in a variety of *Pseudomonas* species. The LapA family of proteins are also secreted by the T1SS, are loosely associated with the cell surface, and are critical for surface adhesion and biofilm formation. The associated LapB, LapC, and LapE proteins are the additional T1SS components that are required for LapA secretion. LapA mutants are deficient in early biofilm formation and do not develop a mature biofilm structure (Hinsa et al., 2003). All RTX adhesins appear to possess a similar structure and molecular mechanism involving a repetitive beta-rich region that extends outward from the cell surface and undergoes Ca²⁺-dependent binding to a variety of surfaces (Guo et al., 2019).

The SasG protein of *Staphylococcus aureus* is another crucial adhesin involved in biofilm development. SasG contains an N-terminal A domain and repeated B domains, with the latter being necessary for biofilm formation. The B domains form Zn²⁺-dependent dimers, a process essential for biofilm accumulation. Notably, SasG undergoes spontaneous cleavage within the B domains at labile peptide bonds, releasing fragments that re-associate with the cell surface, a process required for efficient biofilm development (Geoghegan et al., 2010).

The CshA “Cell surface hydrophobicity” protein found in *Streptococcus gordonii* is another cell wall-anchored protein with an important role in bacterial cell surface adhesion (McNab & Jenkinson, 1998). (McNab et al., 1999) demonstrated that CshA is the structural and functional component of the surface adhesive fibrils (60.7 ± 14.5 nm long). The CshA protein (2508 amino acid residues) is composed of C-terminal repetitive region and N-terminal non-repetitive region. The CshA protein affects the cell-surface hydrophobicity of *S. gordonii* and *S. sanguis* due to the presence of hydrophobic amino acids in the repetitive region (Jenkinson & Demuth, 1997; McNab et al., 1994, 1995). The C-terminal anchor domain of CshA surface protein adheres to fibronectin on human cells via a Catch-Clamp Mechanism (Back et al., 2017; Joh et al., 1999), and adheres to collagen (Patti et al., 1992), and immunoglobulin A and/or G (Kehoe, 1994).

The repetitive biofilm adhesins like SasG and CshA can be more generally described as “fibrillar adhesins” (Monzon & Bateman, 2022). These adhesins have a conserved structural pattern consisting of an N-terminal adhesive domain followed by multiple repeats of a “stalk” that is thought to project the adhesive domain outward toward its binding target (Monzon & Bateman, 2022). Based on sequence homology and structural (Alphafold) modeling, thousands of predicted fibrillar adhesins have been bioinformatically predicted in microbial genomes (Monzon & Bateman, 2022).

1.3 Surface sensing, quorum sensing, and initiation of the biofilm developmental program

While reversible attachment often uses flagella to move toward surfaces and other adhesins to transiently attach to the surface, irreversible attachment involves a programmed initiation of biofilm gene expression including the loss of flagella and further production of adhesive structures like curli or type 1 fimbriae (O'Toole & Wong, 2016). For the transition to irreversible attachment to take place, the cell must first sense the surface to which it is bound (Chang, 2018). One molecular mechanism for “surface-sensing” is through the use of flagellar machinery as mechanosensors, which sense a surface through the inhibition of flagellar rotation upon the initial binding to a surface (Belas, 2014; Hug et al., 2017). Through two-component systems, the cell can detect inhibition of flagellar rotation and signal the increase in other small regulatory molecules, such as the c-di-GMP, a master regulator of biofilm development. Another surface-sensing mechanism includes the *E. coli* type 1 fimbrial adhesive subunit (FimH), which has been suggested to sense shear forces to regulate surface adhesion (Thomas et al., 2002). In *P. aeruginosa*, there appear to be several surface-sensing mechanisms including type IV pili (T4P) mediate surface sensing as well as the membrane bound WspA/WspR system (Chang, 2018; Park & Sauer, 2022). T4P-mediated surface sensing has been shown to regulate cyclic AMP (cAMP) (Persat et al., 2015), which then leads to a cascade of second messengers including ci-di-GMP to regulate surface behaviours (Luo et al., 2015). A common theme among surface-sensing systems in numerous species is the stimulated increase in c-di-GMP, which is a key signal to activate the biofilm developmental program.

After irreversible adhesion and sensing of the surface, bacterial cells initiate a change in gene expression that enables a switch to a surface-associated biofilm lifestyle. Increased intracellular levels of c-di-GMP not only regulate the function of biofilm-associated proteins but activate the expression of downstream genes involved in biofilm formation (Park & Sauer, 2022). In *Pseudomonas aeruginosa*, c-di-GMP regulates biofilm formation by interacting with the transcription factor FleQ, enabling the derepression of target genes at

high intracellular concentrations (Baraquet & Harwood, 2016). c-di-GMP increase therefore leads to sessile phenotypes including biofilm formation, rugose colony morphology, adhesin production, matrix components, and EPS, and represses planktonic phenotypes such as motility through the inhibition of flagellar biosynthetic pathways (Römling et al., 2013). All extracellular matrix components important for biofilm formation appear to be regulated by c-di-GMP (Römling, 2012). Biofilm matrix molecules include polysaccharides, nucleic acids, and proteins, along with accessory components that enhance biofilm formation and adaptability (Mann & Wozniak, 2012).

In addition to c-di-GMP, quorum sensing (QS) also plays a pivotal role in coordinating gene expression related to biofilm development and related physiological processes such as motility, virulence, and EPS production, all of which are vital for biofilm development and maintenance (Zhou et al., 2020). Both Fazli et al. (2014) and Zhou et al. (2020) highlighted QS as an essential process in bacterial communication and common community behaviour, allowing cells to synchronize behaviours such as virulence and biofilm formation in response to population density. This process is mediated by diffusible signal molecules, including autoinducers (AIs) like N-acyl homoserine lactones (AHLs). For Gram-negative bacteria, as population density increases, acyl-HSLs accumulate, enabling bacteria to regulate various physiological processes, from bioluminescence to swarming motility. The first AHL discovered was N-(3'-oxohexanoyl)-L-homoserine lactone (3-oxo-C6-HSL) from *Vibrio fischeri*, which triggers luminescence in this bacterium (Horinouchi et al., 2010). Similarly, QS regulates biofilm formation in species like *Pseudomonas putida*, *Pseudomonas fluorescens*, *Pseudomonas aeruginosa*, and *Burkholderia cenocepacia* through systems that involve AHLs and other quorum molecules, as well as cyclic-di-GMP (c-di-GMP) signaling pathways. A minimum AHL concentration, indicating a threshold bacterial population density, is required for a significant bacterial response. Due to these properties, AHLs are also known as autoinducers or quorum-sensing molecules (Dickschat, 2010).

The role of AHLs, particularly, is well-documented in biofilm regulation. For instance, in *Pseudomonas aeruginosa*, AHLs like N-(3-oxo-dodecanoyl)-L-homoserine

lactone (OdDHL) and N-butyryl-L-homoserine lactone (BHL) are key components of the *las* and *rhl* QS systems, which coordinate the expression of biofilm-related genes such as those involved in the production of extracellular polysaccharides (EPS), DNA, and biosurfactants. These molecules contribute to the structural integrity and virulence of biofilms, enhancing bacterial survival in hostile environments, including resistance to antibiotics. Zhou et al. (2020) emphasize that QS also regulates bacterial motility and the synthesis of extracellular DNA, both essential for biofilm formation and stability.

The integration of QS mechanisms with biofilm development is further evidenced by the discovery of AHLs in various environmental contexts, including aquatic biofilms, confirming the widespread nature of this regulatory system (McLean et al., 2006). An example of an AHL-dependent EPS producer is *Pseudomonas syringae*, which is essential for its virulence in plant diseases causing brown spot disease in beans (Carlier et al., 2015). Additionally, the autoinducer 3-oxo-C6-HSL negatively regulates the biosynthesis of complex extracellular polysaccharides (EPS), which are crucial for virulence, thus controlling biofilm maturation and dispersion (Koutsoudis et al., 2006; Majdura et al., 2023). QS systems using AHL signal molecules play a general role in biofilm formation, while QS systems using fatty acid signals regulate biofilm formation in *B. cenocepacia* and possibly in pseudomonads. In pseudomonads, QS also regulates extracellular DNA, lectins, and biosurfactants production, which are essential for biofilm formation (Fazli et al., 2014).

QS systems are not limited to AHLs. Fatty acid-based QS molecules, such as those found in *B. cenocepacia*, also play critical roles in biofilm regulation. These systems underscore the complexity and diversity of QS-mediated biofilm formation across bacterial species. Zhou et al. (2020) further elaborate on how QS inhibitors (QSIs) and quorum quenching (QQ) enzymes are promising strategies for disrupting QS-regulated biofilm formation, offering potential applications in medical and industrial fields where biofilm-associated infections are prevalent (Zhou et al., 2020).

1.4 Components of the extracellular biofilm matrix

One of the key aspects of biofilms is the molecular composition and function of the biofilm matrix. The biofilm matrix serves as a communal environment for microbial cells, containing extracellular polymeric substances (EPS) like polysaccharides, proteins, amyloids, lipids, secondary metabolites, extracellular-DNA and extracellular-RNA, membrane vesicles, and humic-like substances. These dynamic EPS components stabilize the matrix, acquire nutrients, protect eDNA and exoenzymes, and provide sorption sites for ions and hydrophobic substances. Retained exoenzymes turn the matrix into an external digestion system (Fleming et al., 2022). The EPS also offers structural support and keeps the bacterial cells closely packed, which allows for genetic material exchange and enhances quorum sensing (Wang et al., 2023). Environmental conditions and interactions allow biofilms to form structures like films, colonies, ridges, and bubbles. The matrix's assembly and dynamics are regulated by secondary messengers, signaling molecules, or small RNAs in both medical and environmental biofilms (Fleming et al., 2022).

The structure and composition of the extracellular matrix are key aspects of biofilm development for bacterial species and are crucial for biofilm resilience. The extracellular matrix participates in the mechanical solidity of the biofilm, supporting it to resist substantial shear forces. Tetrasaccharide repeats L-fucose, D-glucose, and D-glucuronic acid have been identified in *Enterobacter aerogenes* (O'Neill et al., 1986). Composed of N-acetyl-D-glucosamine, D-mannose, 6-deoxy-D-galactose, and D-galactose, have been found in *Vibrio cholera* biofilms (Wai et al., 1998). Biofilm formation promotes genetic variants with unique colony morphologies, like rugose small-colony variants and wrinkly spreaders, which overproduce Psl/Pel or cellulose, and mucoid bacteria that overproduce alginate. This emergence of variants shows pseudomonads' ability to use matrix-building subpopulations for collective benefit (Mann & Wozniak, 2012).

Protein components of the biofilm matrix include secreted extracellular proteins, cell surface adhesins, and a significant subset of these proteins are fibrous (e.g., flagella, pili) and

contribute to the structural integrity and function of the biofilm. These proteins play various roles in biofilm formation and dissolution. They help attach cells to surfaces, stabilize the biofilm matrix by interacting with exopolysaccharides and nucleic acids, aid in developing three-dimensional biofilm structures, and dissolve the biofilm matrix through enzymatic degradation of polysaccharides, proteins, and nucleic acids (Fong & Yildiz, 2015).

Increasing evidence points to the role of fiber-forming proteins in providing essential scaffolding within biofilms and also enabling resistance to external threats such as phage predation. Several key fibrous proteins have been identified as contributors to the structural and functional integrity of bacterial biofilms. Major Protein Fibers include TasA, curli fibers, and phenol-soluble modulins (PSM) (Erskine et al., 2018). Curli fibers are among the most well-studied amyloid-like proteins in biofilms, particularly in *E. coli* and *Salmonella*. They are extracellular fibers that contribute to biofilm stability and adherence. Curli fibers are composed of CsgA and CsgB subunits, with CsgA forming the bulk of the fiber and CsgB acting as a nucleator (Barnhart & Chapman, 2006; Van Gerven et al., 2015). These fibers exhibit typical amyloid features, such as resistance to proteolytic degradation and the ability to bind dyes like Congo red and Thioflavin T (ThT), which are commonly used to detect amyloid structures (Chapman et al., 2002). *B. subtilis* biofilms rely heavily on the TasA protein, a non-amyloidogenic fiber-forming protein that plays a crucial role in the biofilm matrix. Although TasA fibers are essential for biofilm formation, their structure does not conform to the typical cross- β sheet arrangement found in amyloids. TasA is instead primarily composed of α -helices but can transition to a more β -sheet-rich structure under certain conditions, such as acidic pH (Erskine et al., 2018; Goyal et al., 2014). In *Staphylococcus* species, particularly *S. aureus* and *S. epidermidis*, the phenol-soluble modulins (PSM) proteins play dual roles as cytotoxic agents and structural components of biofilms. PSMs are unique because they form fibers with a cross- α helical structure rather than the typical amyloid cross- β arrangement. This structural difference highlights the diversity of protein fibers in bacterial biofilms (Erskine et al., 2018; Tayeb-Fligelman et al., 2017).

The biofilm matrix protects biofilms from environmental stresses and enhances nutrient availability. The BslA (Biofilm-Surface Layer Protein) in *Bacillus subtilis* forms a hydrophobic surface layer that protects the biofilm from desiccation and external hydrophilic substances, thereby promoting surface adhesion. Observations using confocal laser scanning microscopy (CLSM) highlight the presence of BslA in the biofilm matrix, where it forms a protective boundary between the biofilm and its environment (Kobayashi & Iwano, 2012). For *Vibrio cholerae*, the protein RbmA also protects the biofilm interior by binding cells to each other and to the matrix polysaccharides (Nadell et al., 2016).

Finally, in addition to providing stability and protection from external forces, the biofilm matrix must also facilitate communication between cells. In *Pseudomonas aeruginosa*, 30% of identified matrix proteins have been shown to be outer membrane proteins, commonly found in outer membrane vesicles (OMVs) (Toyofuku et al., 2012). It was found that while some matrix proteins come from secreted proteins and lysed cells, the majority originate from OMVs (Toyofuku et al., 2012). OMVs released during biofilm formation have been shown to be important for intercellular communication during biofilm development and also facilitating dispersal by coordinating cellular degradation of the biofilm matrix (Cooke et al., 2020).

1.5 Dispersal mechanisms

The final lifecycle stage of surface-attached bacterial communities involves the release of cells to leave the biofilm, return to a planktonic state, and colonize new sites. This process, called biofilm dispersal, is essential for bacteria to adapt to environmental changes or colonize new environments (Christensen et al., 2020). For many pathogenic bacteria, this dispersal is essential for transmission from environmental reservoirs to hosts. During dispersion, the biofilm's interior becomes fluid, and cells start moving actively. They escape through disruptions in the microcolony wall, entering the liquid as a single bacterium and leaving biofilms with central voids. Extensive dispersion can further erode the biofilm structure (Kaplan, 2010; Rumbaugh & Sauer, 2020). The active escape from the protective

biofilm environment is driven by steepening chemical gradients of nutrients, oxygen, and waste products, leading to the accumulation of dispersion-inducing molecules like NO. These conditions create subpopulations within biofilms that are more susceptible to dispersion cues. The dispersed cells are typically more motile, virulent, and adherent, with different metabolic profiles and altered antimicrobial susceptibility, making them distinct from both biofilm and planktonic cells (Rumbaugh & Sauer, 2020).

In *P. aeruginosa*, the dispersion response involves sensing dispersion cues, which is associated with a reduction in the c-di-GMP pool. The *P. aeruginosa* protein, RbdA, for instance, has a phosphodiesterase domain for degrading c-di-GMP and a PAS domain for sensing low oxygen levels. By fusing these two activities, RbdA can trigger biofilm dispersal by facilitating hypoxia-dependent c-di-GMP degradation (An et al., 2010). Low levels of c-di-GMP then activate dispersal (e.g., motility) phenotypes in part through regulatory proteins such as FleQ, the master activator of flagellar gene expression (Hickman & Harwood, 2008). Low levels of c-di-GMP enable FleQ to activate flagellar genes, leading to motility and initiation of the biofilm-to-planktonic transition. At the same time, a mechanism is needed to detach adhesins and release cells from their bound substrates. This is enabled in part by the LapA-LapG system (present widely in species of *Pseudomonas*, *Vibrio*, and other genera). In this system, the cysteine protease LapG cleaves and releases the biofilm adhesin, LapA, from the cell surface to initiate dispersal (Boyd et al., 2014). Upon binding c-di-GMP, a third protein LapD, sequesters LapG and inhibits its activity. Thus, high levels of c-di-GMP keep the LapA adhesin tethered to the cell surface, and low levels facilitate LapA release and dispersal. Figure 1.2 visualizes this system in *V. fischeri*, where the adhesin is known as LapV.

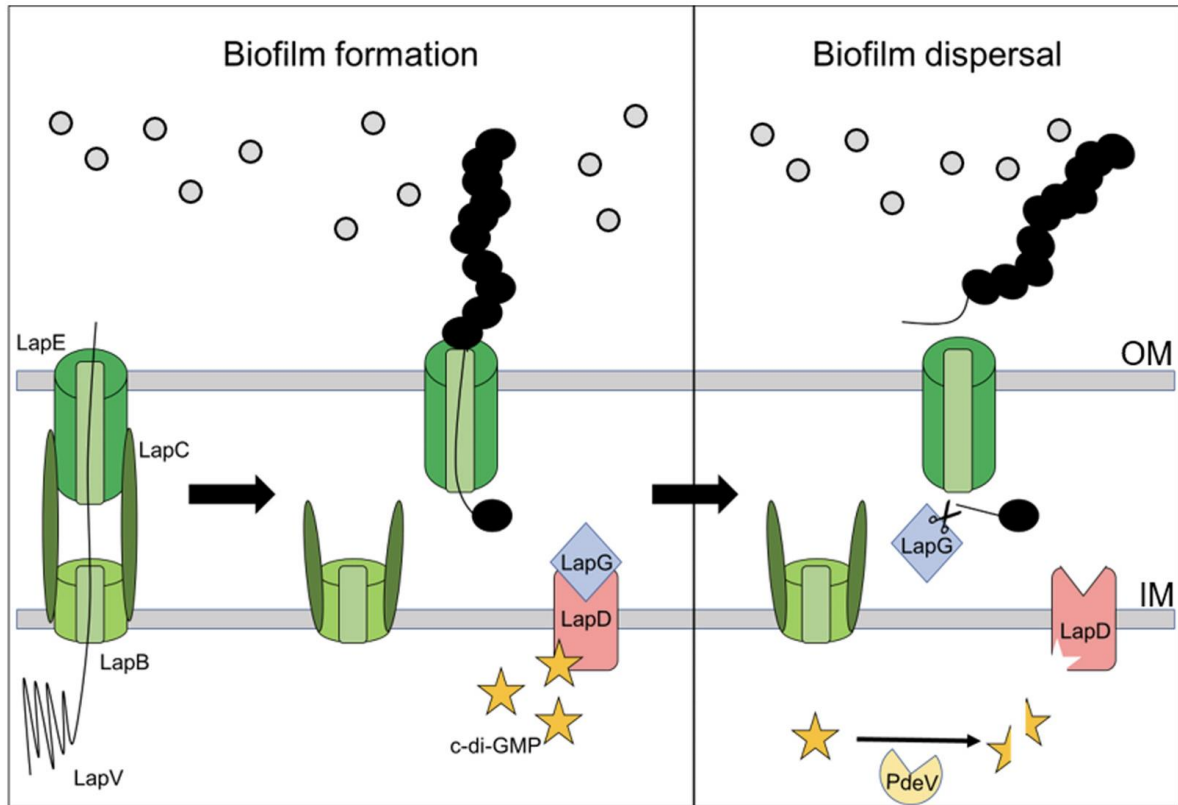


Figure 1.2. The Lap system and mechanism for controlling biofilm formation and dispersal. The large adhesin LapV is secreted through the T1SS components LapB and LapC and remains tethered to the cell. When c-di-GMP levels are high, c-di-GMP binds to LapD, which causes it to sequester the protease, LapG, preventing it from cleaving LapV. However, when the phosphodiesterase, PdeV, degrades c-di-GMP, then LapD no longer sequesters LapG, and it then cleaves the N-terminus of LapV causing it to be released from the cell. Low levels of c-di-GMP therefore enable biofilm dispersal through this system. This figure is obtained from (Christensen et al., 2020).

In addition to releasing adhesins, for dispersal to occur, cells must produce dispersal enzymes that break down the biofilm matrix and free cells from bound polysaccharides, eDNA, and proteinaceous structures. The three major families of biofilm-dispersing enzymes include glycosidases, proteases, and deoxyribonucleases, which target exopolysaccharides, extracellular proteins, and eDNA, respectively (Wang et al., 2023). Dispersin B, a glycoside

hydrolase, is one of the key enzymes involved in biofilm dispersion. It was originally discovered in *Aggregatibacter actinomycetemcomitans*, where it plays a crucial role in degrading poly-N-acetylglucosamine (PNAG), a key polysaccharide component of biofilm matrices in various bacterial species, including *Staphylococcus epidermidis* and *E. coli*. The enzymatic action of Dispersin B breaks down the glycosidic bonds in PNAG, leading to the structural disintegration of the biofilm matrix. By targeting this essential structural component, Dispersin B facilitates the dispersal of bacterial cells, making them more vulnerable to immune responses and antibiotic treatments (Kaplan, 2010; Rumbaugh & Sauer, 2020). For *Staphylococcus aureus*, exo-enzymes and surfactants that degrade the biofilm matrix and release cells have been studied. Key enzymes include secreted cysteine proteases (staphopains), V8 serine protease (SspA), and nuclease (Nuc). These proteases and surfactants are regulated by the *agr* quorum-sensing system, which is a known dispersal mechanism (Lister & Horswill, 2014).

1.6 Biology of *Pseudoalteromonas tunicata*

1.6.1 *P. tunicata* as a model organism for studying biofilm development

Pseudoalteromonas tunicata, a marine bacterium classified under *Gammaproteobacteria* and characterized as heterotrophic and Gram-negative, was originally isolated from the surface of adult tunicate *Ciona intestinalis* off the west coast of Sweden (Holmstrom et al., 1998; H. Holmström & Kjelleberg, 1999; Lovejoy et al., 1998). It is a facultatively anaerobic rod, is motile via a sheathed flagellum, exhibits non-fermentative metabolism, hydrolyzes gelatin, and utilizes mannose as a carbon source (Holmstrom et al., 1998).

P. tunicata demonstrates several characteristics that make it a target for biological study. First, *P. tunicata* exhibits a significant ability to form biofilms in a variety of marine settings (Mai-Prochnow et al., 2004; D. Rao et al., 2005). *P. tunicata* settles on the surfaces of various marine eukaryotic hosts and is known for its “surface-associated lifestyle”,

evidence of which can be seen in its unique proteome (Thomas et al., 2008). Second, *P. tunicata* possesses broad antimicrobial capabilities, including the production of antifungal, antimicrobial, and algicidal molecules, which include pharmaceutically relevant compounds (Bernbom et al., 2013; Bowman, 2007; Mai-Prochnow et al., 2004; Thomas et al., 2008). In part due to the production of these molecules, *P. tunicata* exhibits “antifouling” ability, which aids in its colonization of biofilms and inhibition of other competing species (Davey & O’toole, 2000). This activity impacts a wide variety of marine environments and eukaryotic organisms and is also generally relevant in the context of industrial settings (e.g., water systems) where unwanted biofilms can have undesirable consequences (Bowman, 2007; Saravanan et al., 2006). Flow cell experiments showed that *P. tunicata* can disrupt fungal biofilms, reducing them by 66% (Franks et al., 2006). When tested on the green alga *Ulva australis*, wild-type *P. tunicata* biofilms successfully outcompeted fungal communities, while the antifungal-deficient strain showed no impact. These results underscore the importance of antifungal activity in *P. tunicata*'s ability to dominate biofilm environments (Franks et al., 2006). Third, the genome content of *P. tunicata* also makes it an intriguing model organism for further protein characterization (Thomas et al., 2008). The *P. tunicata* proteome (4,490 proteins) includes 492 “orphan” proteins and 341 “uncharacterized” hypothetical proteins according to the latest Uniprot proteome annotations (UP000006201). Beyond these, the majority of remaining proteins have not been functionally investigated and their functions have been inferred by homology to proteins in other organisms. Previous studies also demonstrate that the *P. tunicata* genome has acquired foreign gene content by lateral transfer (e.g., leptospiral protein LipL32, (Gardiner et al., 2014), further making *P. tunicata* a strategic and characterize novel proteins.

1.6.2 Mechanisms of biofilm development in *Pseudoalteromonas tunicata*

Pseudoalteromonas species are significant contributors to marine biofilm development (Faria et al., 2020). Several previous studies have studied the process of biofilm development in *P. tunicata* (Mai-Prochnow et al., 2004; D. Rao et al., 2005).

The first step in biofilm formation by *P. tunicata* is initial attachment/adhesion to surfaces (Mai-Prochnow et al., 2004). The genome of *Pseudoalteromonas tunicata* encodes a variety of genes for surface adhesion-related proteins. *P. tunicata* also changes its membrane proteome to encode a functional extracellular matrix (ECM)-binding protein LipL32 (immunologically and functionally similar to *Leptospira*'s binding lipoprotein), which is used to adhere *P. tunicata* to *C. intestinalis*'s ECM. In addition, the conserved C-terminal region of LipL32 protein binds selectively to laminin and collagen (Huxley - Jones et al., 2007; Huxley-Jones et al., 2008; Thomas et al., 2008). *P. tunicata* can also adhere to other types of living surfaces for example cellulose and polystyrene via mannose sensitive haemagglutinin MSHA-like pili (Dalisay et al., 2006). Furthermore, *P. tunicata* encodes for the biosynthesis of other cell-surface structures and extracellular attachment components such as type IV pili, curli, chitin and cellulose-binding proteins, and capsular polysaccharide (Hoke et al., 2011; Thomas et al., 2008).

Once adhered to the surface, *P. tunicata* must not only coexist and compete with other prokaryotic and eukaryotic cells but also undergo careful regulation of its biofilm maturation. *P. tunicata*'s transition into a biofilm state involves the action of several proteins and pathways that produce compounds that act as anti-biofouling agents. *P. tunicata*'s antifouling activities are in part due to the production of at least four target-specific compounds and two pigments, yellow and purple, that together give it a dark green appearance (C. Holmström et al., 1998). A study found that 90% of dark-pigmented isolates from marine surfaces inhibited invertebrate larval settlement, suggesting a link between pigmentation and toxicity (C. Holmström et al., 1996). Research has shown that yellow-pigmented mutants retain full antifouling activity, whereas purple and white mutants lose some or all of their ability to

inhibit target organisms (Egan et al., 2002). This indicates that antifouling capabilities are linked to the presence of the yellow pigment rather than the purple pigment. The purple pigment, possibly violacein or phenazine, is known for its antibacterial properties, as seen in bacteria like *Chromobacterium violaceum*, *Pseudomonas*, and *Streptomyces* (Agarwal et al., 2023). The yellow pigment might be a bacterial quinone, which has antifungal, antibacterial, and insecticidal activities (Egan et al., 2002). *P. tunicata* also produces a variety of additional low and high molecular weight compounds, and they include toxic proteins, pyrrole-containing alkaloids, substituted phenolic and polyanionic exopolymers, cyclic peptides, and a range of bromine-substituted compounds (Bowman, 2007). One of the key enzymes involved in the production of these compounds is a long-chain fatty acid-coenzyme A ligase, as demonstrated by an antifungal-deficient mutant (FM3) (Franks et al., 2006).

Several studies have identified proteins that are up-regulated during specific stages of biofilm development in *P. tunicata*. Proteomic analysis revealed four outer-membrane proteins (homologous to a TonB-dependent receptor, OmpW, OmpA porins, and PilF) with increased abundance during biofilm growth (Ritter et al., 2012). Mutants lacking these proteins showed reduced biofilm biovolumes and altered structures (McPhee et al., 2009).

Another biofilm-associated protein produced by *P. tunicata* is the antibacterial protein AlpP, which likely aids *P. tunicata* in competing for space and nutrients on these surfaces (D. Rao et al., 2005). AlpP is an L-lysine oxidase and has been confirmed to possess antimicrobial activity through the generation of hydrogen peroxide (Mai-Prochnow et al., 2008). Through its lysine oxidase activity, AlpP causes cell lysis within biofilms to promote the release of dense clusters of cells and regulate biofilm spatial architecture (Mai-Prochnow et al., 2008). Programmed, localized cell death within biofilm microcolonies is thought to facilitate dispersal, as well as release nutrients and DNA, further aiding the surviving cells in differentiation and dispersal. AlpP-mediated cell death may also regulate biofilm growth in marine hosts. Many sessile algae and animals produce metabolites to prevent fouling, but those lacking defenses might rely on secondary metabolites from surface-associated bacteria like *P. tunicata*. Thus, cell death and dispersal within *P. tunicata* biofilms could protect hosts

from uncontrolled biofilm formation and fouling (Mai-Prochnow et al., 2004; Thomas & Allsopp, 1983). Also, potentially functioning in dispersal is the protein, flagellinolysin, which is a proteolytic variant of bacterial flagellin that is produced by *P. tunicata* (Jenkins, 2024, PhD thesis). Some evidence suggests that flagellinolysin may also function in biofilm development and dispersal by promoting proteolytic release of flagella from bound substrates (Jenkins, 2024).

1.7 Research Objectives and Hypothesis

Despite the wealth of knowledge regarding molecular mechanisms of biofilm development in model species (e.g., *P. aeruginosa*, *E. coli*, *B. subtilis*), there are gaps in our understanding of *P. tunicata* biofilm development. Further characterization of *P. tunicata*'s molecular mechanisms of biofilm development is important to improve our understanding of marine microbial biofilms (in which *Pseudoalteromonas* is a dominant genus). In addition, as a significant fraction of *P. tunicata*'s proteome contains hypothetical or uncharacterized proteins, it is possible that molecular characterization of biofilms may provide a functional context for some of these proteins, enabling basic protein function characterization.

In this thesis, I hypothesize that proteomic analysis of *P. tunicata* biofilms will enable discovery of novel proteins (including hypothetical proteins) with essential roles in biofilm development. The goal of my research is therefore to apply proteomic methods to identify and analyze *P. tunicata* proteins related to biofilm formation. I then aim to identify the top biofilm-associated proteins of unknown function in *P. tunicata* and exploring their functions through molecular, microbiological, imaging, and knockout techniques. My thesis is divided into the following three main data chapters, with objectives summarized below.

Chapter 2: The first study of my thesis conducts a comprehensive proteomic characterization of *P. tunicata*, examining changes in protein expression from the planktonic to biofilm stages. This large-scale survey aims to identify proteins of known function as well as those of

unknown function that may be involved in biofilm development. Hundreds of biofilm-associated proteins are identified, and two hypothetical proteins in particular (EAR28894 and EAR30327) are selected for further characterization in Chapter 3 and 4.

Chapter 3: The second study focuses on further characterization of EAR28894 and determined its role in biofilm development. EAR28894 is identified as the major S-layer protein of *P. tunicata*, and bioinformatic analysis reveals that it forms a unique protein family, designated Slr4. This analysis suggests that in addition to providing the cell with a protective outer proteinaceous layer, Slr4 contributes to the structural integrity and protection of the biofilm matrix.

Chapter 4: The third study performs a characterization of EAR30327, which I statistically identified as the top biofilm-associated protein in Study 1. This research reveals EAR30327 as a novel Ca²⁺ dependent adhesin protein which is required for biofilm formation and adhesion on surfaces and in pellicles.

Together, this thesis research provides a new understanding of the molecular mechanisms underpinning biofilm development in *P. tunicata* and contributes to the broader knowledge of biofilm formation in marine microbial communities.

Chapter 2

Proteomic investigation of biofilm development in *Pseudoalteromonas tunicata*

The material in this chapter has been deposited as a preprint manuscript in bioRxiv:

Sura Ali, Alexander Stavropoulos, Benjamin Jenkins, Sadie Graves, Geoffrey Che, JiuJun Cheng, Huagang Tan, Xin Wei, Suhelen Egan, Josh D. Neufeld, Ulrich Eckhard, Trevor C. Charles, Andrew C. Doxey. Comparative proteomics of biofilm development in *Pseudoalteromonas tunicata* discovers a distinct family of Ca²⁺-dependent adhesins. bioRxiv 2024.10.22.619756; doi: <https://doi.org/10.1101/2024.10.22.619756>

2.1 Introduction

Biofilms are surface-associated, multicellular bacterial communities that are encased within a self-secreted extracellular matrix (ECM). This ECM is spatially organized and composed of exopolysaccharides (EPS), proteinaceous fibers, lipids, and DNA (Beebout et al., 2019). Biofilms provide bacterial cells with numerous advantages, including metabolic resource sharing, physical support, and protection from biotic and abiotic stresses, antimicrobials, and host immune defences (Ge et al., 2016).

Understanding molecular processes that control biofilm development by environmental and host-associated microorganisms is a fundamental area of microbiology, with important industrial and ecological applications. Members of the *Pseudoalteromonas* genus (class *Gammaproteobacteria*) are commonly found in marine environments in association with biological surfaces and diverse eukaryotic hosts and play important roles in the ecology of marine ecosystems (Bowman, 2007; C. Holmström et al., 1998, 2002; Mai-Prochnow et al., 2004). One of the best studied species within this group is *P. tunicata*, a heterotrophic, Gram-negative bacterium first isolated from the tunicate, *Ciona intestinalis* (C.

Holmström et al., 1998). *P. tunicata* is also known to colonize algal host surfaces, sea-water biofilm communities, and likely other yet-to-be-identified living surfaces and host organisms in the marine environment (C. Holmström et al., 1998; Thomas et al., 2008). Among *P. tunicata*'s characteristics is its ability to colonize and outcompete other species in natural biofilms (Rao et al., 2005, 2010), which is in part due to its broad repertoire of antimicrobial capabilities (Bowman, 2007; C. Holmström et al., 1998, 2002; Mai-Prochnow et al., 2004). Characterizing the molecular basis of *P. tunicata*'s biofilm formation, colonization, and antifouling activity is important not only in the context of understanding marine biofilm ecology (Dang & Lovell, 2015; Mai-Prochnow et al., 2004; D. Rao et al., 2005; Rao et al., 2008), but it could also reveal new biotechnological strategies for preventing biofilm formation (e.g., in industrial settings or infections) or controlling biofilm species composition (Asma et al., 2022; Zhao et al., 2023).

The transition of *P. tunicata* to a surface-associated lifestyle involves dynamic changes in its transcriptome and proteome (Hoke et al., 2011), including the production of anti-biofouling agents (Holmström et al., 2002; Stelzer et al., 2006). These include antilarval, antibacterial, antialgal, and antifungal molecules. Transposon mutagenesis studies have identified a ToxR-like regulator, WmpR, as a key regulatory protein that controls stationary phase expression of antifouling inhibitors in *P. tunicata* (Egan et al., 2002). WmpR also controls the production of other bioactive compounds and pigments (Egan et al., 2002), and other proteins associated with adaptation to a biofilm lifestyle such as iron acquisition genes and type IV pili (Mai-Prochnow et al., 2004; Stelzer et al., 2006). One of the proteins produced by *P. tunicata* is an autocidal enzyme called AlpP that causes cell lysis within biofilms (Mai-Prochnow et al., 2004). AlpP is a lysine oxidase that produces hydrogen peroxide (Mai-Prochnow et al., 2008) and exhibits antibacterial activity against other Gram-negative and Gram-positive bacteria (James et al., 1996). Resistance to self-killing by AlpP increases in *P. tunicata* stationary phase cultures (James et al., 1996), which is also regulated by WmpR (Stelzer et al., 2006). The controlled AlpP-mediated autolysis of subpopulations of cells within the centre of biofilm microcolonies is thought to promote the detachment of

dense clusters of cells, regulate biofilm spatial architecture, and facilitate dispersal (Mai-Prochnow et al., 2004). Similar mechanisms have been identified in other Gram-negative bacteria including *M. mediterranea*, *C. violaceum*, and *C. crescentus* (Mai-Prochnow et al., 2008).

Despite previous knowledge of biofilm development in *P. tunicata*, the full repertoire of proteins involved in this species' biofilm-forming activities and surface-associated lifestyle remain uncharacterized. Previous studies have implicated hypothetical proteins as components of *P. tunicata* biofilms or surface-associated states (Ali, Jenkins, Cheng, et al., 2020; Hoke et al., 2011), and there exists hundreds of proteins of unknown function encoded within the *P. tunicata* genome (Thomas et al., 2008), many of which may play important roles in biofilm development that await further characterization. Here, to further elucidate the molecular mechanisms and identify key proteins responsible for biofilm development in *P. tunicata*, I have performed a time-course shotgun proteomic analysis of *P. tunicata* cells from a planktonic to early and late biofilm states.

2.2 Methods

2.2.1 Culturing of *P. tunicata* samples throughout planktonic to biofilm development

A frozen stock of *P. tunicata* strain D2 (provided by Dr. Suhelen Egan, UNSW Sydney, Australia) was streaked on Difco marine agar 2216 and incubated for 48 h at room temperature. An overnight culture was made by inoculating a colony into 4 ml of marine broth, which was incubated overnight at 24°C with 120 rpm. Eight subcultures were made in Erlenmeyer flasks by transferring 1 ml ($OD_{600} = 1.3$) of the overnight culture into 100 ml of marine broth. The flasks were incubated for 8 h at 24°C with gentle shaking (100 rpm). After 8 h incubation, two of these cultures were used as planktonic cultures and considered “T0” samples. The six remaining flasks were used to generate pellicle (air-liquid interface) biofilms, by incubating these flasks statically at room temperature for 3 days. Samples were

collected at 24 h, 48 h, and 72 h of incubation (Figure 2.2.). Duplicate samples were collected from each time point, and they were pooled in one tube. Biofilm samples were collected from the center and the edge of the biofilm in addition to media samples (Figure 2.1.). The entire procedure was repeated three times to provide biological replicates. Thus, a total of 30 samples were collected from four different time points (T) as follows: T0 = [(planktonic 8 h shaking) (n = 3)]; T24 = [24 Biofilm sample center (n = 3), Biofilm sample edge (n = 3), media (n = 3)]; T48 = [48 Biofilm sample center (n = 3), Biofilm sample edge (n = 3), media (n = 3)]; T72 = [72 Biofilm sample center (n = 3), Biofilm sample edge (n = 3), media (n = 3)].

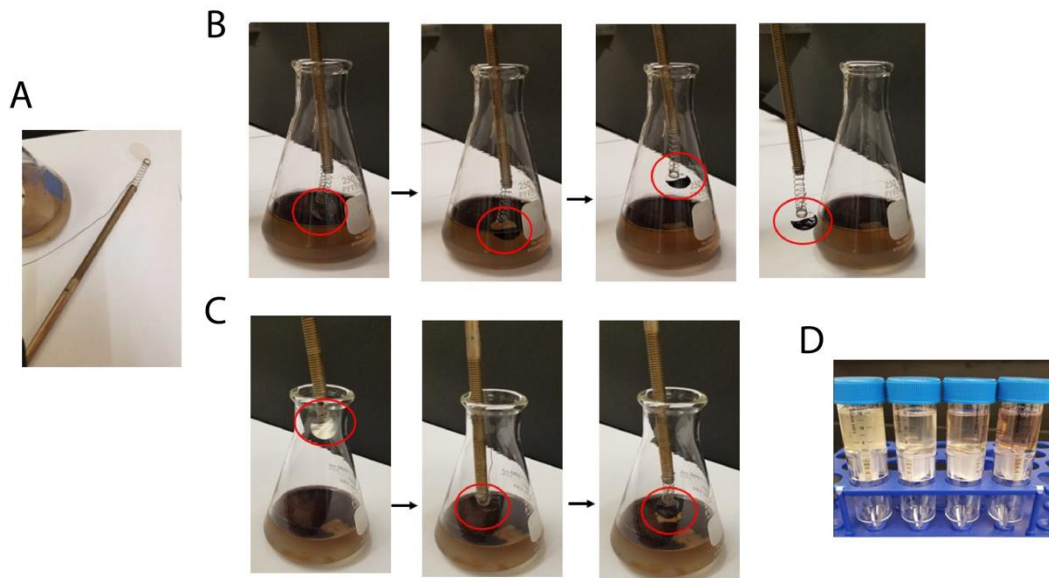


Figure 2.1. Biofilm sample collection tool. (A) A metal dowel was equipped with a tightly coiled spring that held a glass coverslip. The spring was connected to a piece of fishing line, allowing the coverslip to be carefully inserted beneath the film and then raised to collect a portion of the biofilm. (B) Steps of biofilm sample collection from the center. (C) Steps of biofilm sample collection from the edge. (D) Media samples were collected from the same flasks.

A method used by A. J. Park et al. (2014) with some modifications was followed for sample processing. To collect planktonic samples, 7.5 ml was aspirated from each of two flasks using a sterile serological pipette, yielding a total volume of 15 ml. The planktonic cultures were then concentrated to a volume of 2.5–3 ml using a Vivaspin 20 centrifugal filtration unit with a 3 kDa cutoff, operated in a swing bucket at 4000 x g for 140–160 minutes at 4°C. The concentrate (2.5–3 ml) was washed using the same Vivaspin 20 unit with 10 ml of cold Tris-HCl buffer (0.1 M, pH 8.3). This washing step was performed with a fixed-angle rotor at 6000 x g for 10 minutes at 4°C. A final volume of 500 µl of concentrate was collected, and the samples were then frozen at -20°C.

Pellicle biofilm samples were collected using a clean round coverslip (Fisher brand, No. 2 - 0.25 mm thick, Size 18 mm) attached to a custom-designed tool composed of a spring and metal rod shown in Figure 2.1., which was cleaned with water and alcohol after each use. Biofilm samples (18 mm diameter) were collected from the edge and the biofilm's center. The coverslips containing biofilm were placed in a clean tube containing 5 mL of cold Tris-HCl buffer (0.1 M, pH 8.3). Biofilm samples were washed off the surface of the coverslip tube by vortexing gently until the biofilm was completely separated from the coverslip and transferred to clean tubes. The biofilm suspension was centrifuged once at 12,000 x g for 10 min at 4°C. The supernatant was discarded. The pellet was collected and resuspended in 500 µl of cold Tris-HCl (pH 8.3) and vortexed until all the pellet was resuspended. The samples were frozen at -20°C. Media samples were also collected from each biofilm flask after the biofilm samples were taken and prepared using the same protocol as described above for planktonic samples.

2.2.1 Shotgun proteomics

2.2.1.1 Sample processing for LC-MS/MS

Prior to LC-MS/MS analysis, samples were processed for protein extraction and quantification. Three rounds of freeze/thaw cycles were performed using 1 L of liquid nitrogen for 30 seconds followed by transferring to a room temperature water bath. Samples (990 μ l) were then treated with 10 μ l of protease inhibitor cocktail FOCUS ProteaseArrest (G-Biosciences) and kept on ice. A 3 mm sonicator tip (Qsonica Sonicator) was used to sonicate the samples, which were placed in 2 ml round-bottom Eppendorf tubes. Sonication was performed in four cycles on ice, with each cycle consisting of 30 seconds at 30% amplitude, followed by 60 seconds of cooling time between sessions. The sonicated samples were centrifuged (6000 x *g*, 10 min, 4°C) to remove cellular debris, and the supernatants were collected. The samples were stored at -20°C for further processing. To perform LC-MS/MS (Figure 2.2.), at least 50 μ g of protein sample was collected for each sample. The protein concentration in the lysates was measured using the Bradford assay (Bradford, 1976).

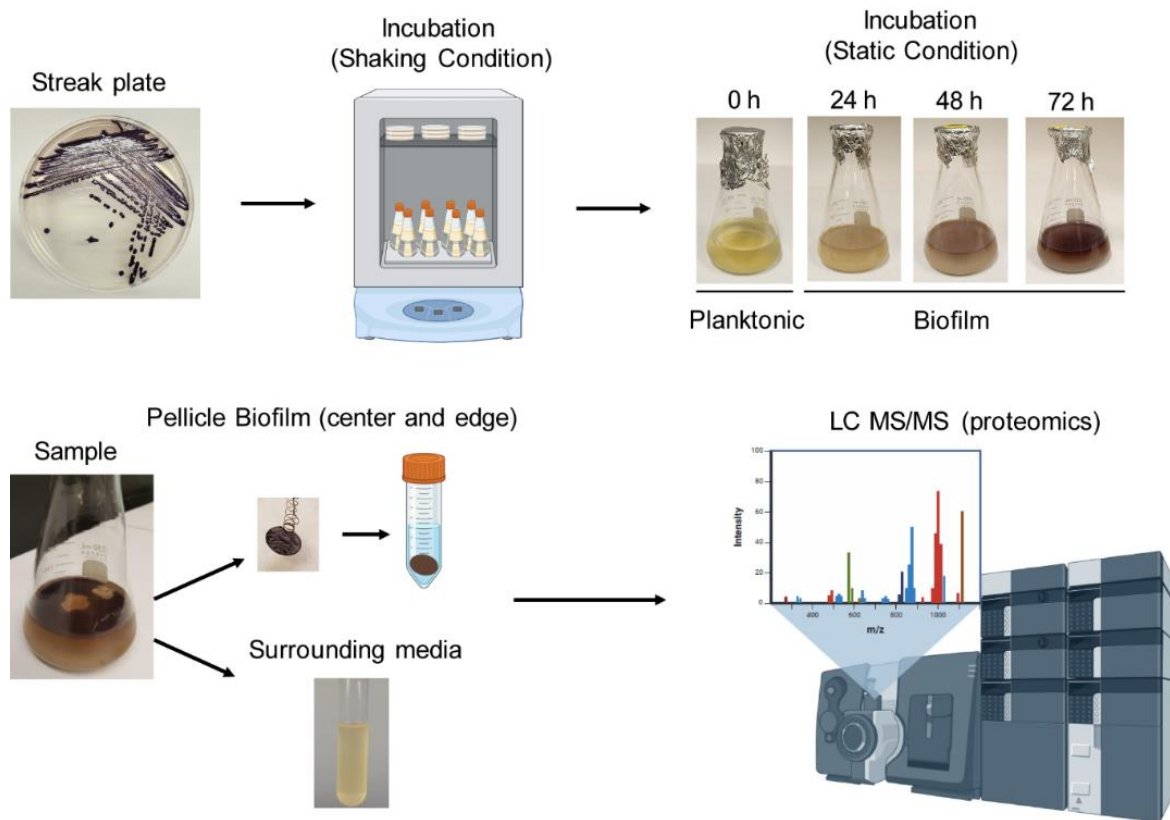


Figure 2.2. Overview of protocol for sampling of *Pseudoalteromonas tunicata* pellicle biofilms and planktonic cultures. *P. tunicata* was cultured on marine agar streak plates, incubated at 24°C for 72 h, and used to make liquid cultures in marine broth. In static (non-shaking) conditions, pellicle biofilms began to develop after approximately 24 h and increase in biomass over time at the air-liquid interface. A device was used to extract circular segments from the pellicle biofilm, which was resuspended in Tris-HCl pH 8.3, and used for LC-MS/MS proteomic analysis. For comparison, samples of liquid media below the biofilm surface were also taken for proteomic analysis.

2.2.2 Proteomics

Ten µg samples were reduced with 10 mM dithiothreitol (Sigma-Aldrich, Missouri, USA) alkylated with 20mM iodoacetamide (Sigma-Aldrich, Missouri, USA), acetone precipitated

and digested overnight with MS grade trypsin (Promega, Wisconsin, USA). Digested samples were lyophilized then resuspended in 0.2% trifluoroacetic acid (TFA) and desalted using a homemade C18 zip tip (resin: Empore, 2215-C18(Octadecyl)). The C18 desalted samples were resuspended in 18 μ l buffer A (0.1% FA buffer pH 2.7). Six microliters of each sample were injected into the *tims*TOF Pro (Bruker Daltronics, Bremen, Germany) using nanoflow liquid chromatography using a Bruker NanoElute chromatography system (Bruker Daltronics, Bremen, Germany). Liquid chromatography was performed at a constant flow of 400 μ l/min and a 15cm reversed-phased column with a 75 μ m inner diameter, packed with Reprosil C18 (PepSEP, Bruker, Germany). Mobile phase A was 0.1% formic acid, and Mobile phase B was 99.9% Acetonitrile, 0.1% formic acid. The *tims*TOF Pro was outfitted with a CaptiveSpray source (Bruker Daltronics, Bremen, Germany), operated in PASEF mode. MS and MS/MS scans were limited to 100 m/z to 1700 m/z, and a polygon filter was applied to the m/z and ion mobility dimensions to select for multiple charged ions most likely to be peptide precursors. Collision energy was applied as a function of ion mobility, using a linear regression with the following parameter settings: 0.85 V·s/cm² at 27 eV and 1.30 V·s/cm² at 45 eV. The TIMS voltage was calibrated using ions from the Agilent Tune Mix (m/z 622, 922, 1222). Active exclusion of MS/MS scans was enabled with a setting of 0.40 min. Quadrupole isolation was set to 2 m/z for ions with m/z less than 700, and 3.0 m/z for ions with m/z greater than 800. All MS experiments were completed at the Bioinformatics Solutions Inc. MS lab (Waterloo, Ontario, Canada).

MS Raw files were processed using PEAKS XPro (v10.6, Bioinformatics Solutions Inc., Ontario, Canada). The data were searched against a custom database containing the *P. tunicata* proteome. Precursor ion mass error tolerance was set to 20 ppm and fragment ion mass error tolerance was set to 0.05 Da. Semi-specific cleavage with trypsin was selected with a maximum of 2 missed cleavages. A fixed modification of carbamidomethylation (+57.02 Da) on cysteine residues was specified. Variable modifications of deamidation (+0.98 Da) on asparagine and glutamine, as well as oxidation (15.99 Da) on methionine, were specified. The false discovery rate threshold was set to 1% for the database search.

Normalized protein abundance calculated by Peaks was further converted to proportions of overall counts using R v4.3.3. Heatmaps of protein abundance were generated using pheatmap (<https://github.com/raivokolde/pheatmap>) with row-normalization applied using the `scale="row"` option. PCA was performed using the “`prcomp`” function in R. Differential analysis of protein abundance was performed using two-tailed t-tests with *p* values adjusted for multiple-hypotheses using `p.adjust` with the Benjamini-Hochberg method (Benjamini & Hochberg, 1995). Differentially abundant proteins were identified as those with \log_2FC values > 0.5 and *q* values < 0.01 .

2.3 Results

2.3.1 Proteomic analysis of planktonic and biofilm proteins in *Pseudoalteromonas tunicata*

To identify potential biofilm-associated proteins in *P. tunicata*, I performed comparative LC-MS/MS shotgun proteomics of *P. tunicata* D2 liquid cultures grown for 8 h (planktonic), 24 h (biofilm), 48 h (biofilm), and 72 h (biofilm). Pellicle biofilms were grown by culturing cells in liquid flasks in non-shaking (static) conditions (see Methods). I also collected protein from the media at 24-72 h time points and performed proteomics on these samples (Figure 2.2.).

For all samples, I identified a total of 942 *P. tunicata* proteins with a coverage of at least one high-confidence peptide assignment Appendix C (C.1.). A subset of 288 proteins excluding low abundance proteins was used to generate a heatmap of relative abundance across all samples (Fig. 2.3.). Proteins clustered into four groups based on their relative abundance profiles: cluster 1 (*n* = 84) was enriched in media samples, cluster 2 (*n* = 54) was enriched in planktonic samples, and clusters 3 (*n* = 69) and 4 (*n* = 81) were biofilm-associated with cluster 4 proteins showing increased abundance at early biofilm stages (24 h) and cluster 3 proteins showing increased abundance at middle to late biofilm stages (i.e., 48 - 72 h).

Planktonic, biofilm, and media samples therefore display unique proteomic profiles. To test this further, I performed principal component analysis (PCA) of all samples based on their proteomic profiles (Figure 2.4.). As shown by the PCA, the samples showed a strong separation according to their category (planktonic, media, biofilm; Figure 2.4.). Biofilm samples also showed some additional separation by time point consistent with the heatmap, but not based on the region of biofilm collected (center versus edge) (Figure 2.4.) Although the heatmap provides a visual overview of protein abundance profiles, differential abundance analysis was required to detect statistically significant differences.

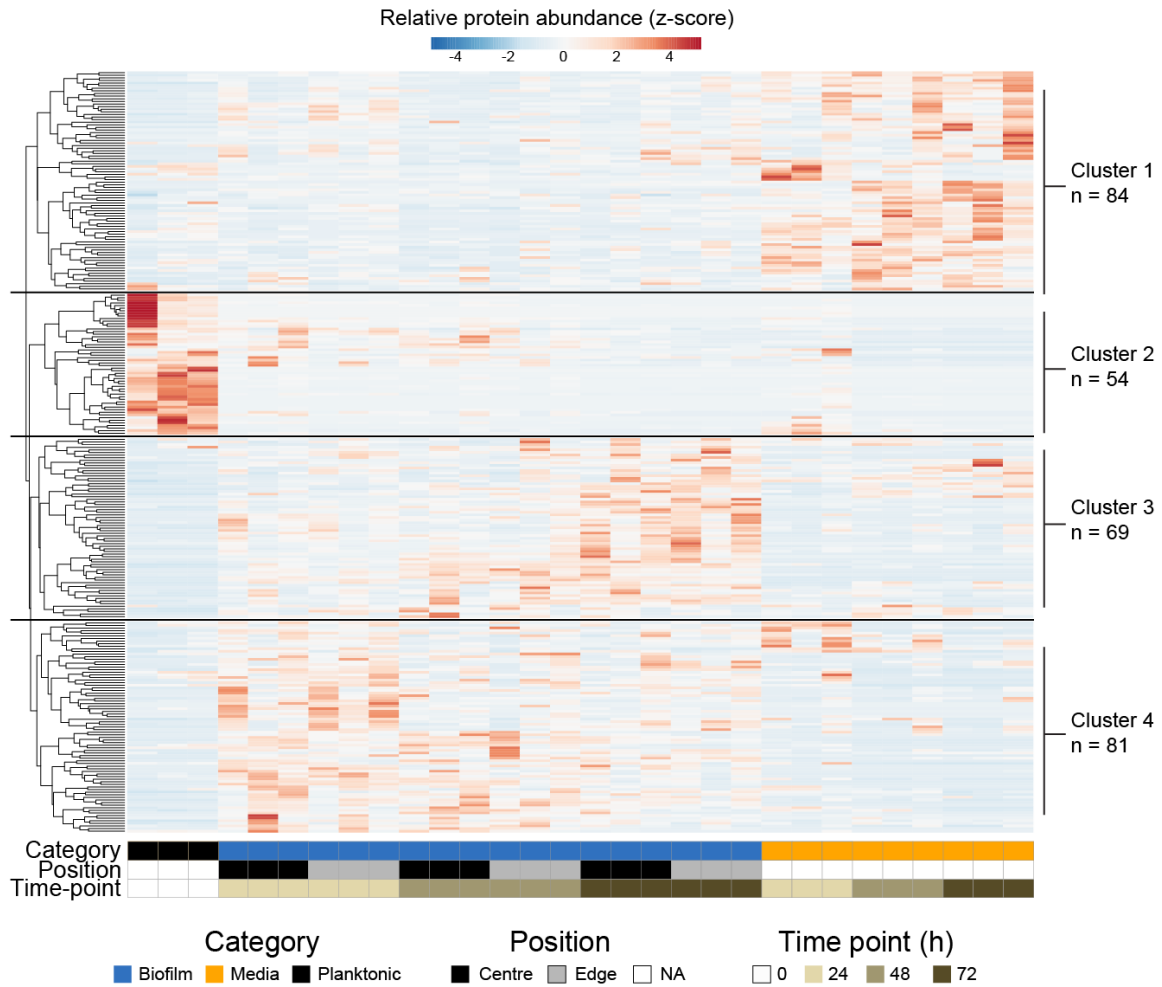


Figure 2.3. Comparative proteomic analysis of *Pseudoalteromonas tunicata* throughout biofilm development. Proteomic abundance heatmap of 288 proteins detected by LC-MS/MS analysis. Per-protein abundances (spectral hits) were row-normalized to Z-scores depicting relative abundance across samples. Proteins clustered into four groups based on their relative abundance profiles across samples. Cluster 1 proteins are media-enriched, cluster 2 proteins are planktonic-enriched, and cluster 3 and 4 proteins are biofilm-enriched, with cluster 3 associated with mid-to-late stage biofilms and cluster 3 associated with early stage biofilms.

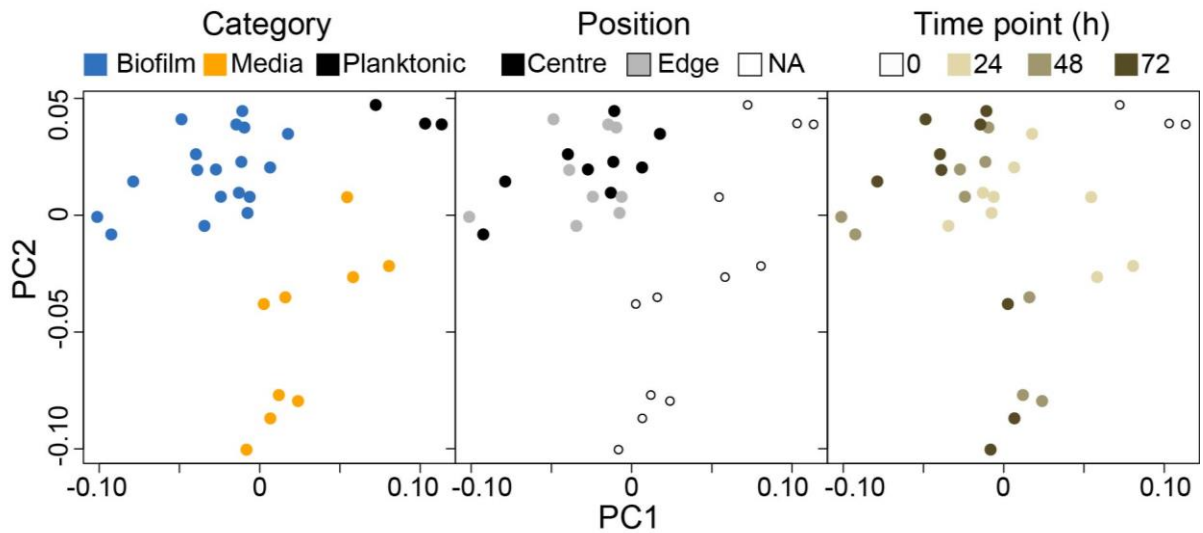


Figure 2.4. Principal component analysis (PCA) plot of samples based on their proteomic profiles. The PCA plot reveals the grouping of samples based on sample type.

I therefore compared normalized protein abundance across biofilm and non-biofilm conditions to detect putative biofilm-associated proteins (Figure 2.5.). Out of the 942 detected proteins (Figure 2.6.) a total of 232 were identified as biofilm-associated based on significant normalized abundance increases ($\log_2FC > 0.5$ and $q < 0.01$, two-tailed t -test, BH adjustment of p values) in biofilm versus planktonic samples (Figure 2.5., Table 2.1). Only 15 proteins were detected with increased abundance in planktonic conditions (Figure 2.5, Table 2.2) which may be due to lower overall proteomic coverage and fewer biological replicates ($n = 3$) of these samples.

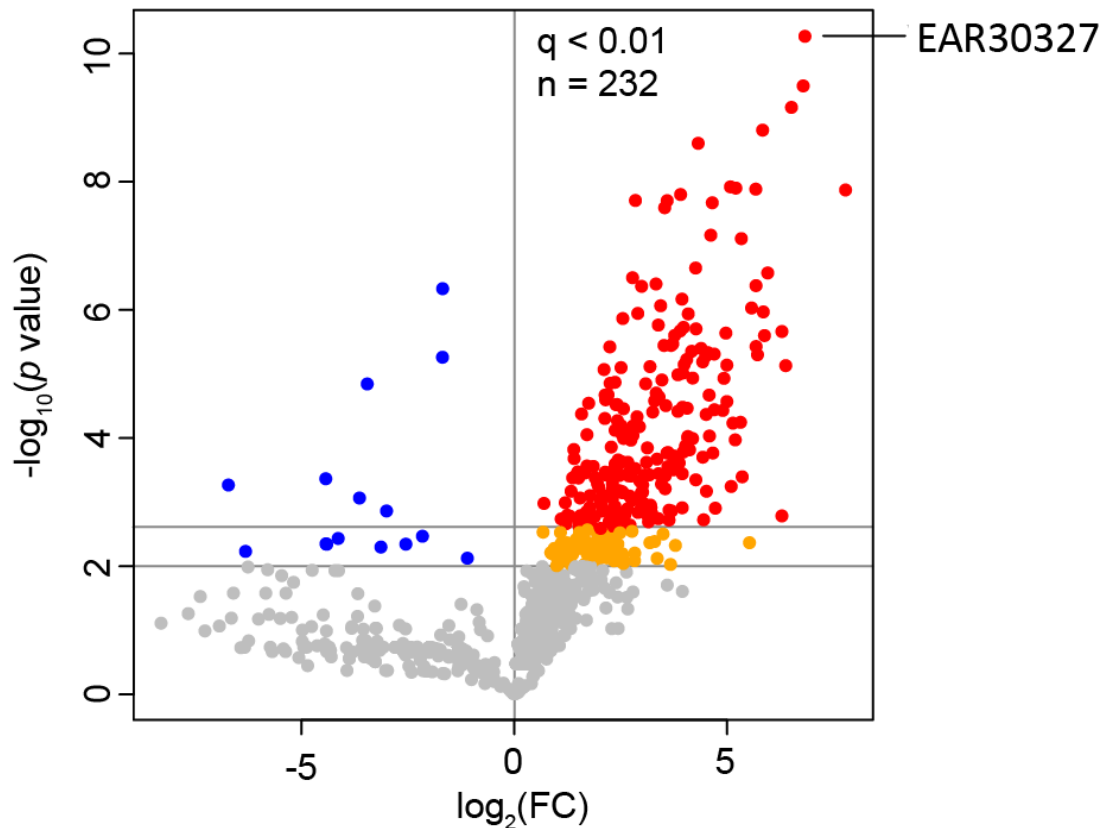


Figure 2.5. Volcano plot depicting differentially abundant proteins in biofilm samples (N = 18) versus planktonic (N = 3) samples. Proteins with significantly increased abundance in biofilms are located in the top right quadrant, with the top-scoring proteins ($q < 0.01$) shown in red. Remaining biofilm-associated proteins with weaker significance ($p < 0.01$) are colored orange. Proteins with significantly increased abundance in planktonic conditions are located in the top left quadrant (colored blue). Non-significant proteins are shown in gray.

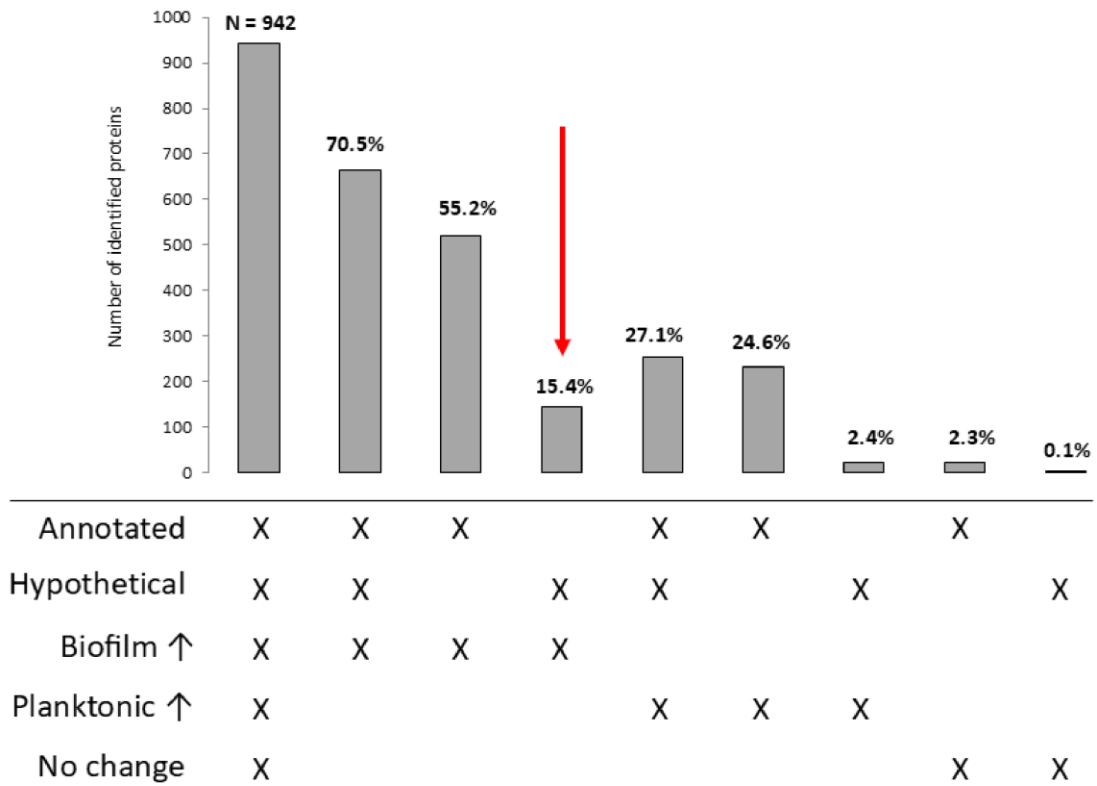


Figure 2.6. Identified *Pseudoalteromonas tunicata* proteins by LC-MS/MS analysis of planktonic and biofilm cultures.

Table 2.1. The top 15 detected biofilm-associated proteins. The full table is found in Appendix C (C.1.).

Rank	logP	log2(FC)	Gene	Description*
1	10.27	6.83	PTD2_02121	EAR30327, Ig-like domain-containing protein, “BapP”
2	9.50	6.79	<i>pal</i>	Peptidoglycan-associated protein
3	9.16	6.51	PTD2_04016	RimK family alpha-L-glutamate ligase
4	8.81	5.83	PTD2_17855	S46 family peptidase
5	8.60	4.32	PTD2_16476	Putative type IV pilus biogenesis protein PilQ (Cytoplasmic ATPase)
6	7.90	5.20	PTD2_14577	PQQ-binding-like beta-propeller repeat protein
7	7.88	5.67	<i>dnaJ</i>	Chaperone protein DnaJ
8	7.87	7.78	PTD2_03531	2' 3'-cyclic nucleotide 2'-phosphodiesterase/3'-nucleotidase bifunctional periplasmic protein
9	7.80	3.91	PTD2_15532	SurA N-terminal domain-containing protein
10	7.67	4.65	PTD2_20877	nitroreductase family protein
11	7.92	5.08	PTD2_09647	FKBP-type peptidyl-prolyl cis-trans isomerase
12	7.60	3.53	<i>ppnP</i>	Pyrimidine/purine nucleoside phosphorylase
13	7.71	2.85	PTD2_18035	Uncharacterized protein
14	7.11	5.33	PTD2_00412	Uncharacterized protein
15	6.58	5.95	PTD2_06994	Uncharacterized protein

*Descriptions are based on annotations of numerous identical proteins collected from NCBI’s “Identical Protein Groups” resource.

Table 2.2. Proteins with increased abundance in planktonic conditions.

Rank	logP	log2FC	Gene	Description
1	6.33	-1.17	<i>panC</i>	Pantothenate synthetase
2	5.26	-1.17	PTD2_19300	Dihydrolipoyllysine-residue succinyltransferase component of 2-oxoglutarate dehydrogenase complex
3	4.84	-2.39	PTD2_15097	Putative orphan protein
4	3.37	-3.07	<i>rpmA</i>	50S ribosomal protein L27
5	3.27	-4.65	<i>rplS</i>	50S ribosomal protein L19
6	3.06	-2.52	<i>csrA</i>	Translational regulator CsrA
7	2.86	-2.08	<i>nusG</i>	Transcription termination/antitermination protein NusG
8	2.47	-1.49	PTD2_10819	Nucleoid-associated protein
9	2.43	-2.87	<i>cpoB</i>	Cell division coordinator CpoB
10	2.35	-3.07	<i>rplL</i>	50S ribosomal protein L7/L12
11	2.34	-1.77	<i>fusA</i>	Elongation factor G
12	2.34	-3.05	<i>tsf</i>	Elongation factor Ts
13	2.30	-2.17	<i>grpE</i>	Protein GrpE
14	2.23	-4.38	<i>tig</i>	Trigger factor
15	2.13	-0.76	<i>ndk</i>	Nucleoside diphosphate kinase

Planktonic-associated proteins included proteins involved in transcription (e.g., NusG), translation (ribosomal proteins, EF-Tu, CsrA), and cell division (e.g., CpoB). This is to be expected since these proteins reflect core physiological processes of intracellular proteins. LC-MS/MS abundance profiles of example planktonic-associated proteins (EF-Tu and rplC) are shown in Figure 2.7. I also detected twenty proteins with significant abundance increases in media samples (Table 2.3). Media-enriched proteins may also reflect the activities of planktonic cells or non-adherent cells and, potentially, dispersed cell populations. Several proteins were detected at high levels in 24 h media samples as well as in planktonic cells (e.g., GroEL chaperone, Figure 2.7.).

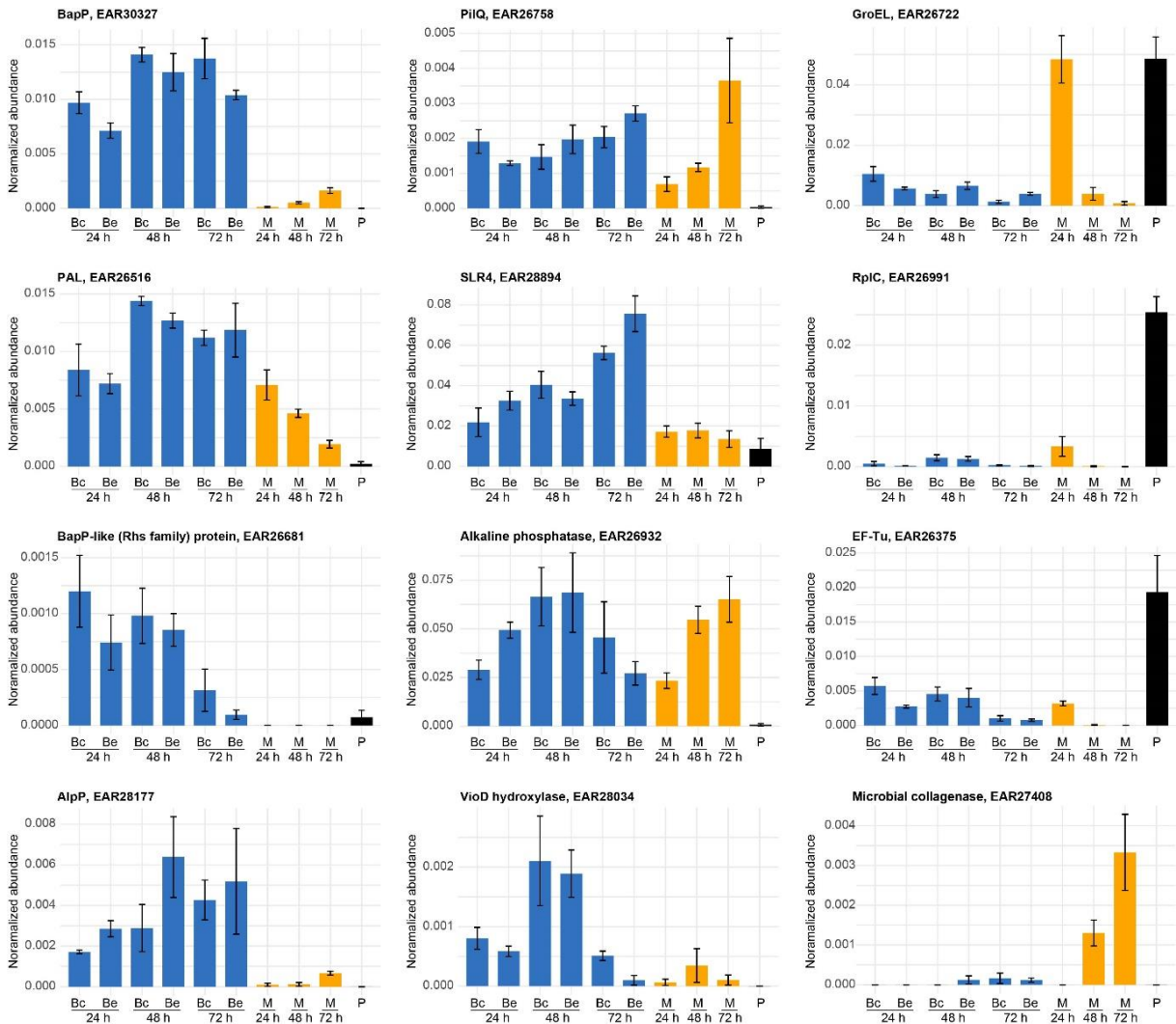


Figure 2.7. Relative abundance of selected proteins across planktonic, biofilm, and media samples based on LC-MS/MS proteomic analysis. Protein abundance was calculated as a percentage of total peptide spectral matches to the *P. tunicata* proteome. Bars represent the mean \pm standard error (SE). The two bolded proteins (EAR30327 and EAR28894) are investigated experimentally in later chapters.

Table 2.3. Top detected media-enriched proteins.

Description	<i>p</i> value	<i>q</i> value	log2FC
Ribulose-phosphate 3-epimerase GN=rpe	1.7E-07	5.2E-05	1.93
Peptide deformylase GN=def	3.9E-06	3.7E-04	3.13
2-3-4-5-tetrahydropyridine-2-carboxylate N-succinyltransferase GN=PTD2_06474	6.4E-06	4.3E-04	3.09
Glutamine synthetase GN=glnA	7.4E-06	4.3E-04	1.29
Putative metal-dependent dipeptidase GN=PTD2_03171	1.1E-05	5.2E-04	1.88
Phosphoribosylamine--glycine ligase GN=purD	2.0E-05	7.3E-04	2.42
Uncharacterized protein GN=PTD2_18035	4.7E-05	1.2E-03	1.24
Protein-export protein SecB GN=secB	5.0E-05	1.2E-03	1.22
Thiol:disulfide interchange protein GN=PTD2_16681	6.8E-05	1.4E-03	2.27
Dihydroorotase GN=pyrC	7.9E-05	1.5E-03	1.30
Uncharacterized protein GN=PTD2_14527	1.4E-04	2.3E-03	2.01
Probable cytosol aminopeptidase GN=pepA	3.1E-04	4.0E-03	4.13
3-methyl-2-oxobutanoate hydroxymethyltransferase GN=panB	3.5E-04	4.4E-03	1.89
Thioredoxin GN=PTD2_09349 PE=3 SV=1	4.7E-04	5.6E-03	2.35
Aspartate-semialdehyde dehydrogenase GN=asd	4.7E-04	5.6E-03	2.45
Putative aminopeptidase GN=PTD2_00911	5.4E-04	6.1E-03	2.47
Cysteine synthase GN=PTD2_18255	6.0E-04	6.4E-03	0.64
Uncharacterized protein GN=PTD2_11539	7.2E-04	7.4E-03	1.60
YkoF domain-containing protein GN=PTD2_07739	8.8E-04	8.7E-03	2.01
6-7-dimethyl-8-ribityllumazine synthase GN=ribH	1.0E-03	9.6E-03	2.94

Among the 232 biofilm-associated proteins are those with known roles in biofilm development (e.g., adhesion proteins, outer membrane proteins, flagellar proteins, type IV pilus proteins, and extracellular DNA processing enzymes (Barken et al., 2008) . The top 15 proteins with increased abundance in biofilms (of 232 total) are listed in Table 2 (full list in Appendix C (C.1). The top identified protein (based on *p* value) was **EAR30327** (Figure 2.5)a hypothetical protein that was chosen for subsequent experimental characterization and **forms the basis of work in Chapter 4**. Also identified was PTD2_22582 or PAL, peptidoglycan-associated lipoprotein, a protein involved in regulation of outer membrane stability, which has been shown to be involved in biofilm development (Solanki et al., 2023). The PAL protein showed a similar abundance profile to EAR30327 (Figure 2.7.) but in media samples was found at higher abundance at earlier (24 h) time points. The chaperone DnaJ was increased in biofilm development, consistent with a previous study demonstrating

that *E. coli* $\Delta dnaJ$ mutants are deficient in biofilm formation (Grudniak et al., 2015). PTD2_03531 (*cpdB*) which encodes 2' 3'-cyclic nucleotide 2'-phosphodiesterase/3'-nucleotidase, was also biofilm associated, which may reflect a putative role of nucleotidases in hydrolyzing extracellular DNA for nutrition (B. Cao et al., 2011). Two alkaline phosphatases (PTD2_10138, PTD2_10143) were also highly abundant in biofilm samples (Appendix Data C.1). Alkaline phosphatases have been shown to be critical for regulating biofilm formation in other organisms (e.g., *P. aeruginosa*) under phosphate depletion stress (Tan et al., 2023). The PTD2_16476 protein was also significantly increased in biofilm samples and media samples, encoding the type IV pilus secretin PilQ (Figure 2.7.). Type IV pili contributes to surface binding and sensing during biofilm formation and may also be involved in uptake of extracellular compounds and DNA (Ellison et al., 2022). The PTD2_09647 protein is a predicted peptidyl-prolyl cis trans isomerase. The protein Ppi-B contributes to biofilm formation of *Mycobacterium tuberculosis* and Ppi-B and is also found in biofilm-forming species like *Pseudomonas aeruginosa* (Ellison et al., 2022). The protein PTD2_12174 encodes the flagellar hook, FlgE, which has been shown to be essential for biofilm formation (Kumar et al., 2019). Other flagellar proteins, including two flagellins (PTD2_12134, PTD2_12124), were enriched in biofilm samples and also were detected in the surrounding media. Detection of flagellar proteins was expected given the role of motility in initial biofilm formation, intra-biofilm motility, biofilm dispersal, as well as the potential role of flagellins as structural components of the extracellular and biofilm matrix (You et al., 2023).

Among the list of 232 biofilm-associated proteins, I also detected several proteins previously shown to be important for biofilm development in *P. tunicata*. For example, the MSHA pilin protein MshA had increased abundance ($\log_2FC = 4.3$, $p = 2e-06$) in biofilms, and the violacein pathway proteins (VioA, C, D, and E) were also significantly increased. The VioD- hydroxylase (VioD) protein showed a unique temporal pattern of expression, because it was at higher abundance at the middle biofilm (48 h) time point (Figure 2.7.). The production of such pigments in *P. tunicata* is correlated with antifouling activity (Hobley et

al., 2015) and its pigmentation is associated with mature biofilms (D. Rao et al., 2005). The autolytic protein, AlpP (PTD2_20217) was also detected at significantly higher abundance in biofilms ($q = 5.5e-04$, $\log_2FC = 5.3$), consistent with previous literature (Mai-Prochnow et al., 2004; D. Rao et al., 2005). AlpP relative abundance increased over time in biofilms, reaching a maximum level in 72 h biofilms (Figure 2.7.). The hypothetical protein EAR28894 or PTD2_07619 (which forms the basis of work in Chapter 3), also increased in abundance throughout biofilm development from approximately 2% abundance in 24 h biofilms to 7.5% abundance in 72 h biofilms (Figure 2.7.). EAR28894 was the second most abundant protein detected overall (alkaline phosphatase PTD2_10138 was number 1) and was also significantly enriched in biofilm compared to planktonic samples ($q = 0.02$, $\log_2FC = 2.3$).

Among the top biofilm-associated proteins are novel/hypothetical proteins whose relevance to biofilm development is unclear, including PTD2_18035, PTD2_00412, and PTD2_06994, which were among the top 15 biofilm-associated proteins (Table 2) and others beyond this list (e.g., PTD2_01831). AlphaFold modelling of PTD2_18035 revealed tandem bacterial immunoglobulin-like (Big) domains similar to the structure of the invasin and intimin family of adhesins (Leo et al., 2015). The predicted structure of PTD2_01831 (AF-A4C3Y7-F1), which was highly abundant in biofilms but also detected in media and planktonic samples, had a predicted beta-helical structure similar to the *S. pneumoniae* surface adhesin, PfbA (Beulin et al., 2014). Thus, in addition to pili, *P. tunicata* appears to produce a variety of surface adhesin proteins involved in biofilm development, most of which are uncharacterized.

2.4 Discussion

Comparative shotgun proteomics detected hundreds of proteins with increased abundance in *P. tunicata* biofilms, many of which are either uncharacterized or have currently unknown roles in biofilm development. Longitudinal analysis over a 24-72 h period also revealed

temporal patterns of protein expression, reflecting changes in biofilm function in different stages of biofilm development. Among the top biofilm-associated proteins detected are proteins that have been previously implicated in *P. tunicata* biofilm development. For example, the autolytic protein AlpP was enriched in biofilm samples and increased in abundance throughout biofilm development. This is consistent with its role in programmed cell lysis to create voids within biofilms that enable cell re-distribution and dispersal (Mai-Prochnow et al., 2004), which may increase in frequency at later stages of biofilm development.

I identified several proteins whose roles in biofilm development are less clear but intriguing. Peptidoglycan-associated lipoprotein, PAL, is known for its role in stabilizing the outer membrane by interacting with the Tol-Pal system (Szczeplaniak et al., 2020). Although the tol-pal system has been shown to be up-regulated during biofilm development in other microorganisms (Solanki et al., 2023; Szczeplaniak et al., 2020), the considerable abundance of PAL in *P. tunicata* biofilms suggests a critical, yet-to-be discovered role. This role may be related to the formation or structure of outer membrane vesicles which are abundant in the biofilm matrix (Ali, Jenkins, Cheng, et al., 2020). In addition, I identified one protein (EAR28894) that was abundant in biofilms, and increased in abundance over time, reaching a maximum of almost 8% of peptide spectra in 72 h biofilms. This protein is pursued experimentally in the following chapter.

There are several limitations of my study that should be addressed by future research. Although my proteomic analysis was able to identify temporal variation in protein expression across biofilm development, I was limited in my ability to detect spatial variation that underlies control of biofilm architecture, which has been demonstrated in other systems (Dergham et al., 2023; Serra et al., 2015; Serra, Richter, & Hengge, 2013; Serra, Richter, Klauck, et al., 2013). Future spatially resolved proteomics or RNA-seq methods could help better understand the relationship between biofilm structure and gene/protein expression patterns. There are also limitations of shotgun proteomics (see previous reviews on this topic (Dupree et al., 2020; Nesvizhskii & Aebersold, 2005), that need to be considered for proper

interpretation of my LC-MS/MS data. These limitations include challenges in quantifying protein relative abundance, variability in peptide detections across samples, and difficulty in detecting low-abundance proteins or proteins with certain post-translational modifications. Thus, although my work has identified a subset of proteins with likely importance in *P. tunicata* biofilm development, others may have been undetected.

Chapter 3

Slr4, a newly identified S-layer protein from marine Gammaproteobacteria, is a major biofilm matrix component

Material in this chapter has been published as part of the following manuscript:

Ali, S., Jenkins, B., Cheng, J., Lobb, B., Wei, X., Egan, S., Charles, T. C., McConkey, B. J., Austin, J., & Doxey, A. C. (2020). Slr4, a newly identified S-layer protein from marine Gammaproteobacteria, is a major biofilm matrix component. *Molecular Microbiology*, 114(6), 979–990. <https://doi.org/10.1111/mmi.14588>

In this chapter, I focus on the experimental characterization of EAR28894, which was identified as one of the most abundant proteins detected in *P. tunicata* biofilms. I demonstrate that EAR28894 is an S-layer protein that is shed into the biofilm matrix. To provide context for understanding the function of EAR28894, below I provide some background information on S-layer proteins in general, their structure and function.

3.1 Background information on S-layer proteins

S-layers are self-assembling, paracrystalline protein layers that form a two-dimensional array on the surface of many bacterial and in nearly all archaeal species. Ubiquitous across a large number of bacteria and archaeal phyla, S-layer proteins can constitute 10% of the proteome of prokaryotic cells, making them one of the most abundant protein polymers found on earth (Qing, 2017). This, combined with their diverse functional roles, which include regulated nutrient transport through porous channels, physical protection of cells against the extracellular environment, targeted cell-adhesion, biofilm interactions, and others, make S-

layers one of the most important cellular structures in the microbial biosphere (Beveridge et al., 1997; Fagan & Fairweather, 2014; Sára & Sleytr, 2000; Sleytr et al., 2014).

S-layers have been extensively characterized in some bacterial species including *Caulobacter crescentus*, *Bacillus anthracis*, *Clostridiodes difficile*, and *Campylobacter fetus*. Electron microscopy (EM) and electron cryotomography studies of S-layers (Bharat et al., 2017) have revealed their exquisite nanoscale organization into paracrystalline arrays formed typically by a single protein or glycoprotein subunits. Depending on inter-subunit interactions between the S-layer protein, S-layer arrays can form different geometries, which include oblique (p1, p2), square (p4), or hexagonal (p3, p6) lattice symmetries (Sára & Sleytr, 2000). Interunit spacing within S-layer lattices can range widely from 4 to 35 nm, depending on the structure of the S-layer subunit and interactions between subunits (Sleytr et al., 2014). Another important feature of S-layer lattices is the presence of pores, which facilitate selective uptake of small molecular weight nutrients and potentially larger compounds in and out of the cell (Arbing et al., 2012). A prime example of S-layer molecular architecture is the RsaA S-layer protein from *C. crescentus*. RsaA forms a hexameric two-dimensional array that is stabilized by Ca^{2+} ions and multiple protein-protein interfaces. The RsaA S-layer lattice contains pore sizes ranging from ~20 Å to 27 Å wide, thus forming a barrier for extracellular attack by phages and most macromolecules (Bharat et al., 2017).

Both Gram-negative and Gram-positive bacteria may possess S-layers as the outermost layer of the cell. In Gram-negative species, S-layers are attached to the outer cell membrane through interactions with surface molecules such as lipopolysaccharide (von Kügelgen et al., 2020). In Gram-positive bacteria, S-layers are attached to secondary cell wall polymers or peptidoglycan through phosphodiester bonds or lipid anchors (Sára, 2001; Schuster & Sleytr, 2014). There are several families of protein domains/motifs that have been shown to mediate S-layer anchoring to outer cell layers. S-layer proteins of some *Firmicutes* species contain S-layer-homologous (SLH) motifs within the N-terminal region, which have been shown to mediate binding to the cell envelope (Mesnage et al., 2000). In other bacteria (e.g., *C. difficile* and other clostridia), CWB2 motifs have been identified as cell wall

anchoring modules (Willing et al., 2015). These anchoring domains have not been identified in all S-layer proteins (e.g., those from Gram-negative bacteria), suggesting distinct cell envelope anchoring mechanisms.

In order to assemble S-layers, bacteria and archaea must be able efficiently secrete large quantities of S-layer proteins across the cell envelope. For instance, it has been estimated that *C. difficile* must secrete ~400 S-layer subunits per second to build a contiguous S-layer composed of ~500,000 subunits (Fagan & Fairweather, 2014). In *C. difficile* as well as *B. anthracis*, S-layer secretion is accomplished through the accessory sec system involving the accessory ATPase SecA2 and a pore containing SecYEG (*C. difficile*) or Sec2YEG (*B. anthracis*). In *Aeromonas*, S-layer proteins are secreted through a dedicated type II secretion system involving a secretion apparatus similar to that of type IV pili (Tomás, 2012). In *Caulobacter* and several other Gram-negative species, S-layer secretion is accomplished through the type I secretion system, which consists of an outer-membrane pore and inner membrane ABC transporter (Awram & Smit, 1998). In *C. crescentus*, these components are genetically encoded immediately upstream of the *rsaA* gene (Awram & Smit, 1998).

Despite their ubiquity across bacteria and archaea, the S-layer proteins of many important lineages of bacteria remain uncharacterized. For example, *Pseudoalteromonas*, an ecologically significant genus of marine Gammaproteobacteria associated with marine eukaryotes and biofilm has not been fully characterized in terms of its surface layer proteins. *Pseudoalteromonas tunicata*, originally isolated from tunicates (Holmstrom et al., 1998; H. Holmström & Kjelleberg, 1999) has become a model organism for studying eukaryotic host-bacteria interactions colonization (Bowman, 2007), in marine environments, and surface-associated lifestyles (Thomas et al., 2008). *P. tunicata* is noteworthy for its “antifouling” activities and ability to colonize mixed species biofilms, where it secretes molecules to inhibit the growth of competing species (C. Holmström et al., 2002; D. Rao et al., 2005, 2010). *P. tunicata* exhibits broad antimicrobial capabilities, and produces antifungal (Franks et al., 2006), anti-nematode (Ballestriero et al., 2010), and algicidal molecules (Egan, James,

et al., 2001; Lovejoy et al., 1998). In addition, *P. tunicata* possesses homologs of virulence factors that aid in host surface colonization (Eckhard et al., 2017; Gardiner et al., 2014). Characterization of *P. tunicata*, its extracellular proteome and biofilm development is thus important to gain insights into the molecular mechanisms and physiology of marine biofilm development (Mai-Prochnow et al., 2004; D. Rao et al., 2005).

3.2 Study objectives

In this study, I report the bioinformatics-aided discovery and characterization of a new S-layer protein from the marine organism *Pseudoalteromonas tunicata* and related species. I identify EAR28894 as the most abundant protein produced by *P. tunicata* planktonic and biofilm cultures and predict its function as an S-layer protein using structure prediction. I then characterize the lattice ultrastructure formed by Slr4 and investigate its presence on cells and in biofilms. I demonstrate that Slr4 forms a new family of S-layer proteins predominantly in marine Gammaproteobacteria, which likely plays an important role in marine microbial physiology and ecology by functioning as a key structural constituent of biofilms.

3.3 Experimental Procedures

3.3.1 Purification of S-layer protein

Pseudoalteromonas tunicata strain D2 (Holmstrom et al., 1998) was routinely cultivated in Difco marine 2216 agar at room temperature. A 13 ml volume of the overnight-grown culture (OD₆₀₀ of 1.3) was subcultured into three flasks with 1 L of marine broth and incubated for 8 hr at room temperature with gentle shaking (100 rpm). Cells were harvested by centrifugation at 12,400g for 20 min at 4°C. The pellet was surface washed with cold phosphate-buffered saline PBS (pH 7.4) by low centrifugation at 7,000g for 20 min at 4°C then resuspended in 60 ml of cold 0.1 M Tris–HCl buffer (pH 7.2). Mechanical cell

disruption was applied to fragment the cell envelope (Sidhu & Olsen, 1997) and remove the capsule (Messner & Sleytr, 1988). This was achieved using a 30-ml tissue homogenizer with a Potter-Elvehjem PTFE pestle with six repetitions (Burden, 2008). The S-layer was recovered by differential centrifugation; first, by pelleting the bacterial cells twice by centrifugation in a fixed angle rotor at 6,000g for 10 min at 4°C; and second, the supernatant was collected. The S-layer in the supernatant was pelleted using a Beckman Coulter Ti 45 fixed angle rotor ultracentrifuge at 169,645g for 3 hr at 4°C. The tightly packed transparent pellet was suspended in 1 ml of cold 0.1 M Tris–HCl buffer and left for 48 hr at 4°C. The suspension was put on ice with 1% v/v final concentration of RIPA solubilization buffer (0.88 g NaCl; 0.15 g EDTA; 1 g NP-40 with a density of 1.06 g/ ml; 1 g sodium deoxycholate; 0.10 g SDS; 2.5 ml of 1 M Tris–HCl buffer, pH 7.6; and H₂O to a final volume of 100 ml) for 30 min to break the non-covalent bonds between the S-layer and the cell wall (Beveridge, 1994; Sidhu & Olsen, 1997). The mixture was swirled occasionally for uniform spreading. A cold 0.1 M Tris–HCl buffer (pH 7.2) was added with a ratio of 3:1 of the mixture. The S-layer was pelleted at 13,000g for 30 min at room temperature. The pellet was washed twice with PBS buffer (pH 7) using a 30 KDa HiPPR detergent column centrifugal filter with centrifugation at 13,000g for 5 min at 4°C. The suspension was aliquoted and stored at –80°C.

3.3.2 Construction of mutant strain

3.3.2.1 Isolation of genomic DNA

P. tunicata D2 was grown at 22°C for 2 days with shaking (170 rpm). Cells were collected by centrifugation and lysed with SDS and proteinase K. Genomic DNA was extracted with phenol, phenol-chloroform and then, precipitated with ethanol. RNA was removed with RNase A. DNA was quantified using a NanoDrop spectrophotometer and checked on 0.8% agarose gel.

3.3.2.2 Plasmid construction

One DNA fragment (1,065 bp) containing the translation start site ATG of PTD2_07619 gene was PCR amplified with primer pair JC491 and JC468 (Table 3.1). Another fragment (991 bp) was obtained by PCR amplification with oligos JC467 and JC492. Following gel purification, the two fragments were combined in equal amounts as PCR templates using primers JC491 and JC492. The 2 kb PCR product was restricted with BamHI and HindIII and inserted into the same sites in pK19mobsacB, yielding plasmid pJC272. The intended deletion region was Sanger sequenced with oligo JC470 (Table 3.1).

Table 3.1. Oligos used for plasmid construction.

Oligo ID	Sequence
JC467	TCAGTTTCATGAAACTTGGAGAATGCTGCAGTAAGCAACCGCTAAGTTTAAGTAGT
JC468	ACTACTTAAACTTAGCGGTTGCTTACTGCAGCATTCTCCAAGTTTCATGAAACTGA
JC470	CGGCAGGCTTAAACTTGCTGCGTT
JC491	GCGGGATCCAAACAATTATTTTAGGTGGTTTAATTAG
JC492	GCGCAAGCTTGCCGATTAATGGACCAAGTGTCAAC

3.3.2.3 Mutant construction by homologous

Plasmid pJC272 was conjugated into *P. tunicata* D2 by triparental mating with the helper plasmid pRK600 (Finan et al., 1986). Single cross-over recombination of the plasmid into *P. tunicata* genome was selected on marine agar with kanamycin (100 µg/ml), and streak purified on the same selection media. A single colony was grown in marine medium, diluted serially, and plated on marine agar containing 5% sucrose. Resulting clones were tested for kanamycin sensitivity (double cross-over and loss of plasmid backbone).

3.3.2.4 Verification of mutation

Genomic DNA was isolated from the assumed mutant. DNA fragments from wild type, the mutant, and plasmid pJC272 were PCR amplified using oligo JC470 and JC492 and resolved with 1% TAE agarose gel.

3.3.3 Negative staining and image analysis

Negative staining was performed following the described procedure (Harris & De Carlo, 2014). Carbon-coated copper grids (Ted Pella, Inc. Formvar W/CARB on 200 M CU; Prod No. 01801) were used with 2.5% w/v ammonium molybdate, pH 5-7. A Philips CM10 microscope running at 60.0 kV was used. TEM micrograph images were analyzed using imageJ (Schneider et al., 2012). To measure inter- unit spacings, five separate square grids of 15 x 15 particles were identified, and the average center-to-center distance was calculated for each axis.

3.3.4 Analysis of Slr4 phylogenomic and metagenomic distribution

Homologs of EAR28894.1 were detected using three iterations of PSI-BLAST (E-value < 0.0001). A sequence alignment was generated using MUSCLE v3.8.31 (Edgar, 2004), and further filtered to remove partial and poorly aligning sequences. A PhyML tree (LG model) as implemented in Seaview (Gouy et al., 2010) was constructed from conserved alignment regions and visualized using ITOL (Letunic & Bork, 2019). The taxonomy of the aligned sequences was used to highlight the bacterial tree of life in AnnoTree (Mendler et al., 2019). A metagenomic survey for Slr4 homologs was performed using the EBI MGnify sequence search at [https:// www.ebi.ac.uk/metagenomics](https://www.ebi.ac.uk/metagenomics) with default settings on May 2, 2019.

3.4 Results

3.4.1 Identification of an abundant protein in cultures of *Pseudoalteromonas tunicata*

Pseudoalteromonas tunicata D2 liquid cultures were initially grown in Difco Marine broth for 8 hr under shaking conditions (Figure 3.1a). Further incubation under static (non-shaking) conditions for 26, 42, and 68 hr produced visible pellicle biofilms that formed at the air-liquid interface with increasing thickness and biomass observed over time (Figure 3.1a). SDS-PAGE analysis of total extracted protein at all stages revealed a dominant band of ~57 kDa (see Figure 3.1b for a representative gel). This protein band was identified by liquid chromatography–tandem mass spectrometry (LC–MS/MS) with spectra matching a ~59 kDa “hypothetical protein” (EAR28894, PTD2_07610) from *P. tunicata* D2 (Figure 3.1c). The LC–MS/MS identification was of high quality with 93% sequence coverage (Figure 3.1c, Tables 3.2 and 3.3). A BLAST search of EAR28894 failed to identify any homologs of known function; all significant matches ($E < 0.001$) were hypothetical proteins. No domains were detected using either the NCBI Conserved Domain Database (Marchler-Bauer et al., 2015) or Pfam (Finn et al., 2014). Shotgun LC–MS/MS analysis of total protein derived from 8 hr (shaking), 26–68 hr (static) cultures confirmed hypothetical protein EAR28894 as the most abundant protein at all time points (Table 3.2).

The data that supports the findings of this study are available Appendix C. 2. This data independently supports the results from Chapter 2, which also identified EAR28894 among the most abundant proteins in *P. tunicata* biofilms.

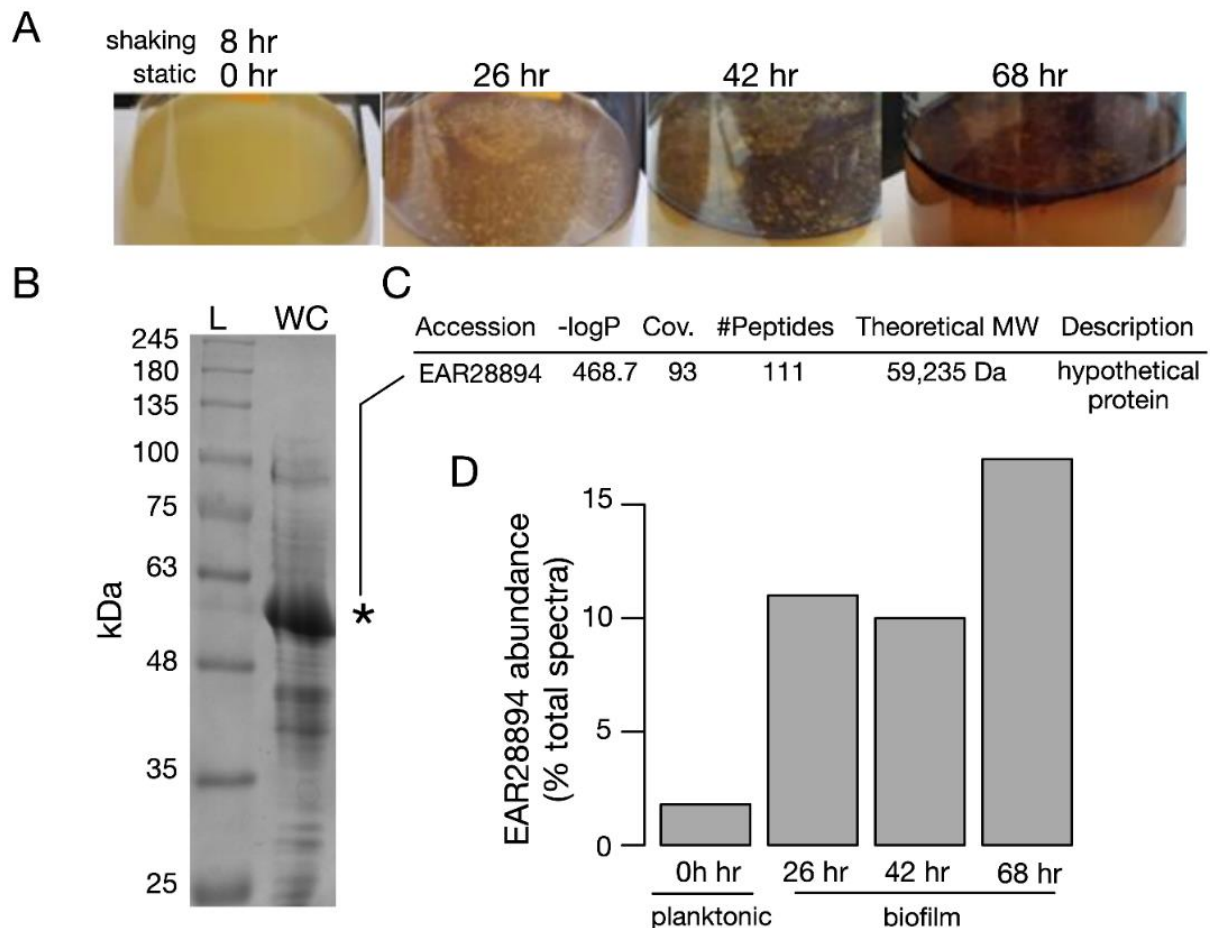


Figure 3.1. Identification of an abundant hypothetical protein in the *Pseudoalteromonas tunicata* proteome. (A) Liquid cultures of *P. tunicata* grown in Difco marine broth for 8 hr with shaking, followed by 26, 42, and 68 hr of static growth (no shaking) to induce pellicle biofilms. (B) SDS-PAGE analysis of whole cell extract from planktonic cultures revealed a dominant band at ~57 kDa. L – ladder; WC – whole cell extract. (C) The ~57 kDa protein was identified by LC–MS/MS as a “hypothetical protein” EAR28894. (D) Shotgun proteomic analysis by LC–MS/MS of *P. tunicata* planktonic and biofilm samples confirmed

EAR28894 as the most abundant expressed protein, constituting ~2% of total spectra in planktonic cultures and 10%–17% of total spectra in biofilms.

Table 3.2. Top proteins identified by LC-MS/MS.

Accession	-10lgP	Cov. (%)	Number Peptides	Number Unique	PTM	Avg. Mass (kDa)	Description
EAR28894.1	468.71	93	111	110	Y	59235	hypothetical protein PTD2_07619
EAR29208.1	170.89	20	12	12	Y	68830	hypothetical protein PTD2_09189
EAR29563.1	133.95	8	3	3	Y	60109	flagellin
EAR27917.1	104.01	5	4	4	N	103265	TonB-dependent outer membrane receptor
EAR28105.1	75.5	6	3	3	N	61087 139223	30S ribosomal subunit protein S1
EAR30644.1	56.2	0	2	2	Y	8	fibronectin type III domain protein
EAR27255.1	53.86	2	2	1	N	67577	putative lipoprotein
EAR28194.1	50.54	3	2	2	N	82187	TonB-dependent receptor
EAR26551.1	48.39	3	2	2	Y	105969	sensor histidine kinase/response regulator
EAR27983.1	44.82	3	1	1	N	63152	putative orphan protein

In planktonic cultures, the hypothetical protein EAR28894 was the most abundant protein and comprised 1.8% of total spectra followed by EF-Tu (EAR26375) at 1.3%. In pellicle biofilms, the relative abundance of EAR28894 peptides increased markedly to 10%–17% of total spectra (Figure 3.1d). The second most abundant identified protein spectra in biofilms were EAR28646, a TonB-dependent receptor, present at 2.1%–2.6% of total spectra.

Although EAR28894 was the most abundant protein according to the percentage of total peptide spectra, these values do not necessarily reflect an accurate measurement of its true protein abundance. Analysis of MS spectra mapping to the EAR28894 protein sequence revealed coverage across the full-length protein, with the exception of an N-terminal segment of 13–27 residues in length which was absent in all four data sets (Figure 3.2). This suggests that EAR28894 is proteolytically processed to remove its N-terminal signal peptide, resulting in a mature protein on the gel (~57 kDa).

8 hrs

EAR28894.1 (100%), 59,234.6 Da
hypothetical protein PTD2_07619 [Pseudoalteromonas tunicata D2]
134 exclusive unique peptides, 222 exclusive unique spectra, 701 total spectra, 541/579 amino acids (93% coverage)

MEIMFKKTL	ALAITGVSV	ANAAVVKTSV	TATTAVLQQT	AIGTAKAHAK	GTAALGASGVF
GTAADATNSA	NCKALAAFY	VSLTKADGTA	AHAVAADGSG	GDVATFADGS	GRELTTVHTT
AANACLATVK	PVLSTTAAKD	GLEYTQATAL	EIKPVI VAGI	GGYKAEDTLT	FQFSGAKL DL
TKTTAPSI TV	AAAGQAGAGV	TFDILDITDS	QIRFTVKATT	PANDFVRGNG	I LELELSNIFLD
STGLAATTSV	MVNSFGTNTS	GTKFDESTAA	TIVSLLPQYT	TEVTTLLDAD	IDVVGKDRQQF
ANNLTADVLA	VKHTKNPTSA	NVLVPANTTY	VVTGDFSWAY	APSVDTNKD	KLSSAELMAA
NVAVLAGGDD	TVKSLALNAT	NTELTIVTNI	VGAALDATNT	ITFNVPGYDS	GKGTNPMISV
QDFTVKVDTM	SDKSVGSKAV	NMPSLAKTAA	GTWKLNGSVV	VVPYVFPGPA	TQPI LRHTNA
GTQTGDI TVR	YMVEGVHTAW	QSLAAAGIKD	AKPGVRDMLG	LVTDALKGE	YDSTTTGFKV
ALEVVTNVP	KDVFVYGGAK	ITAEGQDR IH	LGTFKT NVN		

26 hrs

EAR28894.1 (100%), 59,234.6 Da
hypothetical protein PTD2_07619 [Pseudoalteromonas tunicata D2]
223 exclusive unique peptides, 360 exclusive unique spectra, 852 total spectra, 543/579 amino acids (94% coverage)

MEIMFKKTL	ALAITGVSV	ANAAVVKTSV	TATTAVLQQT	AIGTAKAHAK	GTAALGASGVF
GTAADATNSA	NCKALAAFY	VSLTKADGTA	AHAVAADGSG	GDVATFADGS	GRELTTVHTT
AANACLATVK	PVLSTTAAKD	GLEYTQATAL	EIKPVI VAGI	GGYKAEDTLT	FQFSGAKL DL
TKTTAPSI TV	AAAGQAGAGV	TFDILDITDS	QIRFTVKATT	PANDFVRGNG	I LELELSNIFLD
STGLAATTSV	MVNSFGTNTS	GTKFDESTAA	TIVSLLPQYT	TEVTTLLDAD	IDVVGKDRQQF
ANNLTADVLA	VKHTKNPTSA	NVLVPANTTY	VVTGDFSWAY	APSVDTNKD	KLSSAELMAA
NVAVLAGGDD	TVKSLALNAT	NTELTIVTNI	VGAALDATNT	ITFNVPGYDS	GKGTNPMISV
QDFTVKVDTM	SDKSVGSKAV	NMPSLAKTAA	GTWKLNGSVV	VVPYVFPGPA	TQPI LRHTNA
GTQTGDI TVR	YMVEGVHTAW	QSLAAAGIKD	AKPGVRDMLG	LVTDALKGE	YDSTTTGFKV
ALEVVTNVP	KDVFVYGGAK	ITAEGQDR IH	LGTFKT NVN		

42 hrs

EAR28894.1 (100%), 59,234.6 Da
hypothetical protein PTD2_07619 [Pseudoalteromonas tunicata D2]
212 exclusive unique peptides, 343 exclusive unique spectra, 888 total spectra, 536/579 amino acids (93% coverage)

MEIMFKKTL	ALAITGVSV	ANAAVVKTSV	TATTAVLQQT	AIGTAKAHAK	GTAALGASGVF
GTAADATNSA	NCKALAAFY	VSLTKADGTA	AHAVAADGSG	GDVATFADGS	GRELTTVHTT
AANACLATVK	PVLSTTAAKD	GLEYTQATAL	EIKPVI VAGI	GGYKAEDTLT	FQFSGAKL DL
TKTTAPSI TV	AAAGQAGAGV	TFDILDITDS	QIRFTVKATT	PANDFVRGNG	I LELELSNIFLD
STGLAATTSV	MVNSFGTNTS	GTKFDESTAA	TIVSLLPQYT	TEVTTLLDAD	IDVVGKDRQQF
ANNLTADVLA	VKHTKNPTSA	NVLVPANTTY	VVTGDFSWAY	APSVDTNKD	KLSSAELMAA
NVAVLAGGDD	TVKSLALNAT	NTELTIVTNI	VGAALDATNT	ITFNVPGYDS	GKGTNPMISV
QDFTVKVDTM	SDKSVGSKAV	NMPSLAKTAA	GTWKLNGSVV	VVPYVFPGPA	TQPI LRHTNA
GTQTGDI TVR	YMVEGVHTAW	QSLAAAGIKD	AKPGVRDMLG	LVTDALKGE	YDSTTTGFKV
ALEVVTNVP	KDVFVYGGAK	ITAEGQDR IH	LGTFKT NVN		

68 hrs

EAR28894.1 (100%), 59,234.6 Da
hypothetical protein PTD2_07619 [Pseudoalteromonas tunicata D2]
269 exclusive unique peptides, 488 exclusive unique spectra, 1417 total spectra, 540/579 amino acids (93% coverage)

MEIMFKKTL	ALAITGVSV	ANAAVVKTSV	TATTAVLQQT	AIGTAKAHAK	GTAALGASGVF
GTAADATNSA	NCKALAAFY	VSLTKADGTA	AHAVAADGSG	GDVATFADGS	GRELTTVHTT
AANACLATVK	PVLSTTAAKD	GLEYTQATAL	EIKPVI VAGI	GGYKAEDTLT	FQFSGAKL DL
TKTTAPSI TV	AAAGQAGAGV	TFDILDITDS	QIRFTVKATT	PANDFVRGNG	I LELELSNIFLD
STGLAATTSV	MVNSFGTNTS	GTKFDESTAA	TIVSLLPQYT	TEVTTLLDAD	IDVVGKDRQQF
ANNLTADVLA	VKHTKNPTSA	NVLVPANTTY	VVTGDFSWAY	APSVDTNKD	KLSSAELMAA
NVAVLAGGDD	TVKSLALNAT	NTELTIVTNI	VGAALDATNT	ITFNVPGYDS	GKGTNPMISV
QDFTVKVDTM	SDKSVGSKAV	NMPSLAKTAA	GTWKLNGSVV	VVPYVFPGPA	TQPI LRHTNA
GTQTGDI TVR	YMVEGVHTAW	QSLAAAGIKD	AKPGVRDMLG	LVTDALKGE	YDSTTTGFKV
ALEVVTNVP	KDVFVYGGAK	ITAEGQDR IH	LGTFKT NVN		

Figure 3.2. LC-MS/MS coverage of the EAR28894 protein. Identified peptides mapped across the entirety of the sequence, with the exception of an N-terminal segment consisting of the first 13-27 amino acid residues. Residues highlighted in green represent chemical modifications (e.g., deamidation, oxidation).

Analysis of the MS/MS data also revealed an extreme abundance of non-tryptic peptides associated with EAR28894 (Figure 3.3) indicative of extensive proteolytic processing.

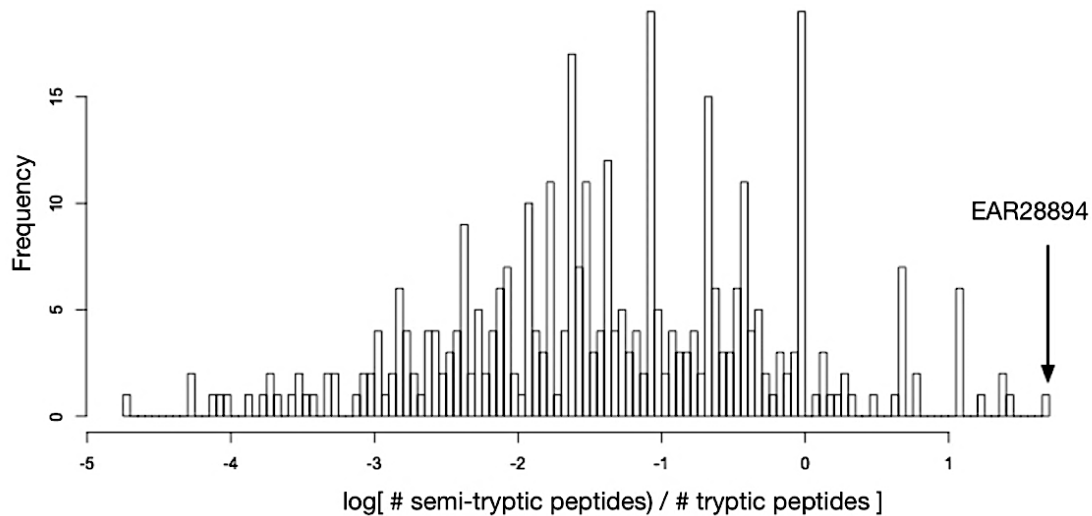


Figure 3.3. Ratio of semi-tryptic to tryptic peptides across all proteins in LC-MS/MS data. EAR28894 deviates from all other proteins in this regard, and therefore is likely to be most heavily processed by non-trypsin proteases.

3.4.2 Protein structure prediction suggests EAR28894 is an S-layer protein

To predict the structure and function of the EAR28894 protein, I applied the I-TASSER pipeline (D. C. Yang et al., 2016). I-TASSER predicted an L-shaped, almost entirely beta-helical fold, and identified the crystal structure of *Caulobacter* S-layer protein RsaA (PDB ID 5n8p) as the top structure template with high estimated model quality (low root-mean squared deviation of 0.98 Å and high model coverage of 98%) (Figure 3.4). Due to the repetitive and beta-rich composition of RsaA, EAR28894 threaded onto different regions of the RsaA structure, resulting in two different high-scoring alignments of only 11%–17%

identity (ranked 1 and 2 in Figure 3.4). Therefore, although a general L-shaped beta-helical fold and S-layer structure/function can be predicted for EAR28894, its relationship to RsaA is unclear. In addition, I examined the genomic context of EAR28894 in *P. tunicata* (Figure 3.5) to determine whether additional evidence could be found supporting its prediction as an S-layer protein. I observed that the EAR28894 gene is located immediately downstream of a putative type II secretion (T2S) pathway operon encoding several T2S genes (T2SG, E, F, K, D, and others), also known as general secretory pathway *gsp* genes (Figure 3.5). Similar genomic arrangements were identified surrounding homologous genes identified in the genomes of other species (Figure 3.5). This suggests the possibility of an evolutionarily conserved operon for EAR28894 secretion by a dedicated T2SS. Also consistent with T2S, signal peptide prediction by Signal P 5.0 predicted a Sec/SPI signal peptide with 98.7% likelihood and a cleavage site at position 23-24 with 89.4% probability, which coincides closely with the absent N-terminal region identified by MS (Figure 3.2). Type II (sec-dependent) secretion pathways have been identified as a dominant secretion mechanism for other bacterial S-layer proteins (Boot & Pouwels, 1996).

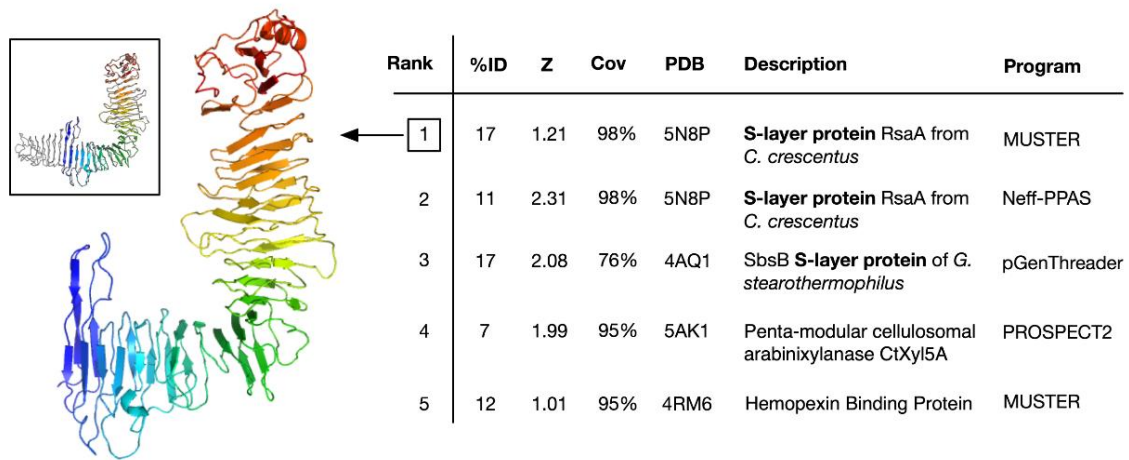


Figure 3.4. Bioinformatic analysis predicts *Pseudoalteromonas tunicata* EAR28894 hypothetical protein as an S-layer protein. Structure prediction by I-TASSER. The top five threading templates are listed on the right, and the structural model for top-ranked template is shown

on the left. EAR28894 threaded onto the structure of Caulobacter RsaA (PDB ID 5n8p) as shown in the top left inset box with the template colored in gray.

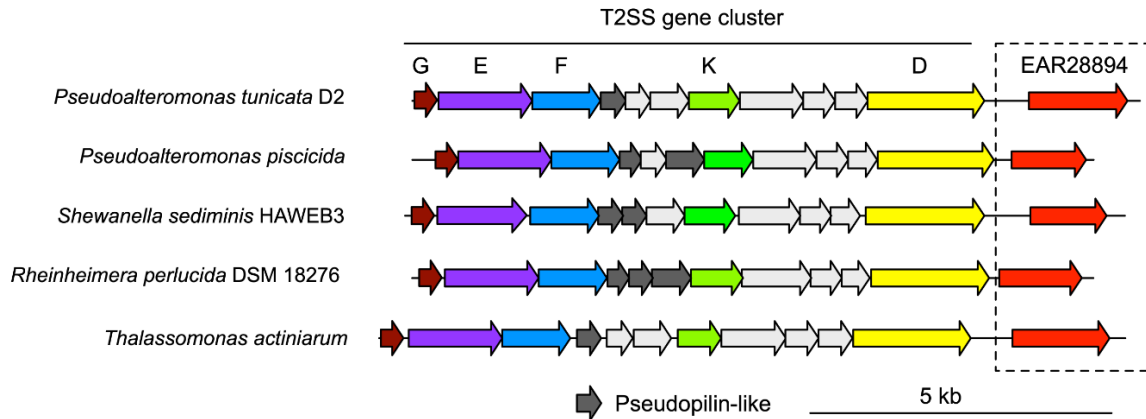


Figure 3.5. Genomic context surrounding the EAR28894 gene in *Pseudoalteromonas tunicata* D2 and related genes in other genomes predicts *P. tunicata* EAR28894 hypothetical protein as an S-layer protein. Immediately upstream of the EAR28894 gene is a type II secretion gene cluster, suggesting a possible dedicated operon for type II S-layer secretion.

3.4.3 Confirmation of EAR28894 as an S-layer protein using TEM and knockout studies

Transmission electron microscopy (TEM) was used to investigate the predicted S-layer structure and function of EAR28894. EAR28894 was isolated and purified using differential centrifugation followed by a detergent wash with radioimmunoprecipitation assay (RIPA) buffer (see, Methods for details) (Figure 3.6). TEM analysis of purified EAR28894 samples revealed S-layer material characterized by a square lattice (p4) symmetry (Figure 3.7a) and (Figure 3.8). Based on repeated measurements using ImageJ (5 independent replicates), the unit cell spacing was determined to be $\sim 9.14 \text{ nm} \pm 0.27$ (Figure 3.7b). This is consistent with

the expected range of an S-layer unit cell (4 to 35 nm). This protein was designated EAR28894 as “Slr4” given its identification as an S-layer protein producing a fourfold symmetric lattice. Using homologous recombination, I generated a $\Delta slr4$ deletion mutant.

The coding region (1,737 bp) of the *slr4* gene (EAR28894) was replaced with a PstI restriction enzyme site (CTGCAG), which was verified by PCR amplification (Figure 3.9) and Sanger sequencing.

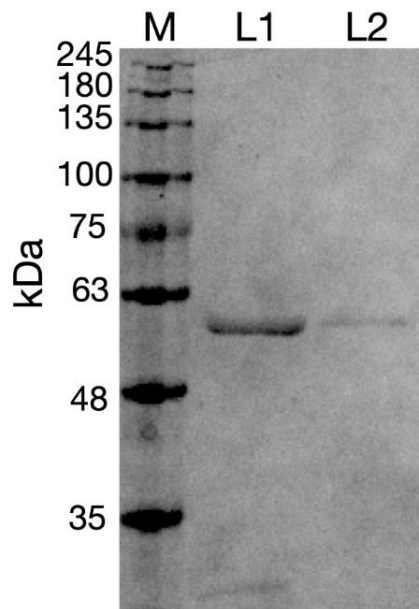


Figure 3.6. Purification of EAR28894 by ultracentrifugation (L1) followed by detergent washes (L2). L1 samples predominantly contain the ~57 kDa band (EAR28894) but also contained other impurities. L1 was, therefore, further purified using RIPA detergent washes to L2, which produced a single band on the gel.

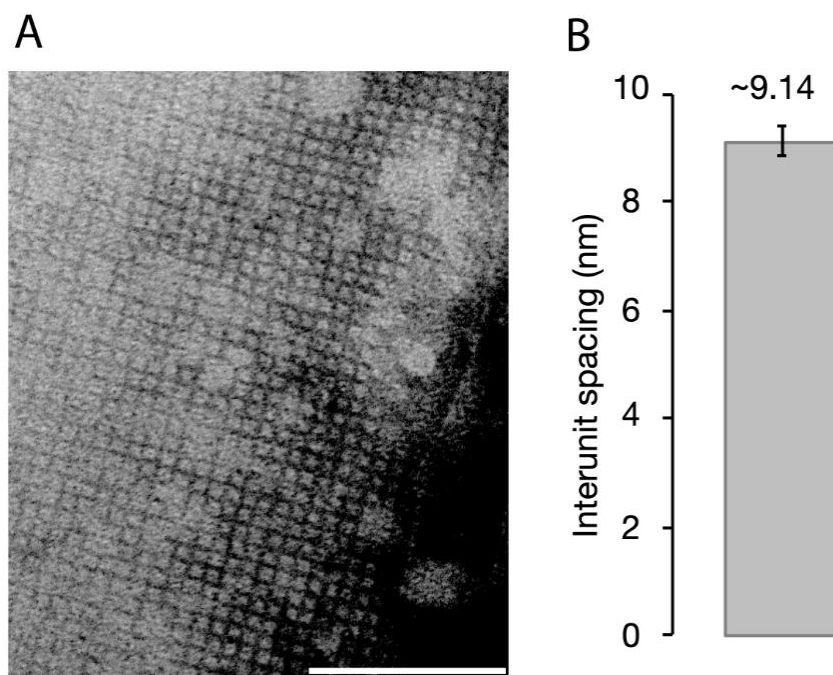


Figure 3.7. TEM imaging of purified EAR28894 reveals a paracrystalline lattice with square (p4) symmetry. (A) TEM imaging reveals a paracrystalline lattice with a square (p4) symmetry. There are approximately 11 subunits per 100 nm, suggesting an interunit spacing of approx. 9.1 nm. (B) Quantitative estimate of inter-unit spacing based on averages of $N = 5$ independent measurements from TEM images. Scale bars = 100 nm.

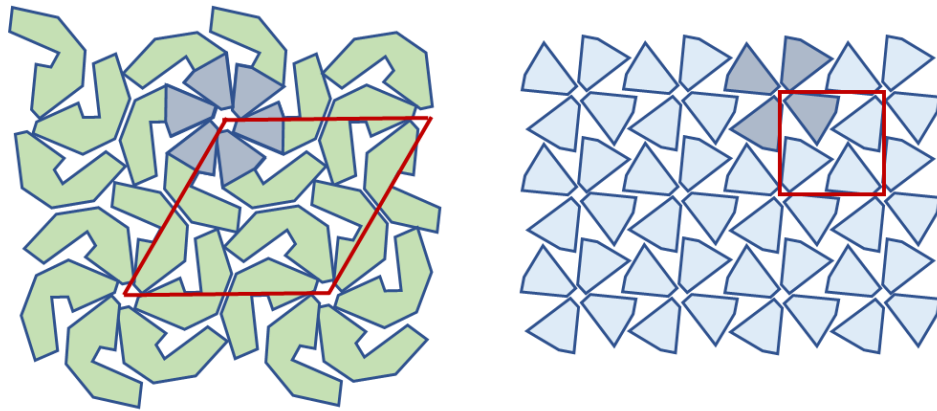


Figure 3.8. Hypothetical model of Slr4 S-layer lattice assembly (right) compared to RsaA S-layer assembly (left). A smaller (truncated) S-layer subunit relative to *rsaA* could alter inter-subunit interactions to result in a four-fold symmetric pattern (right) instead of a six-fold hexagonal symmetry (left). The model is consistent with the top-down view of a square lattice as observed in Figs. 3.7a and 3.13a, as well as the side-view showing V-shaped cups as shown in Fig. 3.13a.

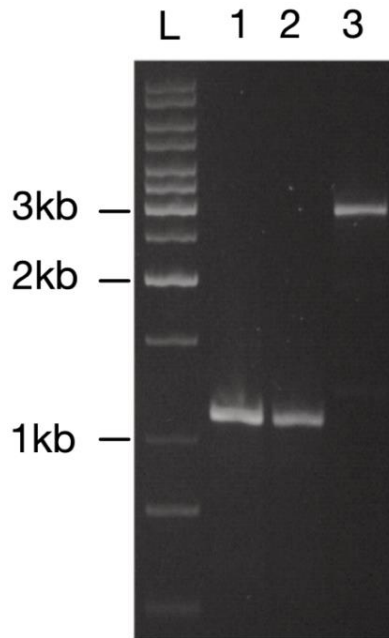


Figure 3.9. Verification of Δ slr4 (EAR28894 gene deletion) mutant in

Pseudoalteromonas tunicata PnAD3. PCR amplification of the PnAD3 genomic DNA with oligo JC470 and JC492 yielded a DNA fragment of same size (1,086 bp) as that from plasmid pJC272, but a 2814-bp product was obtained from wild type (WT) DNA. Lane L, DNA marker; lane 1, *P. tunicata* PnAD3; lane 2, plasmid pJC272; lane 3, *P. tunicata* WT D2.

The Δ slr4 mutant was also confirmed by SDS-PAGE, which demonstrated a lack of the ~57 kDa band identified previously as EAR28894 (Slr4) (Figure 3.10).

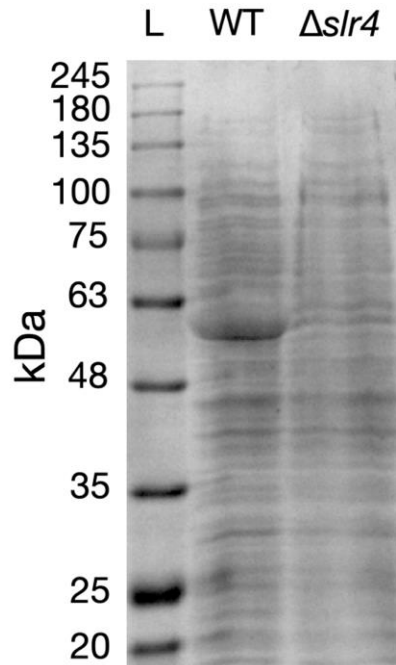


Figure 3.10. SDS-PAGE analysis of whole cell extract of WT versus $\Delta slr4$ *Pseudoalteromonas tunicata* strains. A missing band ~57 kDa in $\Delta slr4$ strains that is present in WT.

The $\Delta slr4$ mutant strain was capable of growth in marine media (liquid and plates), formed colonies with similar morphology to the WT, and formed pellicle biofilms with similar appearance to the WT (Figure 3.11).

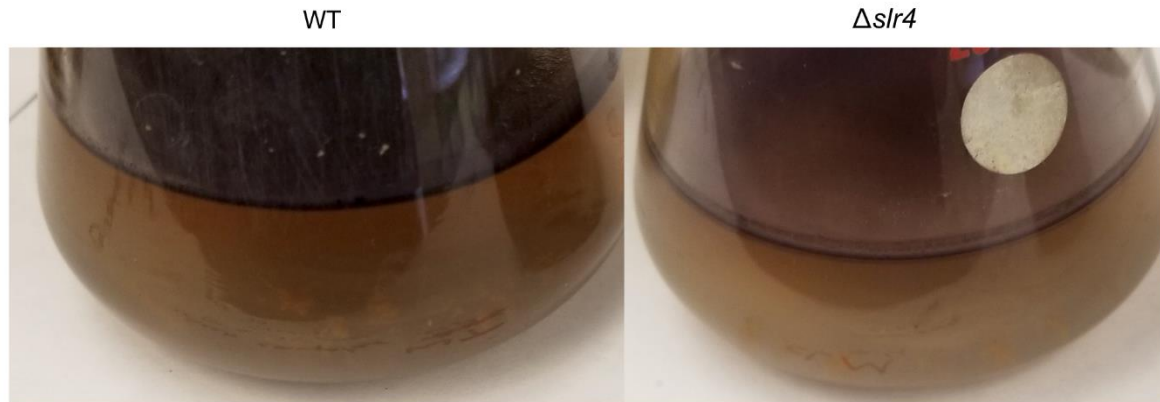


Figure 3.11. Pellicle biofilms formed by the WT vs $\Delta slr4$ mutant strain. Liquid cultures were grown for 8 hours (shaking) in liquid Difco marine broth media, followed by 72 hours of static (nonshaking) incubation.

P. tunicata WT and $\Delta slr4$ cells were then visualized and compared by TEM. In untreated samples, S-layers were difficult to observe on WT cells due to the presence of an apparent outer capsular polysaccharide layer (Figure 3.12). Indeed, a capsular polysaccharide gene operon is present in the *P. tunicata* genome (Thomas et al., 2008) and has been identified in closely related species (Zeng et al., 2019). We, therefore, treated the cells with 0.1M Tris–HCl and a tissue homogenizer to remove the capsular layer and reveal the underlying S-layer, similar to that done previously for the *Bacillus anthracis* S-layer (Mesnage et al., 1998).

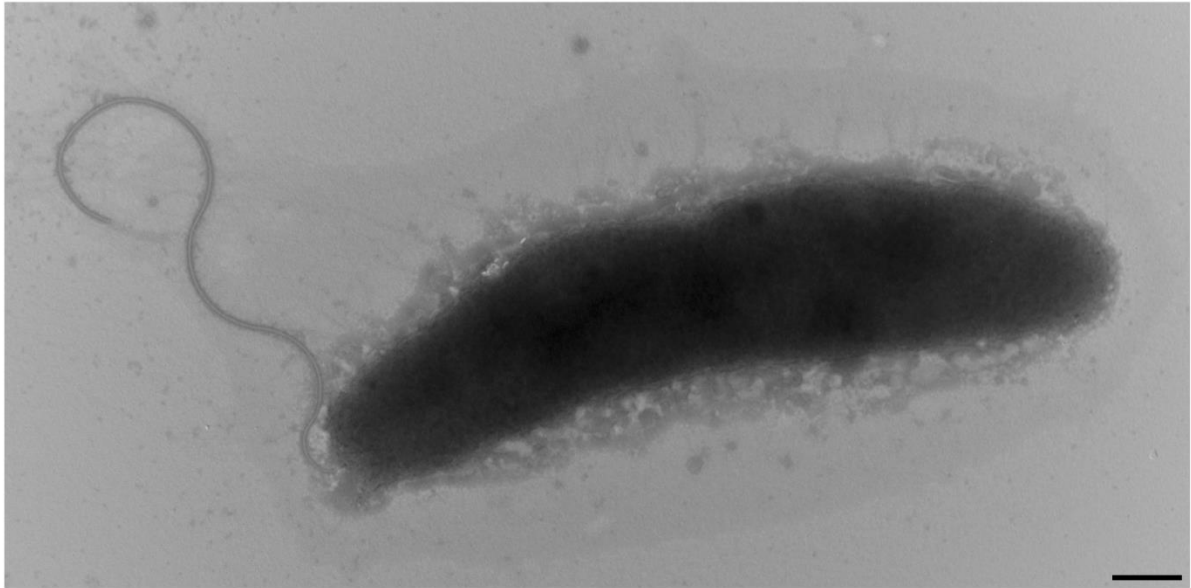


Figure 3.12. TEM micrograph of a *Pseudoalteromonas tunicata* cell revealing the presence of a putative outermost capsular layer. Scale bar = 500 nm.

In TEM micrographs of treated WT cells, an S-layer lattice was observed completely surrounding the outer membrane of intact *P. tunicata* cells (Figure 3.13a) with an identical square lattice structure and geometry to that observed in purified Slr4 samples (Figure 3.7a). Visualization of cells also revealed a “side view” of the S-layer edge consisting of “V” shaped subunits (see arrow in Figure 3.13a). As predicted, the paracrystalline S-layer was completely absent in TEM micrographs of $\Delta slr4$ mutants (Figure 3.13b) confirming that $\Delta slr4$ is required for assembly of an S-layer in native cells.

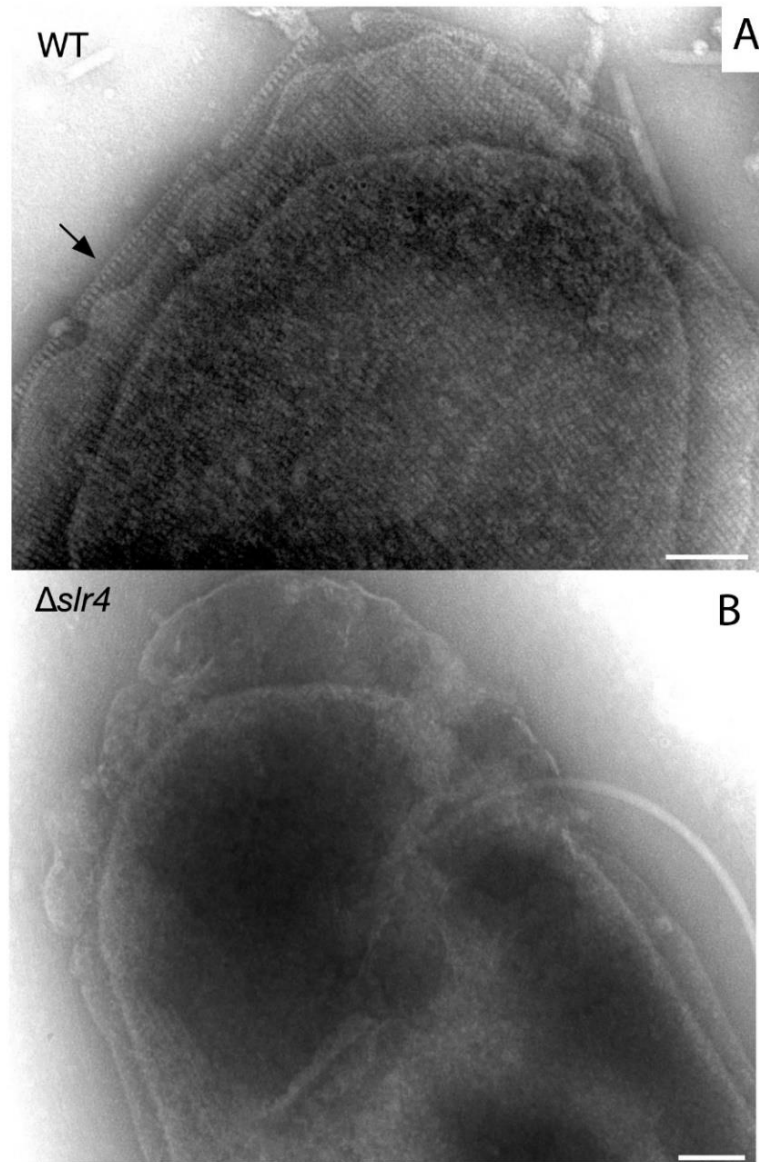


Figure 3.13. Electron micrographs of *Pseudoalteromonas tunicata* revealing presence/absence of a square grid S-layer in WT and $\Delta slr4$ cells, respectively. (A) TEM micrographs of WT vs (B) $\Delta slr4$ cells, revealing the presence and absence of an S-layer, respectively. A side-view of S-layer revealing V-shaped subunits is indicated by an arrow in (A). Samples were derived from liquid cultures grown in marine Difco broth for 8 hr in shaking conditions. Scale bars = 100 nm.

3.4.4 S-layer is shed from cells and is a major component of the biofilm matrix

Exclusively in the WT S-layer producing strain, I observed an abundance of extracellular material containing S-layer that appeared to be “shed” from the cell (Figure 3.14) as described for other bacteria (Chandramohan et al., 2019; Schultze-Lam et al., 1992). Extracellular matrix containing material resembling S-layer was observed outside of planktonic cells (Figure 3.14a) as well as surrounding microcolonies of cells in biofilms (Figure 3.14b). The biofilm extracellular matrix also contained outer membrane vesicles (OMVs), tubular structures, and filaments (Figure 3.14b). Closer examination of purified extracellular matrix revealed S-layer associated with outer-membrane vesicles, (Figure 3.14c) and surrounding networks of filamentous structures including putative flagella, flagellar sheaths, pili, and prosthecae (Beurmann et al., 2017) (Figure 3.14d). S-layer coated vesicles have been reported in archaea, where the S-layer may provide physical stabilization at extreme conditions (Marguet et al., 2013; Rodrigues-Oliveira et al., 2017).

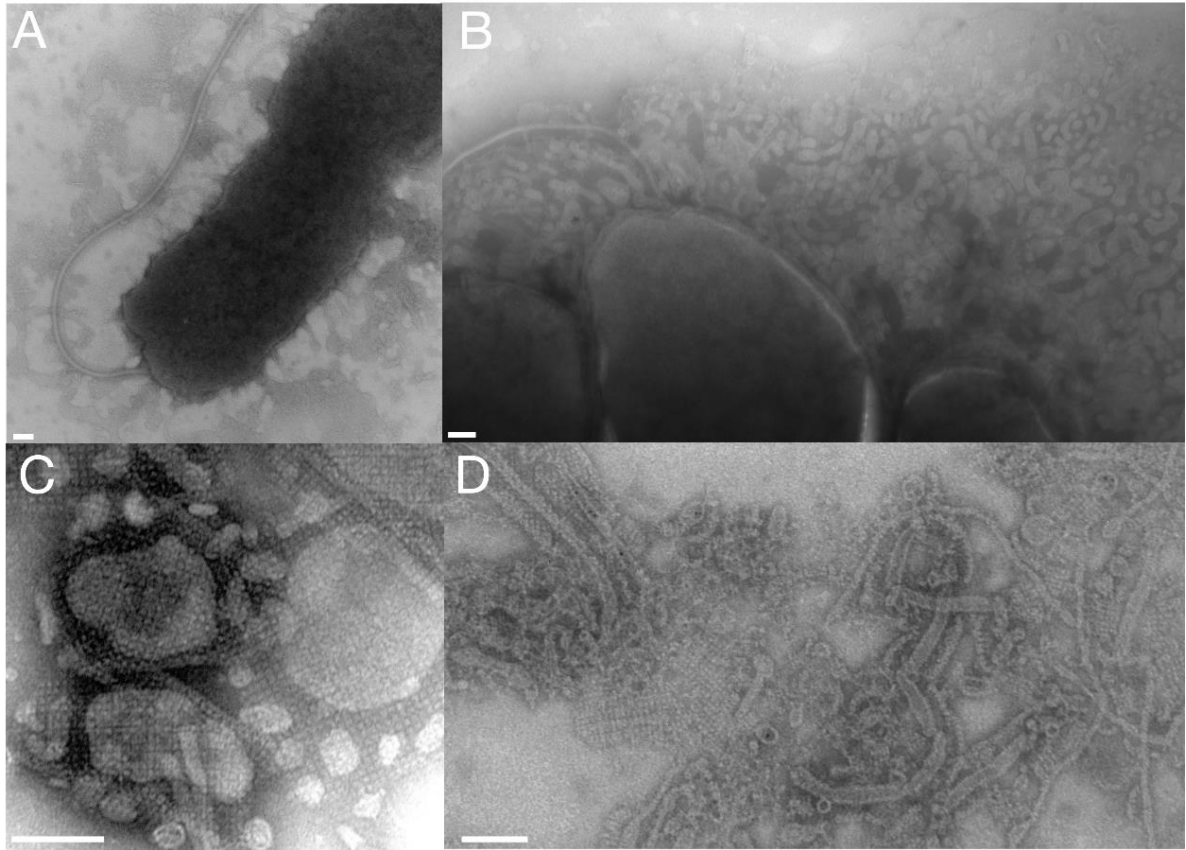


Figure 3.14. S-layer is present in the *Pseudoalteromonas tunicata* extracellular environment and biofilm matrix. (a) A TEM micrograph showing a *P. tunicata* cell as well as “shed” extracellular material layer that is nearby but distinct from the cell body. (b) Three adjacent cells within a microcolony with a substantial amount of secreted outer membrane vesicles (OMVs) and a sheathed flagellum. (c) TEM micrograph of an extracellular protein fraction showing S-layer associated with outer membrane vesicles of various forms. (d) TEM image taken from a WT pellicle biofilm, which shows S-layer material in association with outer membrane vesicles, and fibrous and tubular structures. (e.g., see high-magnification image shown in c) representing possible pili, flagella, prosthecae, or flagellar sheaths. Scale bars = 100 nm.

TEM imaging of WT 48 hr pellicle biofilms also revealed dense clusters of cells that were interconnected by S-layer-associated biofilm matrix components (Figure 3.15). TEM micrographs of $\Delta slr4$ mutant biofilms revealed cell clusters connected by biofilm matrix components but without any S-layer material as expected (Figure 3.15). The $\Delta slr4$ mutant biofilms also contained cells with deformed cell shapes (Figure 3.15) consistent with previous studies demonstrating the involvement of S-layers in cell-shape determination (Poppinga et al., 2012). These observations together with the high abundance of Slr4 protein detected in biofilm versus planktonic samples (Figure 3.1) suggests that Slr4 S-layer material is a dominant component of the biofilm matrix, where it form a self-assembling proteinaceous layer surrounding not only cells but also a wide variety of extracellular matrix components.

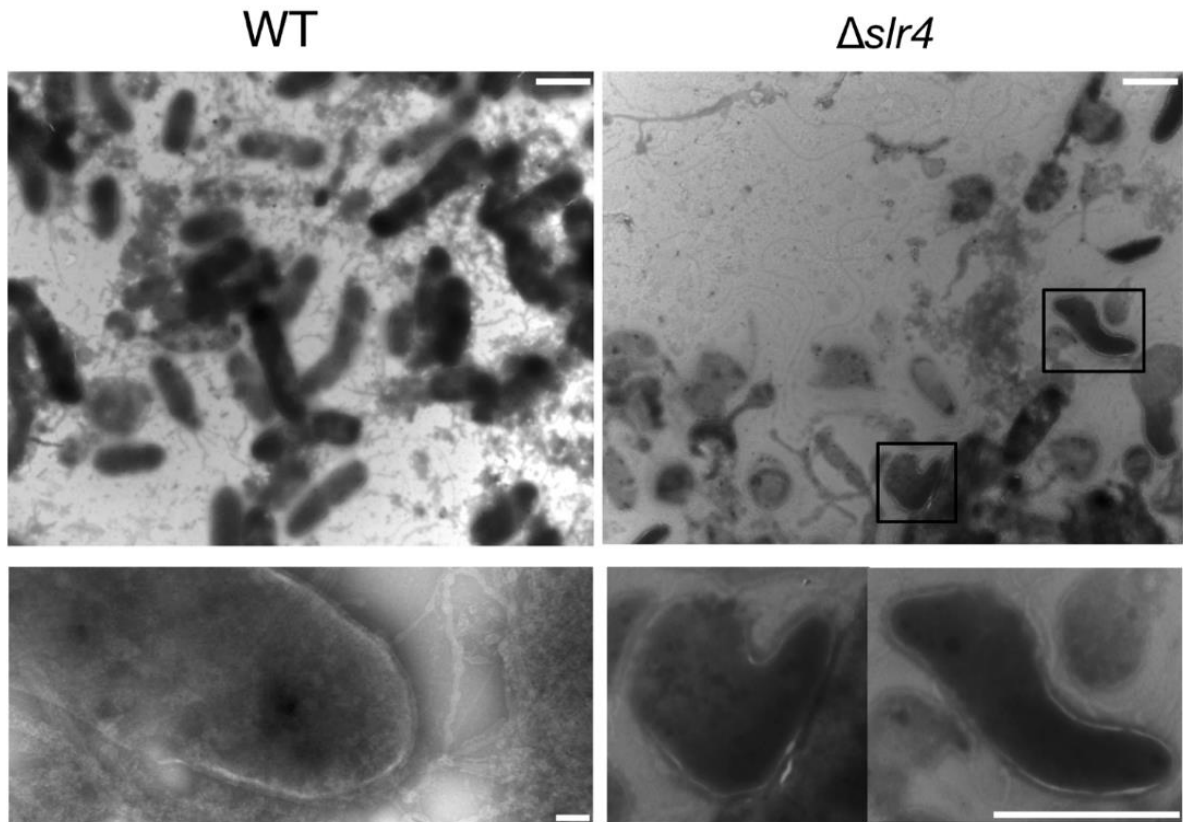


Figure 3.15. TEM micrographs of 48-hr pellicle biofilms (WT versus $\Delta slr4$ mutant strain). Top left – dense cell clusters in the WT strain interconnected by biofilm matrix material. Bottom left – a WT cell within a biofilm with extracellular biofilm matrix including fibrous structures coated by S-layer material. Top right – image taken from a $\Delta slr4$ biofilm showing a sparser cell distribution that is not connected by S-layer associated matrix material. Bottom right – two examples from the image above of deformed cell shapes. Scale bars are 2 microns, with the exception of the bottom left image where it is 100 nm.

3.4.5 The Slr4 protein family is widespread in marine bacterial genomes and metagenomes

Using PSI-BLAST, I identified 108 Slr4 homologs in available genomes, ranging in sequence identity from 13% to 60%. I then examined their distribution across the bacterial tree of life using AnnoTree (Mendler et al., 2019) (Figure 3.16) and constructed a protein phylogeny (Figure 3.17). Slr4 homologs were identified in 79 species, 19 genera, and 1 phylum. Most (98%) of these homologs (including the most closely related sequences) occur within neighboring lineages of Gammaproteobacteria, specifically within the Order Enterobacterales (GTDB nomenclature) (Figure 3.16). These include additional species of *Pseudoalteromonas*, but also *Idiomarina*, *Colwellia*, *Shewanella*, *Thalassomonas*, and *Vibrio* (Table D.2).

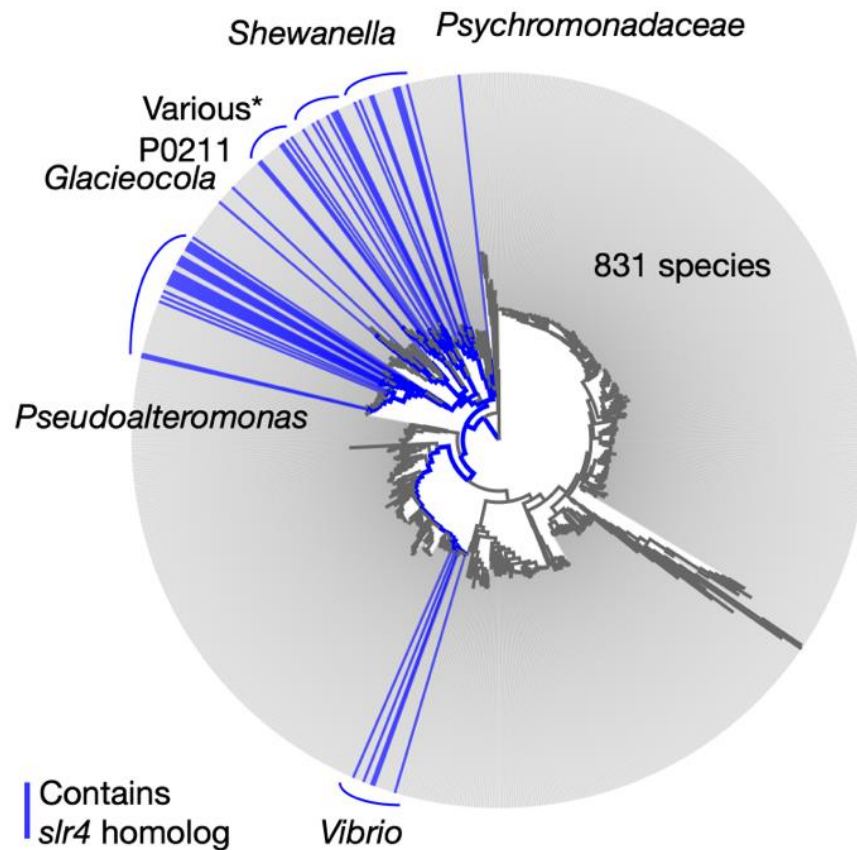


Figure 3.16. Taxonomic distribution of Slr4 homologs. Distribution of Slr4 homologs in the bacterial tree of life generated using AnnoTree. Lineages (genus-level) containing PtSla homologs are shown in blue. Slr4 homologs were detected largely within the order Enterobacterales (GTDB taxonomy), class Gammaproteobacteria. Several instances of Slr4 were detected outside of this lineage (see Table D.2). The group labeled as “Various” includes the genera *Colwellia*, *Thalassomonas*, *Thalassotalea*, and *Lacimicrobium*.

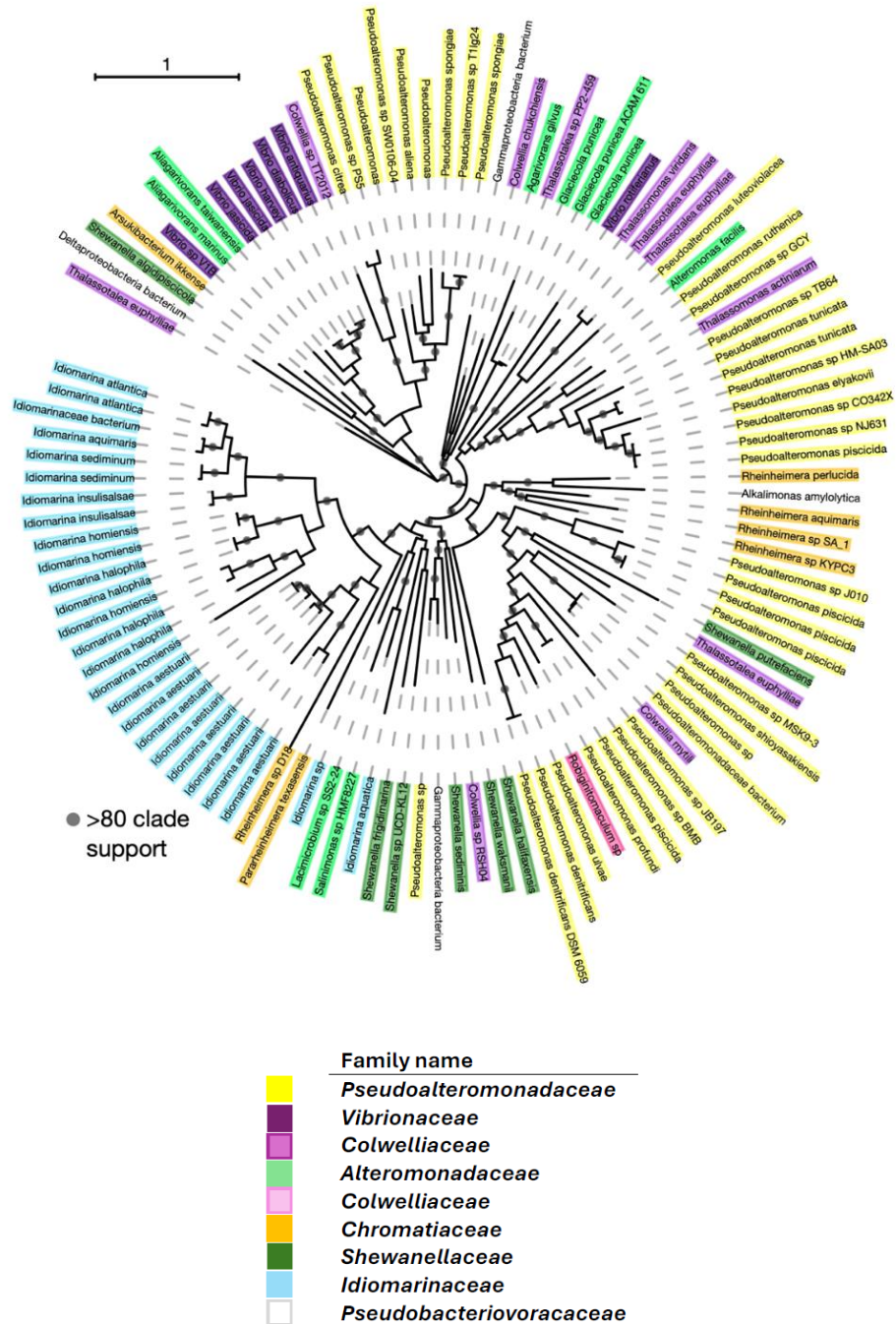


Figure 3.17. Phylogeny of Slr4 homologs. Phylogenetic tree of Slr4 homologs colored according to taxonomic family. Clades with aLRT (SH-like) branch support > 0.8 are indicated. The phylogeny was visualized using iTOL4.

According to the phylogeny, much of the Slr4 protein family has diversified consistently with taxonomy (e.g., a large Slr4 clade is specific to the genus *Idiomarina*). However, there are also examples that are inconsistent with phylogeny (e.g., Slr4 homolog from *Thalassomonas actiniarum* nested within a *Pseudoalteromonas* Slr4 clade), indicative of horizontal gene transfer (Figure 3.16). Niche analysis of Slr4-containing species revealed that 73/79 (~92.4%) could be associated with marine habitats, and 78/79 (98.7%) with aquatic (including freshwater) habitats (Table D.2). The only Slr4-containing species not associated with aquatic environments was *Pseudoalteromonas* sp. JB197, isolated from cheese rind. A total of 27/73 (37.0%) of the marine Slr4-containing species were found to be host-associated (Table D.2). To further explore the association with marine environments, I searched for homologs of Slr4 within available metagenomes from the EBI MGnify metagenomics resource (Mitchell et al., 2020) including marine, freshwater, human microbiome, soil, and engineered environments. Homologs were detected exclusively in marine metagenomes (Figure 3.18).

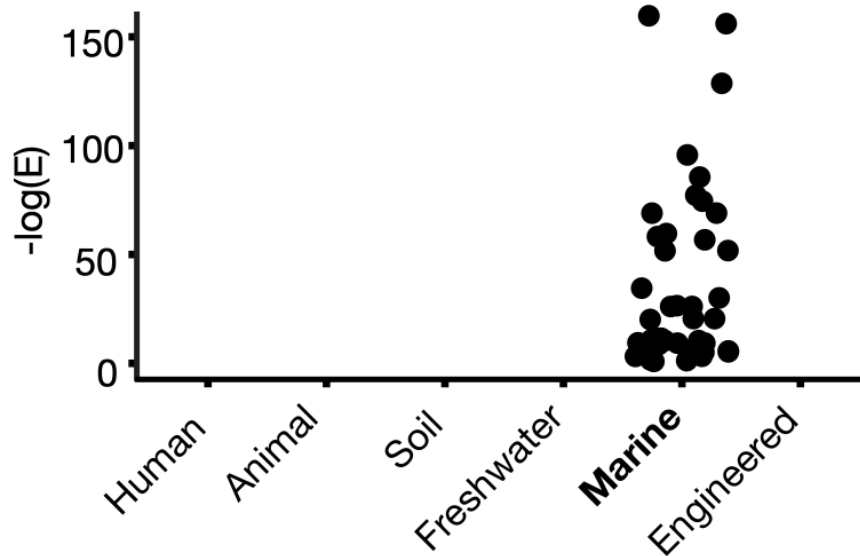


Figure 3.18. Metagenomic occurrence of Slr4 homologs. Metagenomic survey for Slr4 homologs using the EBI MGnify metagenomics database. The plot shows the $-\log(E)$ for all significant (phmmer E-value < 0.01) Slr4 homologs were detected exclusively in marine metagenomes.

3.5 Discussion

I identified an abundant protein (EAR28894, now designated “Slr4”) produced in cultures of the marine bacterium, *P. tunicata* D2, and predicted its function as an S-layer protein using structural bioinformatics. The purified Slr4 protein was capable of forming square (p4 symmetry) paracrystalline lattices, and these S-layer lattices were also present and absent on the outer-membrane of WT versus $\Delta slr4$ mutant cells, respectively. Consistent with the substantial increase in Slr4 relative abundance in biofilm (10%–17% of total spectra) compared to planktonic samples (2%), I observed S-layer material shed outside of *P. tunicata* cells and identified S-layer as a dominant component of the biofilm matrix where it is

associated with OMVs and other filamentous structures. Phylogenomic and metagenomic analysis showed that Slr4-related proteins are conserved in related species and abundant in marine Gammaproteobacteria and marine metagenomes.

3.5.1 Sequence-to-structure relationship

The confirmation of Slr4 as an S-layer protein raises several questions regarding its similarity to other S-layer protein families. Is Slr4 truly homologous to these proteins, and if so, what structural features and regions are conserved/lost between Slr4 and other S-layer proteins? Furthermore, what sequence or structural differences account for the unique square lattice geometry of Slr4 compared to the hexagonal symmetry of RsaA (Bharat et al., 2017)?

Given the low sequence identity (~17% in the threading alignment) of Slr4 to the *Caulobacter* RsaA S-layer protein, it is unexpected that I-TASSER was capable of detecting this relationship and correctly predicting an S-layer function for Slr4. A potentially significant sequence relationship could also be detected by pairwise alignment via the PredictProtein server (Yachdav et al., 2014); however, no relationship was detected when the BLAST compositional bias filter was used. This suggests that I-TASSER's prediction of an S-layer structure/function may have occurred in part because of a highly repetitive beta-rich sequence composition that is shared with other beta-rich S-layer proteins (Baranova et al., 2012; Bharat et al., 2017). This also offers an explanation for why I-TASSER's threading algorithms aligned Slr4 to different regions of the RsaA template. A beta-helical fold may represent an ideal structural solution for S-layers due to the high propensity for self-assembly of beta-rich proteins (e.g., beta amyloid proteins) (M. K. Tiwari & Kepp, 2015). Despite the distant sequence similarity between Slr4 and RsaA, previous cryo-EM structures of RsaA (Bharat et al., 2017) can be used to speculate on the spatial organization of Slr4 lattices (Figure 3.8). Since Slr4 mapped onto a portion of the RsaA structure, it is possible that a truncated beta-helical L-shaped fold would result in different higher-order interactions with

its crystal form, shifting it from a hexagonal pattern (p6 symmetry) to a square grid (p4 symmetry). Based on the observed inter-subunit spacing of ~9.1 nm which is similar to the length of the predicted Slr4 protein structure along its long axis (also ~9.1 nm), I hypothesize that four Slr4 subunits may interact within a unit cell, rather than six within the RsaA lattice. This could result in fourfold symmetric interactions, producing the square grid lattice pattern observed in TEM (Figures 3 and 4). This model could also provide an explanation for the “side view” of Slr4 S-layers observed in TEM (Figure 4c) since a side view of interacting Slr4 monomers could result in apparent “V”-shaped patterns. Future structural studies involving cryoEM and x-ray crystallography are needed to confirm this model and further investigate the structure of the Slr4 S-layer lattice.

3.5.2 A putative role for Slr4 in marine biofilms

My finding that Slr4 is the dominant protein within *P. tunicata* pellicle biofilms, together with the observation of S-layer “shedding” from cells, suggests that Slr4 may play a functional role in the biofilm matrix. Although the biological role of Slr4 in biofilms is unknown at this point, I hypothesize that it may provide protection not only to cells but also to extracellular matrix structures (e.g., filaments, OMVs, etc.) that are important for biofilm structural integrity and/or cell-cell communication. In addition, it may provide a physical barrier shielding a larger biofilm community against external forces including predation and attack by viruses, bacteria, or eukaryotes. The role for S-layer proteins in biofilms is not unprecedented, as numerous studies have implicated S-layer proteins in biofilm-related processes such as cell adhesion to substrates, promotion of cell-cell aggregation, and initial biofilm establishment (Beveridge et al., 1997; Dapa et al., 2013; Gerbino et al., 2015; Janesch et al., 2013). For example, the *Bacillus subtilis* S-layer protein (BslA) has also been shown to play a critical role in formation of pellicle biofilms (Hobley et al., 2013; Kobayashi & Iwano, 2012; Liu et al., 2017). BslA forms a hydrophobic surface layer, which aids in the formation of a biofilm at the air-liquid interface (Kobayashi & Iwano, 2012). In addition to

playing a role in the process of biofilm formation and cell-cell aggregation, S-layers have also been suggested to provide protective roles within biofilms, in which defenses must be heightened due to increased phage and antimicrobial attacks. A bacteriophage of *Caulobacter crescentus*, for example, is known to use the *Caulobacter* S-layer as a receptor for invasion (Edwards & Smit, 1991). In addition, the S-layer of *Aquaspirillum* spp. and *Aeromonas salmonicida* A449 protects the bacteria against predation by *Bdellovibrio bacteriovorus* (Koval & Hynes, 1991). The role of Slr4 in defense against bacteriophages and predatory bacteria will be an interesting avenue for future work. A key finding from my bioinformatic analysis is that homologs of Slr4 were detected predominantly in Gammaproteobacteria and marine metagenomes (Figure 3.16). Indeed, Gammaproteobacteria, including species of *Pseudoalteromonas* and *Vibrio*, are known to be particularly important members of marine biofilm communities (Longford et al., 2007; Mai-Prochnow et al., 2004; D. Rao et al., 2005). A recent study also revealed a high level of species and functional novelty in marine microbial biofilms, with marine Gammaproteobacteria contributing the largest number of gene clusters (Zhang et al., 2019). In addition to the conservation of the Slr4 gene, the adjacent putative T2SS gene cluster was also found to be highly conserved among marine Gammaproteobacteria.

This is an intriguing finding because T2S pathways are known to play a significant ecological role in marine nutrient cycling (Evans et al., 2008) and secretion of biofilm matrix proteins for surface colonization and biofilm development (Dang & Lovell, 2015). Thus, it is tempting to speculate that the Slr4 family of S-layer proteins are uniquely adapted to marine microorganisms, and perhaps more specifically, marine biofilms. For instance, perhaps the structure and geometry of Slr4 S-layers are adapted for high salinity and/or regulated exchange of marine micronutrients. Or perhaps Slr4 provides biofilms with a level of hydrophobicity and/or cohesion that is required to withstand the constant hydrodynamic forces of marine environments. Although previous oceanic surveys of microbial diversity have focused on planktonic microorganisms, marine biofilms also impact biogeochemical cycling and ecosystem dynamics (Zhang et al., 2019). Surface-associated biofilm lifestyles

provide numerous benefits to bacterial communities including resource sharing, physical support, spatial organization for enhanced nutrient acquisition and flow, and protection against phages, other bacteria, predators, antibiotics, and chemical toxins (Dang & Lovell, 2015). Cell surface associated and extracellular matrix components that protect biofilms against these agents are fundamental elements of marine microbial ecology by providing a foundation for biofilm development. It will be important to further explore the contribution of Slr4 to *P. tunicata*'s biofilm structure and physiology. It will also be important to study the flow cell systems and mixed-species biofilms under natural conditions and examine the role of Slr4 in protecting not only cells but also biofilm matrix components against natural stressors such as antimicrobials, oxidative stress, desiccation, chemicals, temperature, and phage attack. I postulate that Slr4 plays a role in protecting both cells and biofilm matrix components against some of these stressors, thereby benefiting the fitness of marine biofilms.

Chapter 4

Comparative proteomics identifies a Ca²⁺-dependent adhesin required for biofilm formation in *Pseudoalteromonas tunicata*

The material in this chapter has been deposited as a preprint manuscript in bioRxiv:

Sura Ali, Alexander Stavropoulos, Benjamin Jenkins, Sadie Graves, Geoffrey Che, JiuJun Cheng, Huagang Tan, Xin Wei, Suhelen Egan, Josh D. Neufeld, Ulrich Eckhard, Trevor C. Charles, Andrew C. Doxey. Comparative proteomics of biofilm development in *Pseudoalteromonas tunicata* discovers a distinct family of Ca²⁺-dependent adhesins. bioRxiv 2024.10.22.619756; doi: <https://doi.org/10.1101/2024.10.22.619756>

Proteomic analysis in Chapter 2 identified hundreds of candidate biofilm proteins, including hypothetical proteins and proteins of unknown functions. In this Chapter, I focus on the top-scoring biofilm-associated protein that was identified in Chapter 2, EAR30327, and investigate its biological function using additional structural analysis, knock-out studies, and biofilm assays. I identify EAR30327 as a Ca²⁺-dependent adhesin protein involved in surface adhesion of *P. tunicata* cells to surfaces.

4.1 Introduction

Several previous studies have investigated the molecular processes underlying biofilm development in *P. tunicata* (Mai-Prochnow et al., 2004; D. Rao et al., 2005, 2010), which share several general mechanisms with other biofilm-forming bacteria. The first step in *P. tunicata* biofilm formation is the initial attachment/adhesion to surfaces (Mai-Prochnow et al., 2004). Typically, these initial interactions involve weak and reversible binding to a

surface substrate, using adhesive structures such as flagella and pili (Berne et al., 2018). The genome of *P. tunicata* encodes a variety of flagellar genes including a proteolytically active variant of flagellin that might be involved in flagella-mediated interactions with surfaces or host cells (Eckhard et al., 2017, 2020). In addition, the *P. tunicata* genome encodes a diversity of surface adhesion-related proteins capable of binding diverse substrates in the marine environment. These include genes for the biosynthesis of type IV pili, curli, capsular polysaccharide, chitin, and cellulose-binding proteins, as well as specialized proteins for binding to extracellular matrix (ECM) components abundant in eukaryotic host surfaces (Hoke et al., 2011; Thomas et al., 2008). Among these is the ECM-binding protein, LipL32, which has laminin- and collagen-binding activity (Gardiner et al., 2014) and facilitates adhesion of *P. tunicata* (Eckhard et al., 2017) to the ECM of its *C. intestinalis* host. In addition, *P. tunicata* can adhere to other types of surfaces, such as cellulose and polystyrene, via mannose sensitive haemagglutinin MSHA-like pili (Dalisay et al., 2006).

In addition to surface adhesion and production of antimicrobial molecules, another key aspect of *P. tunicata* biofilm development is the structure and composition of its extracellular biofilm matrix. In biofilm-forming species, the extracellular matrix is critical because it participates in the mechanical solidity of the biofilm, supporting it to resist shear forces as well as other external factors such as predation and phage infection. Previous studies have shown that biofilm matrices can be composed of polysaccharides, proteins, and nucleic acids. For example, the polysaccharides Pel, Psl, and alginate have been identified as constituents of *Pseudomonas aeruginosa* biofilms (Friedman & Kolter, 2004). However, the molecular composition of the *P. tunicata* biofilm extracellular matrix is relatively uncharacterized. A recent study described in Chapter 3 of this thesis, identified and characterized a novel protein, Slr4, as the major S-layer protein of *P. tunicata* (Ali, Jenkins, Cheng, et al., 2020). Slr4 not only forms the protective S-layer around cells in a planktonic state, but it is highly abundant in the extracellular matrix where it coats other extracellular structures, including outer membrane vesicles and filaments (Ali, Jenkins, Cheng, et al., 2020). Thus, in addition to the likely components, polysaccharides, and eDNA, *P. tunicata*'s

biofilm matrix also appears to contain proteinaceous structures and surface-associated proteins that facilitate cell-cell adhesion and attachment to different biotic and abiotic substrates.

In this study, I investigated the top biofilm-associated protein identified by proteomic analysis of *P. tunicata* biofilms in Chapter 2. This protein, EAR30327, is previously uncharacterized and is described as an “Ig-domain containing protein”. This work establishes EAR30327 as a novel Ca²⁺ biofilm adhesin that is a determinant of biofilm formation and adhesion in *P. tunicata* and likely in many related bacterial species.

4.2 Methods

4.2.1 Bioinformatic analysis of EAR30327

4.2.1.1 Sequence and structural modeling of EAR30327

Structural modeling was performed using ColabFold’s implementation of AlphaFold v2.0 (Jumper et al., 2021; Mirdita et al., 2022), and further edited and visualized in PyMol v3.0 (Schrödinger, 2024). Internal sequence repeats based on the structural model were further aligned using MUSCLE (Edgar, 2004) and further edited and visualized using AliView (Larsson, 2014).

4.2.4.2 Phylogenomic and metagenomic analysis

A comprehensive set of EAR30327 homologs were identified by BLAST analysis of 80,789 proteomes from the GTDB R214 database using EAR30327 as a query and an E-value threshold of 0.001. The taxonomic distribution of genomes possessing one or more EAR30327 homologs was summarized and visualized using AnnoTree (Mendler et al., 2019). A smaller set of more closely related homologs was identified by a BLAST search of

the NCBI nr database on July 1, 2024, using an *E*-value threshold of 0.001 and a query coverage threshold of 50%. Gene neighborhoods of identified homologs were visualized using AnnoView (Wei et al., 2024). A phylogenetic tree of EAR30327 and close homologs from other *Pseudoalteromonas* species was produced using PhyML v3.1 (Guindon & Gascuel, 2003) using 1018 sites and the LG model with 4 rate classes. Categories of metagenomic datasets containing *P. tunicata* EAR30327 genes identified using PebbleScout (Shiryev & Agarwala, 2024).

4.2.2 Construction of EAR30327 (BapP) deletion and rescue plasmids

4.2.2.1 Bacterial strains, plasmids, and growth media

Bacterial strains and plasmids used in this study are derived from earlier work (Finan et al., 1984; C. Holmström et al., 1998; Schäfer et al., 1994; Table 4.1). *E. coli* strains were grown at 37°C in LB medium (1.0% tryptone, 0.5% yeast extract and 0.5% NaCl). *P. tunicata* was grown in Difco marine broth 2216. Enzymes were obtained from New England Biolabs (NEB). Antibiotics were used at the following final concentrations: kanamycin, 50 µg/ml for *E. coli* or 100 µg/ml for *P. tunicata*; chloramphenicol, 20 µg/ml.

4.2.5.2 Plasmid construction

Q5 high-fidelity DNA polymerase (NEB) was used for plasmid construction and confirming constructs. The upstream region (1,469 bp) of *bapP* gene and 23-bp downstream of the gene were PCR amplified using oligos JC559 and JC560 (Table 4.2., Figure 4.1.) and its downstream region (1,690 bp), 20-bp upstream of the ORF and start code (ATG) were obtained using primers JC561 and JC562. Both DNA fragments were gel purified and pooled in equal amount as PCR template using JC559 and JC562. The PCR product was digested

with EcoRI-XbaI and then inserted into the same sites in pK19mobsacB, yielding plasmid pJC296.

Table 4.1. Bacterial strains and plasmids were used in this work.

Bacteria and plasmids	Characteristics	References
<i>E. coli</i> DH5a	<i>F</i> Φ 80 <i>lacZ</i> Δ M15 Δ (<i>lacZYA-argF</i>) U169 <i>recA1 endA1 hdr17 phoA supE44 thi-1</i> <i>gyrA96 relA1</i>	Lab collection
<i>P. tunicata</i> D2	Wild type	(C. Holmström et al., 1998)
ADx1	<i>P. tunicata</i> D2, in-frame BapP deletion	This work
ADx2	BapP ⁺ rescued ADx1	This work
Plasmids		
pK19mobsacB	Cloning vector, <i>sacB</i> , Km ^R	(Schäfer et al., 1994)
pRK600	Helper plasmid, Cm ^R	(Finan et al., 1984)
pJC296	pK19mobsacB carrying in-frame BapP deletion, <i>sacB</i> , Km ^R	This work
pJC302	pK19mobsacB carrying BapP ⁺ ORF, <i>sacB</i> , Km ^R	This work

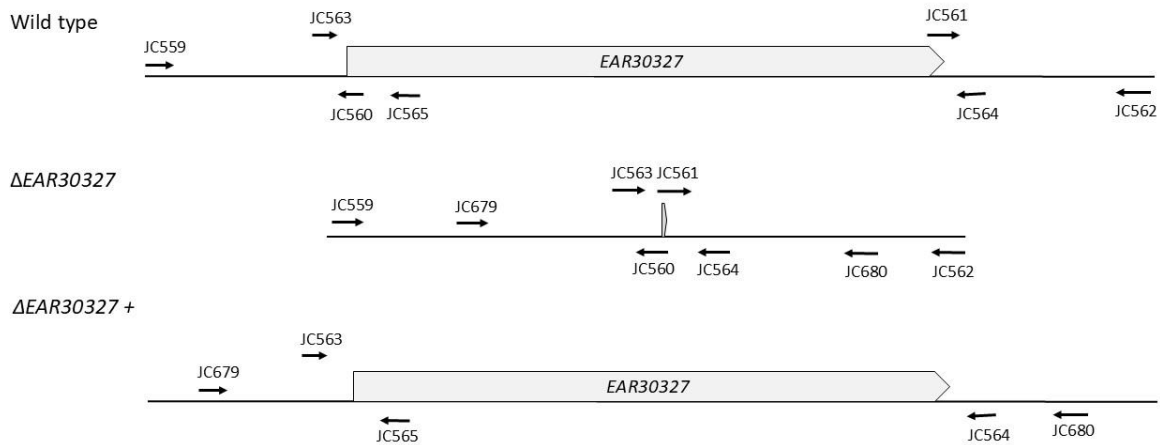


Figure 4.1. PCR primer binding regions in *Pseudoalteromonas tunicata* genomes.

A DNA fragment (6,818 bp) containing EAR30327 (*bapP*) ORF, upstream and downstream regions (989 bp and 1,014 bp respectively) of the gene were PCR amplified using oligos JC679 and JC680 (Table 4.2., Figure 4.1.). After gel purification, the amplicon was restricted with EcoRI-XbaI and then cloned into the same sites in pK19mobsacB, to obtain plasmid pJC302. The plasmid constructions were verified by restriction enzyme mapping.

4.2.5.3 Construction of *Pseudoalteromonas tunicata* strains

Plasmid pJC296 was conjugated into *P. tunicata* D2 with the helper plasmid pRK600 (Finan et al., 1986). Single cross-over recombination of the pJC296 into *P. tunicata* genome was selected on marine agar with kanamycin. A single colony was streak purified on a fresh plate. A colony was grown in Difco marine broth 2216, diluted serially, and plated on marine agar plates containing 5% sucrose. Resulting clones were tested for kanamycin sensitivity (double cross-over and loss of plasmid backbone). Genomic DNA was isolated from the Kan^S clones. DNA fragments were PCR amplified using primer pairs of JC563- JC565 and JC563-JC564.

The products were resolved with 1.5% TAE agarose gel. The amplicon generated with oligos JC563 and 564 was also Sanger sequenced at The Centre for Applied Genomics (Toronto, Ontario).

In order to rescue *bapP* ORF in the in-frame-deletion $\Delta bapP$ mutant, plasmid pJC302 was transferred into the $\Delta bapP$ mutant strain with the plasmid pRK600. Following selection of single cross-over recombination on marine agar with kanamycin, one transconjugant clone was streak purified on a new selection plate. A Kan^R colony was then incubated overnight in marine medium, diluted serially, and plated on marine agar with 5% sucrose. Resulting clones were screened for kanamycin sensitivity (*bapP* ORF inserted and loss of plasmid backbone). In order to detect the replacement of in-frame $\Delta bapP$ ORF in mutant, Genomic DNA was extracted, and PCR amplification was performed using primer pairs of JC563-JC565 and JC563-JC564.

Table 4.2. Sequences of primers used in this work.

Oligo ID	Sequence
JC559	GCGCG <u>GAATTC</u> CGTGAAACGTA CTACGTTGACATG
JC560	CTAACAGACTAGATTAACGCTTAGGATCCCATGCCGAGCTCCGTAAATCGTG
JC561	CACGATTTACGGAGCTCGGCATGGGATCCTAAGCGTTAATCTAGTCTGTTAG
JC562	CGCGT <u>CTAGAG</u> TATTCGAGATATGTGCCAACATTC
JC563	CGCGTGAATGTTAAGGGTGCCCGTTTTAT
JC564	CGCGCAATCGATTACAAAGTGGGTTAGGTC
JC565	CGCGGTGAGTCAATCGTTGAGCCTGTTAC
JC679	GCGCGAATTCGAGCAGATTAATATTGGTTCAATGC
JC680	CGCGTCTAGATTCAACAGTATGAACAGCTCTAAAC

Note: Restriction sites are underlined

4.2.3 Crystal Violet Biofilm Assays

A modified protocol based on a previous study (O'Toole, 2011) was used to perform crystal violet assays. The WT, $\Delta bapP$, and rescue ($\Delta bapP+$) strains were grown overnight in Difco marine broth 2216 at 24°C with shaking at 120 rpm. Overnight cultures were diluted to an OD₆₀₀ of 0.01 with Difco marine broth 2216, and 900 μ L of each subculture was dispensed into regular retention 1.5 ml microcentrifuge tubes (GeneBio). The centrifuge tubes were incubated statically at room temperature for 24 h. Five replicates were made for each sample, and the entire experiment was replicated three times to ensure reproducibility. After the appropriate incubation time, the culture was discarded. The biofilm adhered to the walls of the microcentrifuge tubes was stained by adding 950 μ l of 0.1% crystal violet to each microcentrifuge tube and left to stain for 15 min. Then the stain was disposed, and the excess stain was removed by shaking out the tube, and slowly washing with water three times. The trapped water was shaken out, the biofilm was left to dry overnight. To quantify the biofilm, the concentration of crystal violet was measured. A total of 1.1 ml of 30% acetic acid was added to each microcentrifuge tube to solubilize the crystal violet for 15 min. The same volume of acetic acid was added to three microcentrifuge tube to serve as a blank. The absorbance was quantified using a spectrophotometer (BioSpectrometer, Eppendorf) at 550 nm.

The same procedure described above was then used to investigate the effects of CaCl₂ on BapP biofilm formation with one modification: the overnight cultures of WT and $\Delta bapP$ strains were grown in Complex Media “CM1” broth (tryptone 10 g, yeast extract 5 g, NaCl 10 g, MgSO₄ 0.150 mg, deionized water 1 L) with five different levels of CaCl₂ (0, 0.138, 0.277, 0.832, 1.8 g/L; 0, 1.24, 2.49, 7.50, 16.2 mM). Each culture was diluted to an OD₆₀₀ of 0.01 with a volume of the corresponding CM1 broth. Then each subculture was dispensed into microcentrifuge tubes. Three replicates were made from each subculture, and the entire experiment was replicated three times to ensure reproducibility.

4.2.4 Confocal Laser Scanning Microscopy

Pellicle biofilm samples were collected using a clean square coverslip (Fisher brand, No. 1.5 - 0.17mm thick, Size 18X18 mm) and the same custom-designed tool that was described earlier to collect the biofilm samples for proteomic analysis. The coverslip was immediately inverted on a clean microscopic slide and the edges of the coverslip were sealed with a transparent nail polish to avoid biofilm dryness. Slides were examined within one hour of preparation using a Zeiss LSM 700 confocal microscope with the differential interference contrast (DIC) II condenser setting at magnifications of 40X and 63X.

4.2.5 SDS-PAGE

The WT, $\Delta bapP$, and $\Delta bapP^+$ strains were grown overnight in 4 ml Difco marine broth 2216 at 24°C with shaking at 120 rpm. Overnight cultures were subcultured, by first standardizing the overnight to an OD₆₀₀ of 1.0 with Difco marine broth 2216. The diluted overnight cultures were then subcultured to 1:99 dilution into fresh marine broth. A total volume of 4 ml was prepared and incubated for 5 hours at 24°C with shaking at 120 rpm. Each culture was centrifuged at 5000 x g and 4°C for 15 min. The supernatant was transferred to a new container and centrifuged again under the same conditions. The resulting supernatant was treated with two different protease inhibitors to prevent protein degradation: 10 µl of FOCUS ProteaseArrest added to 990 µl of the sample, and 10 µL/mL of 0.5 M EDTA. The samples were stored at -20°C. On the following day, samples were subjected to an SDS-PAGE (10% SDS) for protein separation based on molecular weight. A 25 µl of samples were loaded into the gel. In addition, 5 µl of BLUelf prestained ladder with MW 5- 245 kDa (FroggaBio) was loaded. The gel was run at 90 kV for 20 min, and 140 kV for 60 min. The SDS-PAGE gel was stained using silver staining (Pierce silver stain for Mass Spectrometry, Thermo Scientific) following the kit protocol.

4.3 Results

4.3.1 EAR30327 is the top biofilm-associated protein in *P. tunicata*

As mentioned in Chapter 2, the top identified protein (based on *p* value) was EAR30327 (Figure 2.5). EAR30327 was detected at high relative abundance in all biofilm time points, was virtually undetected in planktonic cells, and was also detected at low abundance in the media, which increased over time (Figure 4.2).

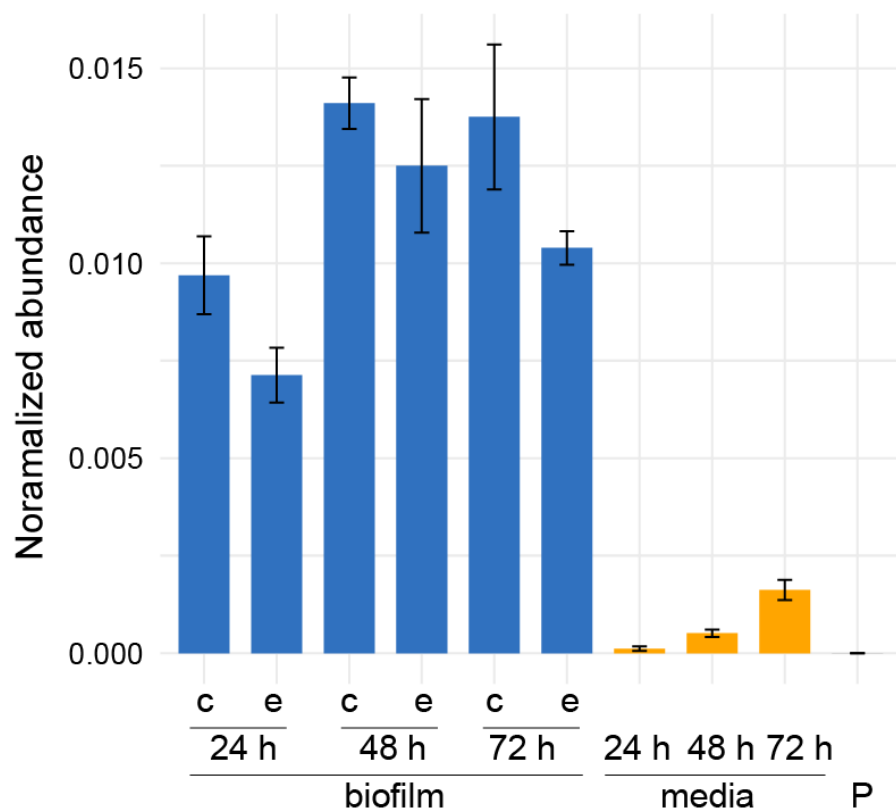


Figure 4.2. Abundance of the EAR30327 protein across samples based on LC-MS/MS shotgun proteomic data. EAR30327 is significantly increased in biofilm samples at all time points. Center biofilm samples = c; edge biofilm samples = e; Planktonic = p. Bars represent the mean \pm standard error (SE).

4.3.2 EAR30327 (“BapP”) predicted as a Ca²⁺-dependent outer membrane adhesin

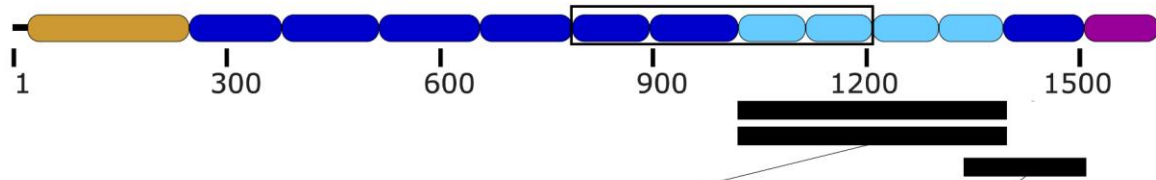
I investigated the top identified biofilm-associated protein EAR30327 (Figure 2.5, Figure 4.2) also labeled as “Ig domain containing protein” in the NCBI protein database. I used Alphafold 2.0 to predict the structure of this protein (Figure 4.3a) and sequence/domain analysis using multiple tools to predict its domain architecture (Figure 4.3b).

The predicted structure of EAR30327 has an N-terminal beta-propeller domain followed by 12 repeats of β -sandwich folds. Upstream of the N-terminal domain is a predicted Sec/SPI signal peptide (amino acids 1-20), indicating that the protein is translocated into the periplasm and/or extracellular space via the secretory pathway. My shotgun proteomic data (Ali, Jenkins, & Doxey, 2020) of *P. tunicata* was consistent with signal peptide cleavage between residues 20 and 21, as this region was missing in mass spectral coverage completely (data not shown). The N-terminal domain (residues 21-246) has a 5-bladed propeller structure in the Alphafold model (Figure 4.3.a). The top structural matches to this domain based on a FoldSeek search were TolB-related domains, which adopt a 6-blade propeller fold. Based on sequence alignments, the 12 β -sandwich repeats following the N-terminal domain can be subdivided into three classes of internal repeats (Figure 4.3.b, 4.3.c). The first six repeats (R1-R6) and also a seventh repeat (R7) found closer to the C-terminus, adopt a cadherin-like Greek-key structure that possess matches to the Calx- β PFAM (PF03160) domain. Calx- β domains were originally described in eukaryotic Na⁺-Ca²⁺ exchangers and play a role in Ca²⁺-binding. Calx- β like domains have also been identified in the large adhesin protein, LapA (Boyd et al., 2014). A second class of shorter repeats match the bacterial immunoglobulin 9 (Big_9) PFAM (PF17963) family (Figure 4.3.b, 4.3.c). FoldSeek searches using the tandem beta-sandwich region of EAR30327 revealed similarities to eukaryotic cadherin proteins as well as a variety of bacterial adhesins. For example, the Big_9 repeat region is predicted to be structurally similar to the adhesin region of AF-A0A066UXP9 from *Vibrio fortis*, which encodes a LapA like protein with an N-terminal LapA retention module (Smith et al., 2018).

and CabD, with significant *E*-values and identities exceeding 30% (Figure 4.4.). Within the *P. tunicata* EAR30327 sequence, I also identified matches to putative Ca-binding motifs identified previously in bacterial CHDL domains, including two matches to the PxAxxD motif, three matches to Dx Dx D, and two matches to the YT[V/I][S/T]D motif (L. Cao et al., 2005) (Figure 4.3.c). Twelve Dx D motifs were also found throughout the tandem beta-sandwich repeat domains (Figure 4.3.c). Combined, these results imply a Ca-binding adhesin function for *P. tunicata* EAR30327. I therefore designated this protein as *Pseudoalteromonas tunicata* biofilm adhesin protein or BapP.

I also observed that the N-terminal domain, which is predicted to adopt a beta-propeller fold, did not align to the N-terminal domains of other known adhesins. Given that other RTX adhesins contain a retention module as the N-terminal domain that anchors the protein into the outer membrane (Smith et al., 2018), I hypothesize that this beta-propeller domain in BapP may play a similar role.

BapP (*Pseudoalteromonas tunicata*)



CadB (*Saccharophagus degradans*)

%identity = 36%, E-value = 3e-49

```

BapP 1014  DNGAPIATDDSAFVNEDSLANNIDVLGNDSDFEN----DKLTVASATSNEGVVQININGT 1069
      +N AP+AT D+A  ED+  IDVL ND+D +N  D  T+A  +  ++G
CadB 1861  ENDAPVATSDTASTPEDT-PPTIDVLVNDNDIDNGDSVDGTTLAIIVSQPVNATASVVSGE 1919

BapP 1070  LNFQPDITNFNGIATITVVVDFEGG-EDTAYVSVNVVLPVNDAPLARPDLAKVSEDSQDNI 1128
      + F+P+ +FNG T TY V D+ G  + A V VNV  VND P+A  D A + ED  +
CadB 1920  IYFEPNEHFNGSTTFTTYTVDQNGATSNVATVLVNVTVGNLDLVALGDSASLDEGDSVEV 1979

BapP 1129  IVVLSNDEIDID---KDTLSVTSASANNQTVIINIDGTVYTPPMANFTGDTISYSVSDG 1184
      V L+ND DID  T+SV S +N GT +  G +TTFP ANF G+DT +Y V D
CadB 1980  DV-LANDSDIDGTIDPSTVSVLSDASNGCTSVNTTGGVITYTPPANFNGSDTFTYVQDN 2038

BapP 1185  KGG-SASSTVTVTVDNQNDAPTAAPFTAIVDEDSLNNVIDVSAYLADNENDTLTL---- 1239
      GG SA++TV+VTV + NDAP  TA + ED+  I+V  +D D + S
CadB 2039  DGGSSAATTVSIVTASINDAPNGVADTAALMEDN-PTTINVLGNDSVDGSIIVTSQIV 2097

BapP 1240  -SPAAMNGVTVVNDKILYTPKPGFVCSDTITVYVSDGKG-FAQGVITMTRVNVNDAP 1297
      PA  +G V V+ NG +TY+P  + G D+ TY V D +G  +++  + +TV +VNDAP
CadB 2098  TGPA--DGTVEVLANGSITVSPOTNYGDDSTYQVQDNEGAWSESSTVNVTVSSVNDAP 2155

BapP 1298  VAKPKAVEVNEQSNNIITLADVLEADND-----VLTVTNISAQHGTVTLQNGQLVYT 1351
      +A  +V +E++ +I +A+  D+D D  L + + A  V  +G +YT
CadB 2156  LANNDVSTDEDTAVSIDLIAN---DSDADGLDSSSLVIVSAPANGALVNDLGTVYTT 2212

BapP 1352  PQASYSAGEITVYVSDGKGSQAQ-GYVEVTKFVNATISLIAVNGASREEGQTATYRIV 1410
      P A Y G+D TY + D G S+  V +TI PVN  +  AS E  +Y +
CadB 2213  PSADYFGSDSFTYQIDDDSDSSNTAAVTITINPVNDAPQISGTPAASVNEDSVSYTPI 2272

BapP 1411  LMQAISNDATIEVQ 1424
      +  ++D +  ++
CadB 2273  SSDIEADLDSFSIE 2286
  
```

LapA (*Pseudomonas fluorescens*)

%identity = 31%, E-value = 1e-10

```

BapP 1330  TVTNISAQHGTVTLQNGQL-----VYTFQAS---YSGADEITYVSDGKGSQAQ 1375
      T+TN +  TVTL NG +  V P + Y A + T+++ GG+ +
LapA 3903  TLTRNAGSFVTVLNSGAVITIDAGKTTGTVVPAPADDVYKDGANVQATITNATGGNFE 3962

BapP 1376  GYVEVTKFVNATISLIA-----VNGA-SREEGQTATYRIVLQQAISNDATIEVQVINGT 1429
      V T V +  I  + G+ S  EGQTA+Y + L  + T+++ V +GT
LapA 3963  NLVTSTTPAVTSVTDITDITTVSITGTSVTEGQTASYVSLTHPAQTEVTLKI-VYSGT 4021

BapP 1430  AFKGSDFSTNTMTVPAQQTSEVNFVTEDESHEELEDVHVKI-----IAKSN 1479
      A GSDF+ T + +PAG +S +FNV TI+D  E E++ VKI  +A S+
LapA 4022  AADGSDFTGVYTVKIIFAGASSAQFNVATIDDKITEGTFVVKIDSATGONFENLAVSS 4080

BapP 1480  ATGTAQLKRAVIVDDDCPL 1497
      G +  I+D+D P
LapA 4081  TWG--SVSTSIIDNDAPP 4096
  
```

Figure 4.4. Partial sequence homology between a putative binding region in BapP and binding domains from other biofilm adhesins. A domain architectural model of BapP is depicted above, and two regions corresponding to significant BLAST alignments are shown below, the first of which is similar to a region from the CadB adhesin from *S. degradans*, and the second of which is similar to a region from *P. fluorescens* LapA.

4.3.3 EAR30327 (“BapP”) required for proper biofilm formation and surface adhesion

To test the predicted function of BapP as a biofilm adhesin, I generated a $\Delta bapP$ knockout mutant and verified it by PCR (Figure 4.5) and sequencing of amplified PCR product from its genomic DNA (see Methods).

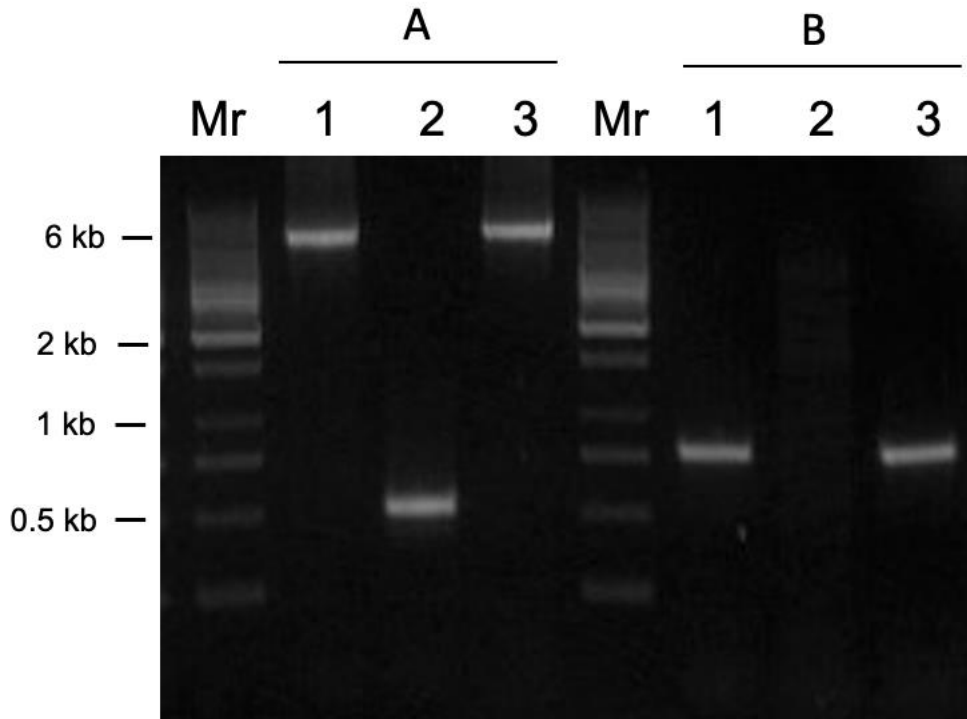


Figure 4.5. Verification of *Pseudoalteromonas tunicata* strains by PCR amplification.

Verification of *P. tunicata* strains by PCR amplification. Mr, DNA ladder, lane 1, wild type; lane 2, $\Delta bapP$ mutant, lane 3, $\Delta bapP^+$. (A) PCR products amplified with primers JC563 and JC564. An amplicon of 510-bp was expected in $\Delta bapP$ mutant, and a 5301-bp fragment was present in both wild type and $\Delta bapP^+$ strains. (B) PCR amplification with primers JC563 and JC565. A 722-bp fragment was present in wild type and $\Delta bapP^+$, but absent in $\Delta bapP$ strain due to absence of JC565 binding site.

A silver stain SDS-PAGE gel of WT supernatants revealed a distinct band that matched BapP by LC-MS/MS analysis (Table 4.3) and this band was absent in the $\Delta bapP$ strain, again confirming successful deletion of the *bapP* gene (Figure 4.6). This result also suggests that BapP is at least partially released extracellularly or, alternatively, that it is loosely associated with the cell surface. This is consistent with the biology of non-fimbrial adhesins involved in biofilm formation (Baps, biofilm-associated proteins), which are secreted by the T1SS and loosely attached to the cell surface and often released into the extracellular space (Berne et al., 2015).

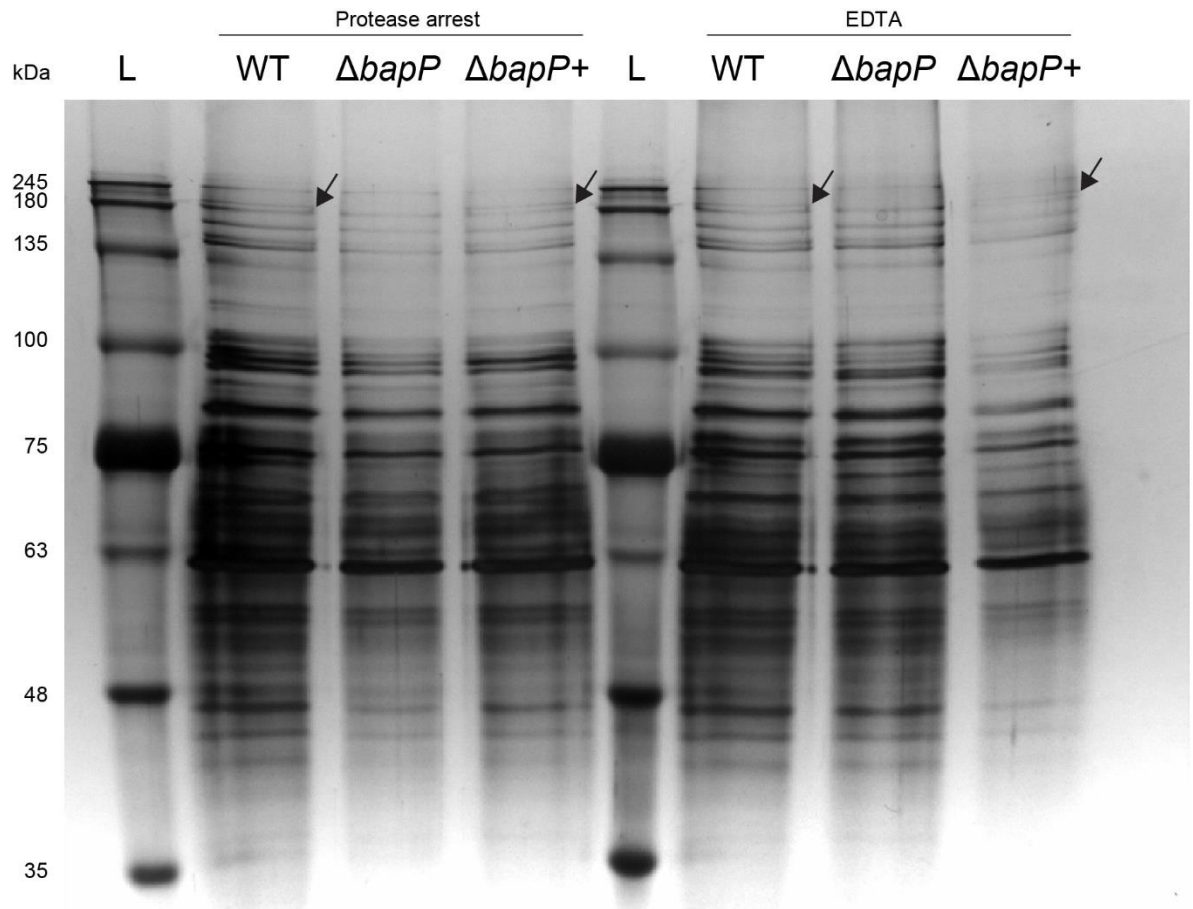


Figure 4.6. SDS-PAGE gel of supernatant protein collected from the WT, $\Delta bapP$, and $\Delta bapP+$ strains. Loss of BapP reduces biofilm formation and surface adhesion. Silver stain SDS-PAGE gel of supernatant containing extracellular proteins. A unique band was observed in WT supernatants and missing in $\Delta bapP$. The band was excised from the gel and identified as BapP by LC-MS/MS. Protease arrest and EDTA were added to minimize protein degradation. A unique band (arrow) appeared at ~180 kDa in the WT and $\Delta bapP+$ strains, and not in the $\Delta bapP$ deletion strain, and was identified as BapP by LC-MS/MS proteomics.

Table 4.3. Identified peptides for top-matching *P. tunicata* proteins by LC-MS/MS.

Accession	10LgP	Coverage (%)	Coverage (%)	Number Peptides	Number Unique	Number Spec	Average Mass	Description
A4C445 A4C445_9GAMM	59.8	7.94	7.94	10	10	10	172055.48	PTD2_02121
A4CAM5 A4CAM5_9GAMM	51.1	8.43	8.43	6	6	7	119094.73	Ribonuclease
A4CFX2 A4CFX2_9GAMM	16.4	1.01	1.01	1	1	1	154389.08	DNA-directed RNA polymerase subunit beta

I cultured pellicle biofilms and examined their morphology over a 24-72 h period. As seen after 72 h, the WT formed robust pellicle biofilms with high cell density, whereas the $\Delta bapP$ mutant formed thin fragile biofilms with a loss of cohesion between cells (Figure 4.7).

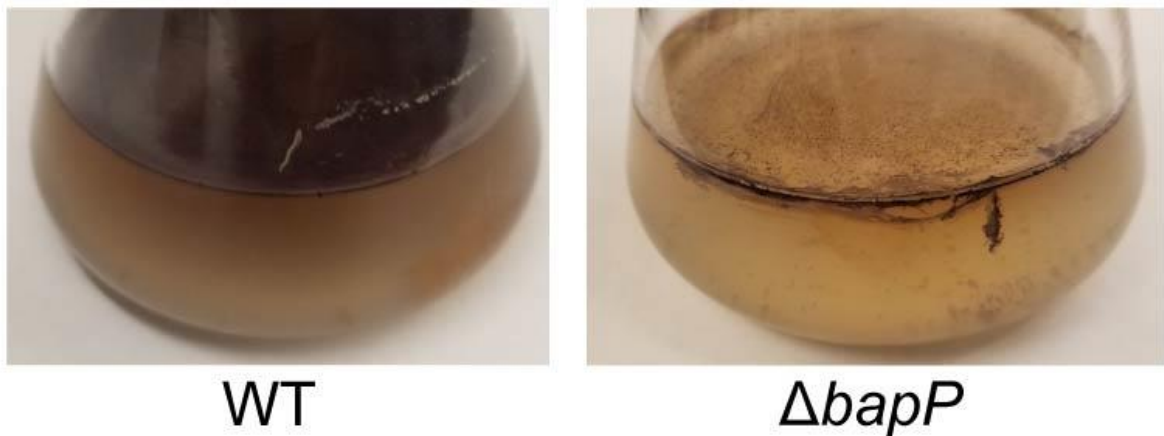


Figure 4.7. Loss of BapP reduces biofilm formation and surface adhesion. Pellicle biofilms of WT versus $\Delta bapP$ formed by 72-hour incubation in marine broth under static conditions.

Regions of the $\Delta bapP$ biofilm were also visibly detached from the glass substrate. Similarly, confocal microscopy revealed a dense and homogeneous layer of cells in WT biofilms, whereas $\Delta bapP$ had a fragmented and heterogeneous biofilm with a loss of cell-cell cohesion (Figure 4.8).

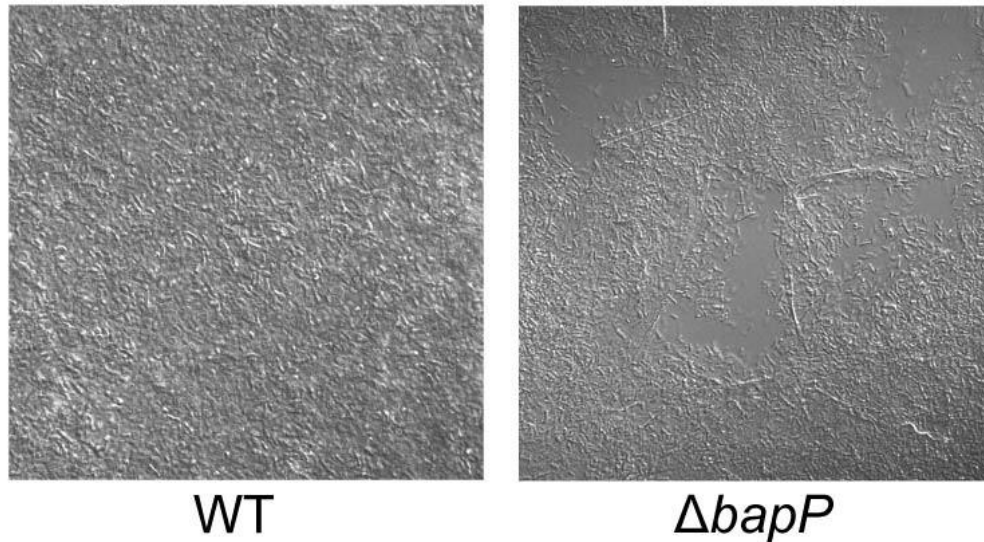


Figure 4.8. Loss of BapP reduces biofilm formation and surface adhesion. Confocal microscopy of 72-hrs pellicle biofilms (63 X magnification).

To examine the reduced biofilm-forming capability of the $\Delta bapP$ mutant quantitatively, I performed crystal violet biofilm assays using centrifuge tubes. The WT formed robust biofilms on these tubes within a 24 h period, reaching a maximum OD₅₅₀ of 2.0 units, whereas there was a significant (5.7-fold) reduction in biofilm formed in the $\Delta bapP$ mutant ($p = 8.6 \times 10^{-19}$; Figure 4.9). To verify the genotypes, I generated a rescue mutant by replacing the in-frame $\Delta bapP$ (ATGGGATCCTAA) with the wildtype *bapP* gene in the genome of the $\Delta bapP$ strain, which was then verified by PCR amplification (Figure 4.5).

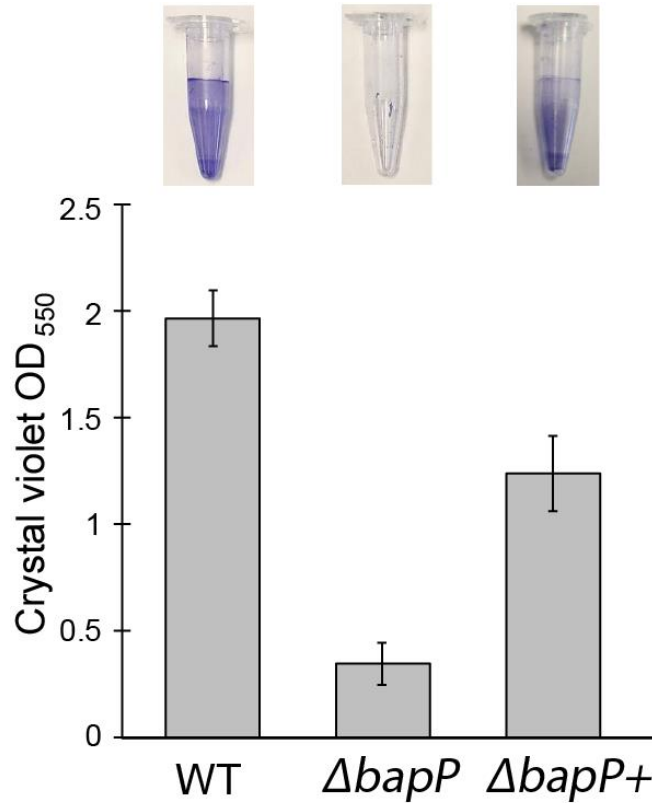


Figure 4.9. Loss of BapP reduces biofilm formation and surface adhesion. Crystal violet assays of WT, $\Delta bapP$, and rescue ($\Delta bapP+$) strains were cultured for 24 h in centrifuge tubes containing marine broth. 95% confidence intervals are shown as error bars.

The $\Delta bapP+$ rescue mutant successfully restored biofilm formation in the crystal violet assay (Figure 4.8.). The BapP band also reappeared in the supernatant of the $\Delta bapP+$ strain confirming successful mutant rescue (Figure 4.6).

4.3.4 Ca²⁺-dependent BapP-mediated biofilm formation

Given the presence of bacterial cadherin-like domains in BapP and numerous putative Ca²⁺-binding sites (Figure 4.3) I investigated the influence of Ca²⁺ on biofilm formation in the WT versus $\Delta bapP$ strain. To control the CaCl₂ concentration, I used non-marine complex media (“CM1”) as described in the Methods. Crystal violet assays were then performed with varying levels of CaCl₂ added to the CM1 media, and the optical density of attached cells was measured at 24, 48, and 72 h. In the WT strain, I observed a strong relationship between added calcium and biofilm formation, especially by the 72-h time point ($R^2 = 0.67$), with OD₅₅₀ readings increasing from a mean of 1.5 units (no added CaCl₂) to a mean of 4.4 units (1.8 g/L added CaCl₂) (Figure 4.10, Figure 4.11). By comparison, in the $\Delta bapP$ strain the addition of Ca²⁺ had a significantly weaker influence on biofilm formation than the WT ($p < 0.05$), with OD₅₅₀ readings increasing from 0.6 units to 1.7 units (Figure 4.10, Figure 4.11). Despite the reduction in Ca-dependent biofilm formation in $\Delta bapP$, a positive relationship was still detected ($R^2 = 0.37$). This may be due to the presence of additional Ca²⁺-dependent biofilm adhesins in *P. tunicata* beyond BapP (e.g., PTD2_14577, see Table 4.1.).

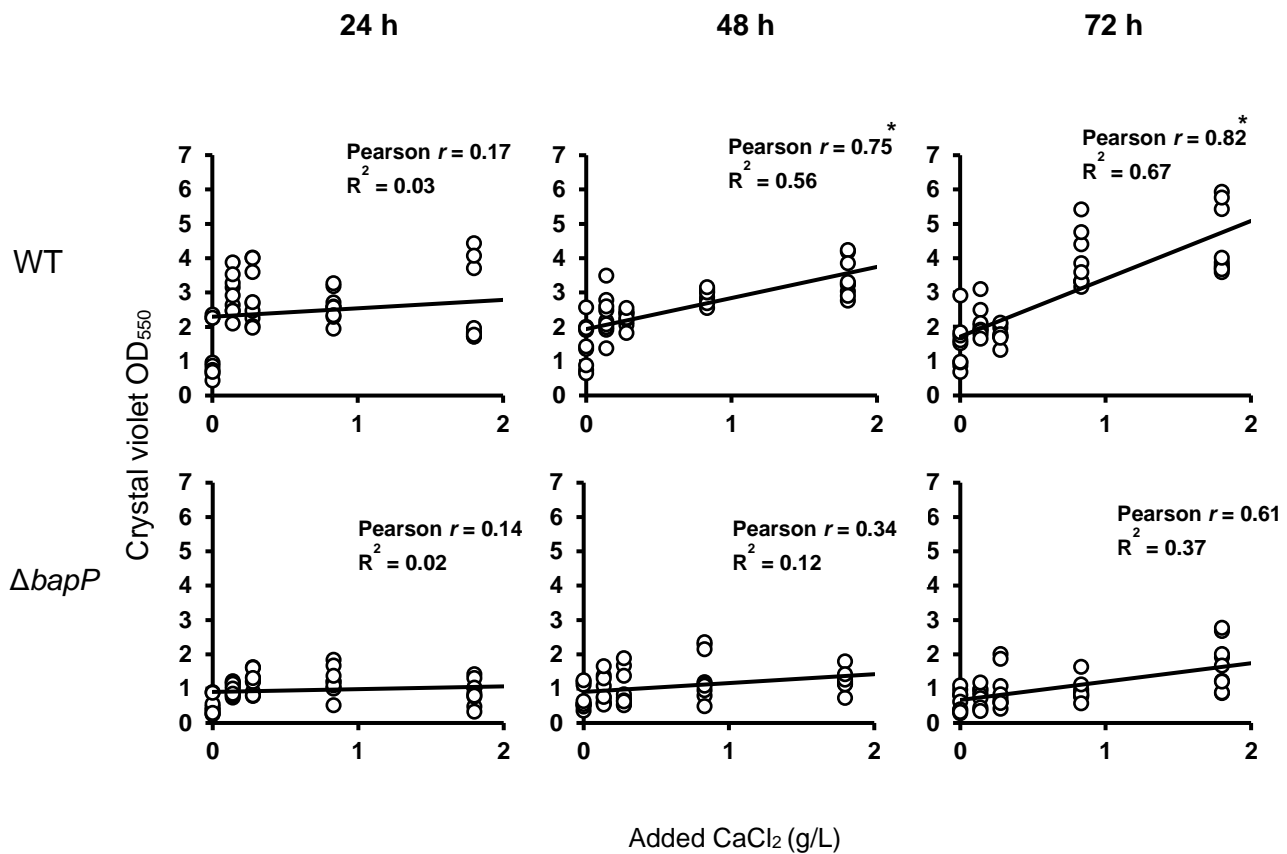


Figure 4.10. Quantification of the effect of Ca²⁺ addition on biofilm formation.

Scatterplots depicting correlations between biofilm growth, quantified via 550 nm absorbance of attached cells, and added CaCl₂. The asterisks (*) indicate time points for which the Pearson correlations (Ca²⁺ vs biofilm OD) are significantly greater for WT than $\Delta bapP$ strains (Fisher's z-Test, $p < 0.05$).

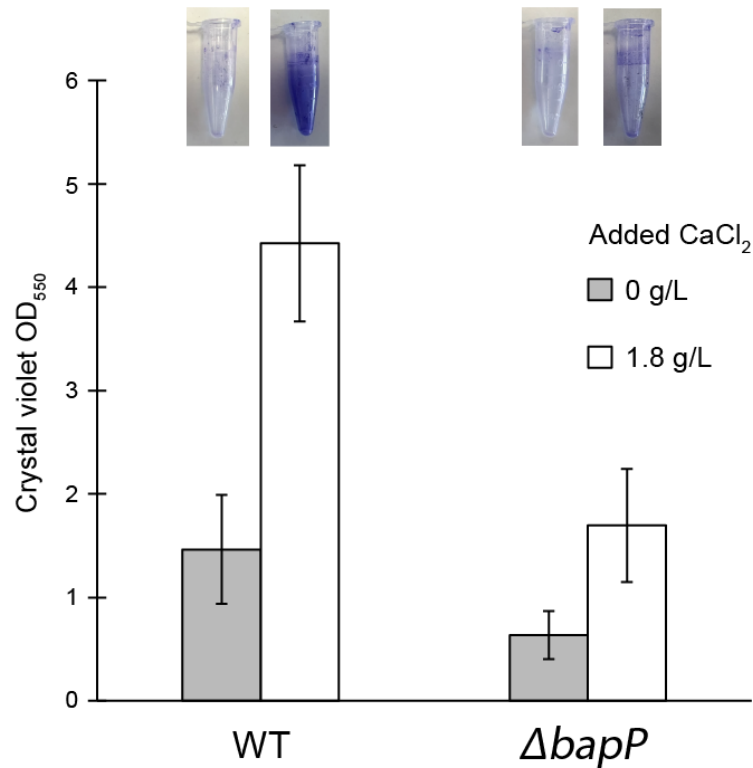


Figure 4.11. Quantification of the effect of Ca²⁺ addition on biofilm formation. Crystal violet biofilm levels at 72 h for WT and $\Delta bapP$ with and without added Ca²⁺. Added Ca²⁺ results to an approximately 4.5-fold increase in biofilm formation in the WT strain, but only a ~1.5-fold increase in the $\Delta bapP$ strain, consistent with the prediction of BapP as a Ca²⁺-dependent biofilm adhesin. Two representative centrifuge tubes from this experiment are shown above the bar plots. The 95% confidence intervals are shown as error bars.

To account for the possibility that $\Delta bapP$ had a growth defect, I measured the OD₆₀₀ of all cells in the centrifuge tubes including the media (Figure 4.12). Despite the WT showing increased biofilm formation based on crystal violet assays, the total concentration of cells in the tubes including the media was higher for $\Delta bapP$ than that of the WT. This indicates that

the observed effects (Figure 4.10, Figure 4.11) are not due to growth artifacts, and that the majority of $\Delta bapP$ cells remained in solution, non-attached to the substrate.

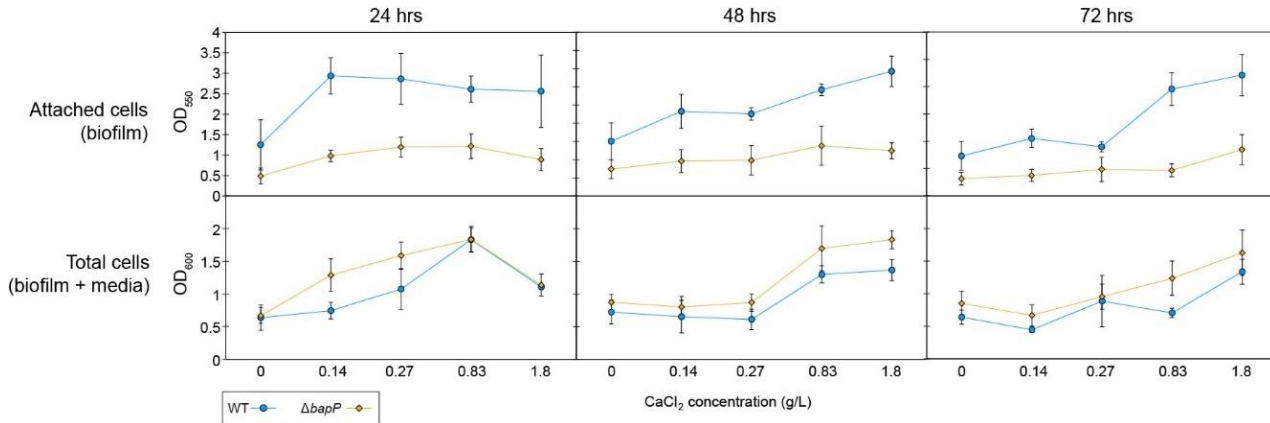


Figure 4.12. Line graphs depicting biofilm growth, quantified via 550 nm absorbance, and total cell growth, quantified via 600 nm absorbance, against added CaCl₂. Across all timepoints and CaCl₂ levels, the density of WT biofilms exceeds that of $\Delta bapP$ ($p < 0.05$, two-tailed t-test). However, the total cell growth (attached + non-attached cells) of $\Delta bapP$ matched or exceeded that of WT cultures. Error bars represent 95% confidence intervals.

4.3.5 Phylogenomic analysis and distribution of the *Pseudoalteromonas* BapP adhesin family

I used AnnoTree (Mendler et al., 2019) to explore the broader phylogenomic distribution of BapP homologs. A BLAST search identified proteins with at least partial homology to BapP in 13,729 (17%) genomes out of 80,789 total genomes in the GTDB R214 database (Figure 4.13).

Distant & partial homologs

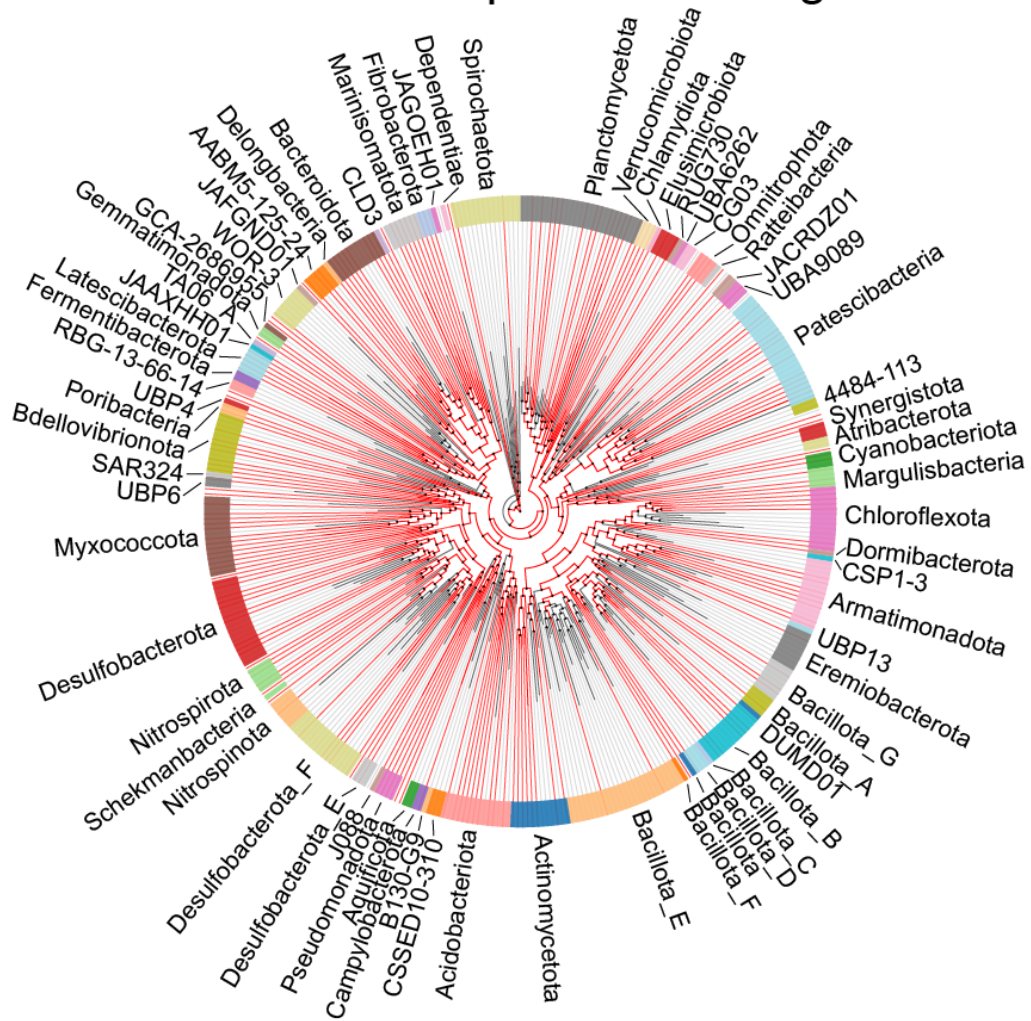


Figure 4.13. Phylogenomic distribution of *Pseudoalteromonas tunicata* BapP homologs available metagenomes. Distribution of BapP-related proteins across the bacterial tree of life using AnnoTree. The branches of the tree represent individual classes, and the outer ring annotation shows the phylum. Branches in red represent classes that contain one or more BapP homologs. Homologs were defined as any significant ($E < 0.001$) matches based on a BLAST search including partial homologs with low query alignment coverage.

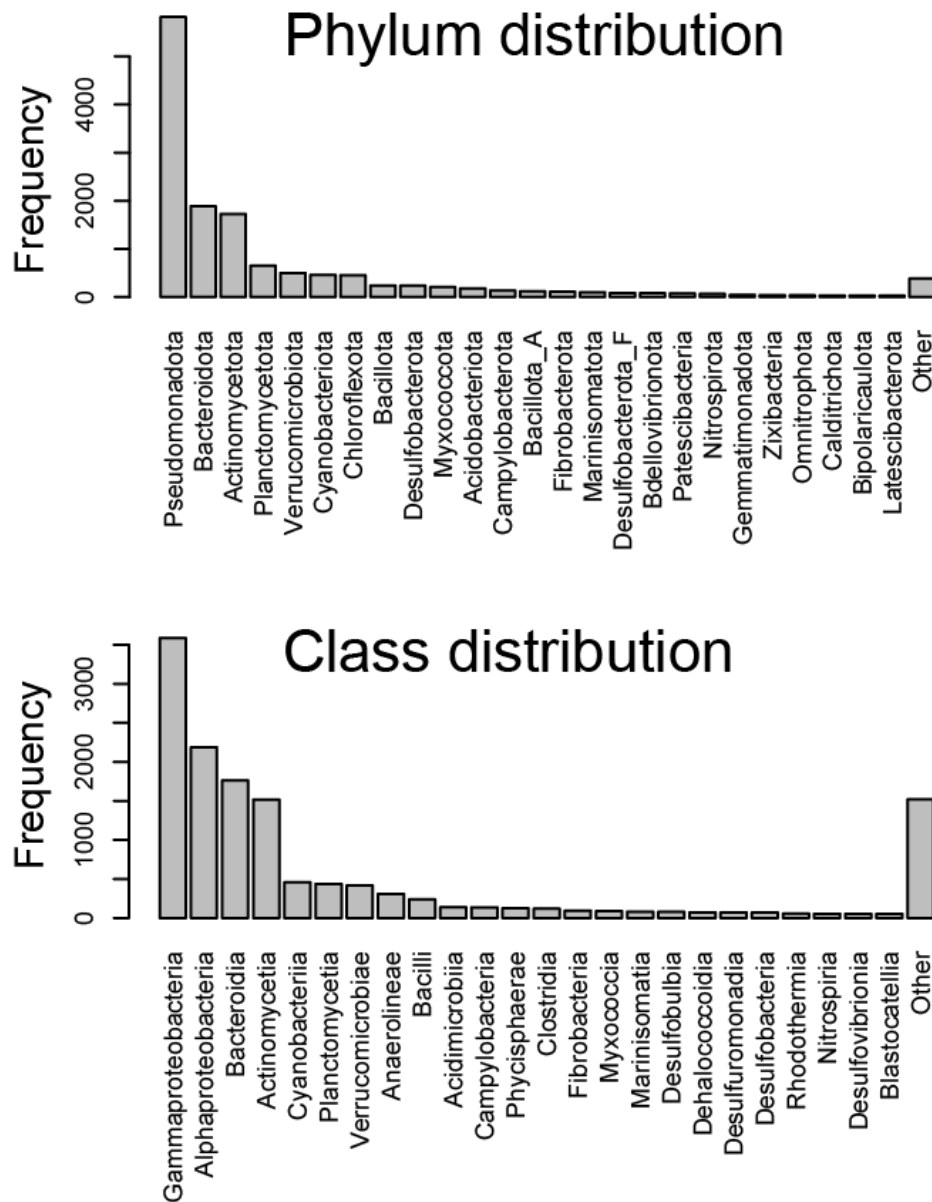
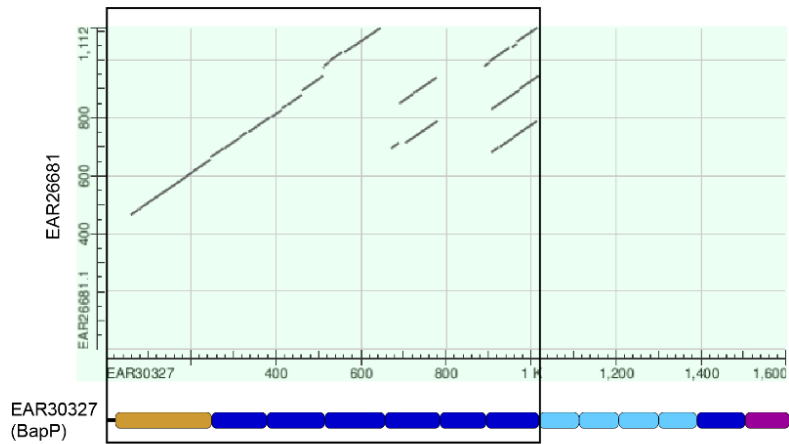


Figure 4.14. Occurrence of BapP of *Pseudoalteromonas tunicata* available metagenomes.

Frequency histograms that show the number of genomes containing BapP homologs subdivided by bacterial phylum and class.

An additional homolog was detected in the *P. tunicata* genome (EAR26681, PTD2_17117, annotated as “Rhs family protein”), with significant sequence similarity (29% identity, 46% similarity, $E = 1e-55$) (Figure 4.15). This protein sequence aligned to 37% of the BapP sequence (residues 59-646) including the N-terminal beta-propeller domain and the first four beta-sandwich repeats (Figure 4.15). A unique feature of EAR26681 is that it also possesses an N-terminal “Choice of anchor A” domain, which has been identified in proteins from the microbial surface component recognizing adhesive matrix molecule (MSCRAMM) family (Deivanayagam et al., 2002; Xu et al., 2004). Like BapP, this protein was also detected among the group of 232 biofilm-associated proteins (\log_2FC increase of 1.7, $q = 8.3e-03$). Therefore, this BapP-like protein (EAR26681) may function along with BapP in extracellular adhesion and/or interaction with other extracellular matrix molecules.

The largest number of BapP-related proteins occurred in the *Gammaproteobacteria* (Figure 4.16). An analysis using PhyloCorrelate (Tremblay et al., 2021) suggests that BapP is associated with biofilm-forming species, as “Biofilm formation – *Pseudomonas aeruginosa*; map02025” and “Biofilm formation – *Vibrio cholerae*; map05111” were the top two enriched pathways ($q < 4e-06$) among proteins that co-occurred with BapP. The majority of BapP-related proteins detected by BLAST possess only partial detected homology across the full length BapP sequence, which can arise due to the presence of common domains in BapP, such as the calx- β motif (IPR003644), which I detected in 10,874 genomes (Mendler et al., 2019).

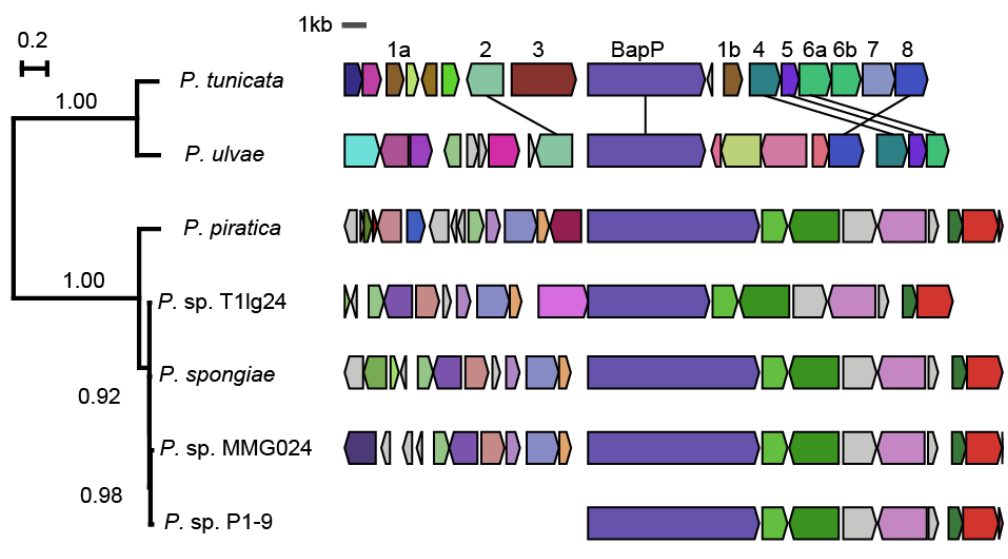


Score	Expect	Identities	Positives	Gaps		
199	bil.s	(506)	1e-55	190/664 (29%)	307/664 (46%)	95/664 (14%)
Query	59	SDATAYQESTDRLYVYVTKPVNG--KPRIYVYVDMATFQHVVDVAATTGTYRIA FSPDGQTLW	116			
Sbjct	466	SDAAY I DRLYYITK VNG KP I YVIM T I V IA G YRL FSPD LI SDAVAYDKINDRLYYITK-VNGALKPKVAYVNMQTGEDVKLAEIDGGYRLVFSPPSSQLF	524			
Query	117	GSS EDTVFNINTNDGTVSNKVTLTGFATDADKLGDI VFNINDTLHIVTNKKLFAVDLAAG	176			
Sbjct	525	SS + TN G V +K++L. GD+VFT D I+IV+ I. VDI. ASSCRDIVEINPTTCAVISKISLKSNDSEITFCMGDLVFIQDELYIVSGLHLKVDLVNK	584			
Query	177	TVREVGMIINLS-VTGSTIDSLGOLLVSS-NAGNNKTDLYTLDPAKPSLLSSINYRIND	234			
Sbjct	505	+G H ++ TG+ +DS G LL+S N +T +Y+++ K + ++++Y IND QATVVLGKHGVNGATGAEVDSGNLLISKINNATAQTIIYSINVTELKATAVAIVDYAIND	644			
Query	235	LATRIVVQPACT-----QLQDNVSSVEAIKNNVSEGGVQLHARVHFEQPISTDTVIYL	286			
Sbjct	645	LA R + C ++ ++ ++E I + VEG L A+V F + + IATRHFDFGKTCNTDPVDPVFPKSSIVATELTSDRQVRGDDIVAKVMFSG--GFFAQINT	702			
Query	287	NFNASAQKNADFDFRVELSFDNGMTWTS---VKNITSTIATTDAPKGLSHFDVRIHSFKD	343			
Sbjct	703	N I + IA +ADE V +SFDIG TW I KN S +A L ++IH+ D NLSSTIADIDAEFTSKVSVSFDGGIWLTDLEAKNGSSVTPENAKSAL----IKLHTLTD	758			
Query	344	GDIEGNEFVLE-AWNEGQADKKSRIFTIVDQSSSPDVTSVTLTSENVEGVMVADVV	402			
Sbjct	759	++E +E+ LE ++ + KS + TLVD+ + +P+ F+ A + TEVENDESLRLEVSFAHDPVVKSELLTIVDKPTGGDTCCGDAC---EMPKVSFITALSI	815			
Query	403	LSQATTSFHDHY-----IQIVTNSNPAYSALNEDFTGQI-EISFNRGISWQSIGLVGR	455			
Sbjct	816	I T I I I IQ + PA N F IL I I I I I V FNGEYTDQSKAFTYEGGEMQFEVGFDDGPA--KCGNPFQFKLNDIETTQRLDYALVSVSS	873			
Query	456	L IKAR-----IYEGVSEYKLRKRVYSDGVTEGAETAALISISASSDGLFAL	500			
Sbjct	874	L + EG + +R K +D E E +S+ SD LTNENWLNNVNVALGSATYAVQREGDEGFTVRVKTLADTTKERNEVFTLSVMNKSQSDVK	933			
Query	501	ERPFTI-NDAV-----KSC-----LPKVMYTIALP---	524			
Sbjct	934	+ +T N+A SC +P + + AI. YKDUSIENNAATDVDDGTPGTGGGTPGTGPGNGNTDPDSCSSEDELPAKKEITALSVDI	993			
Query	525	-NPFSEDCYMFVEVGYRSEAKCDGQYKFLVETSISYVDKAKKGVDFSTLVDIKDINSR	582			
Sbjct	994	F+ E G M++ G+ EA C G + E + D KGV+ST VD1+ + + GRSPTKREGKMEYYAGFAKEASCSTPYFSPAD-----DHITTKGVDYSTNVDTQTWD-K	1046			
Query	583	FFRQPAVDASGVVTTDVPKGSAGFVVRVYKPKDDITEGPREPSTNAWASPDQSDI.FFKDT	642			
Sbjct	1047	I QI VDAI IIV KCIAGF I I DD E EE I I W D+SDL KD QPAQYNVDAANGAAVNVKGIAGFTIITLTLADDEAEEREYFLHITWRKADKSDLKIKDH	1106			
Query	643	TILD 646				
		TI+D				
Sbjct	1107	TIVD 1110				

Figure 4.15. BLAST alignment dot plot depicting regions of similarity between BapP (x-axis) and a related *Pseudoalteromonas tunicata* protein (EAR26681). The region of similarity (boxed) covers the N-terminal domain and first six beta-sandwich repeats.

I restricted my BLAST search to identify *close homologs* possessing both significant sequence similarity ($E < 0.001$) and alignment coverage across the majority ($\geq 50\%$) of the BapP sequence. This search identified only 13 proteins within the NCBI nr database, all of which occur within genomes from the *Pseudoalteromonas* genus. After removing redundant sequences, the remaining BapP-related proteins were found in seven *Pseudoalteromonas* species (Figure 4.16). Phylogenetic analysis showed that *P. tunicata* BapP is most closely related to an orthologous protein from *P. ulvae*, an organism associated with the host, *Ulva lactuca* (Egan, Holmström, et al., 2001) (Figure 4.16). Five BapP-related proteins form a second cluster, which is more distantly related. The *P. tunicata* gene neighborhood surrounding BapP that I analyzed using AnnoView (Wei et al., 2024), shows some syntenic conservation with that from *P. ulvae* (Figure 4.16) but not with the other five genomes, suggesting that genomic rearrangements have occurred. The gene neighborhood of *P. tunicata* BapP encodes several proteins related to outer membrane systems including ABC transporter components as well as the HlyD family efflux transporter periplasmic adaptor subunit (Figure 4.16). In a more distantly related *Dickeya dadantii* genome, immediately downstream of a BapP-related protein (WP_284601796.1) is the *tolC* gene, which is also a component of the T1SS.

Close homologs (*Pseudoalteromonas*)



- 1 - transporter substrate-binding domain-containing protein
- 2 - alanine/glycine:cation symporter family protein
- 3 - DUF2339
- 4 - HlyD family efflux transporter periplasmic adaptor subunit

Figure 4.16. Phylogenetic tree of *Pseudoalteromonas tunicata* BapP along with its the top six identified homologs (all with coverage exceeding 50%). The corresponding protein accessions are: *P. tunicata* (WP_009836625), *P. ulvae* (WP_086743690.1), *P. piratica* (WP_040136050.1), *P. sp. MMG024* (WP_237129147.1), *P. sp. P1-9* (WP_054980746.1). Clade support values are shown next to nodes. On the right of the phylogeny the gene neighborhoods surrounding BapP homologs are shown, as generated using AnnoView (Wei et al., 2024).

I used Pebblescout (Shiryev & Agarwala, 2024) to search the NCBI sequence read archive for metagenomic datasets containing reads matching BapP (Table 4.4).

Table 4.4. Pebblescout results for Sequence Read Archive datasets of the top 30 results containing matches to the *P. tunicata* BapP protein.

Subject ID	Raw Score	Coverage (%)	PBS score	Bio Sample	Title
SRR12112860	486	99.8	99.8	SAMN15346752	Manipulative experiment on <i>Ulva australis</i> surface-associated bacterial community Raw sequence reads
SRR12112859	469	96.31	96.3	SAMN15346753	Manipulative experiment on <i>Ulva australis</i> surface-associated bacterial community Raw sequence reads
SRR1586370	458	94.06	94.1	SAMN03081543	Epidermal mucus from <i>Anguilla anguilla</i> Metagenome
SRR16282460	435	89.34	89.3	SAMN22190879	Metagenomic investigation of antibiotic resistance genes in aquacultural farms in Vietnam
SRR12112861	434	89.14	89.1	SAMN15346751	Manipulative experiment on <i>Ulva australis</i> surface-associated bacterial community Raw sequence reads
SRR7253989	424	87.09	87.1	SAMN09302799	Baltic Sea viral metagenomes
SRR7254007	421	86.48	86.5	SAMN09302802	Baltic Sea viral metagenomes
SRR6319735	376	77.25	77.2	SAMN08093733	marine metagenome Metagenome
ERR1992810	339	69.67	69.7	SAMEA103954417	Semi-synthetic marine metagenomes for metagenomic pipeline assessment
ERR1992808	331	68.03	68.0	SAMEA103954398	Semi-synthetic marine metagenomes for metagenomic pipeline assessment
ERR2185279	331	68.03	68.0	SAMEA104351855	Semi-synthetic marine metagenomes for metagenomic pipeline assessment
ERR3986938	329	67.62	67.6	SAMEA6617236	Biofilms on microplastics $\sqrt{t, \zeta''}$, Åú composition, genetic potential, and function examined by meta-proteogenomics
ERR1992809	322	66.19	66.2	SAMEA103954416	Semi-synthetic marine metagenomes for metagenomic pipeline assessment
ERR2696420	322	66.19	66.2	SAMEA4786491	Semi-synthetic marine metagenomes for metagenomic pipeline assessment
ERR1992807	278	57.17	57.2	SAMEA103954418	Semi-synthetic marine metagenomes for metagenomic pipeline assessment
ERR2696419	278	57.17	57.2	SAMEA4786490	Semi-synthetic marine metagenomes for metagenomic pipeline assessment
SRR11803501	262	53.89	53.9	SAMN14935076	Rhode River viral and microbial metagenomes
SRR7253990	258	53.07	53.1	SAMN09302798	Baltic Sea viral metagenomes
SRR16282462	253	52.05	52.0	SAMN22190877	Metagenomic investigation of antibiotic resistance genes in aquacultural farms in Vietnam
ERR2206792	249	51.23	51.2	SAMEA104408630	Baltic Sea reference metagenome assembly and data sets; transect and redoxcline.
ERR1992794	231	47.54	47.5	SAMEA103954396	Semi-synthetic marine metagenomes for metagenomic pipeline assessment
SRR6869395	213	43.85	43.8	SAMN08714533	marine biofilm metagenome

ERR2206788	198	40.78	40.8	SAMEA104408626	Baltic Sea reference metagenome assembly and data sets; transect and redoxcline.
SRR3727517	191	39.14	39.1	SAMN05150094	Baltic Sea (Asko 2011) Metagenomes
SRR16282464	190	38.93	38.9	SAMN22190875	Metagenomic investigation of antibiotic resistance genes in aquacultural farms in Vietnam
SRR6319734	171	35.04	35.0	SAMN08093733	marine metagenome Metagenome
SRR15221283	162	33.2	33.2	SAMN19735983	study the efficiency of preservation
SRR3747824	152	31.15	31.1	SAMN04943415	Baltic Sea Metatranscriptomes 2009-2012
SRR6787537	148	30.33	30.3	SAMN08606345	Coupling biogeochemical process rates and metagenomic blueprints of coastal bacterial assemblages in the context of environmental change in the Baltic Sea Metagenome
ERR3534981	141	28.89	28.9	SAMEA5789077	Metagenomes of epibacterial communities of Agarophyton vermiculophyllum varying salinity

I examined the top 100 datasets and categorized them using their metadata (Figure 4.17). The analysis reveals that BapP-related sequences can be found broadly within marine metagenomes associated with biofilm samples and also on the surfaces of marine eukaryotic hosts, consistent with the known biology of *Pseudoalteromonas* species.

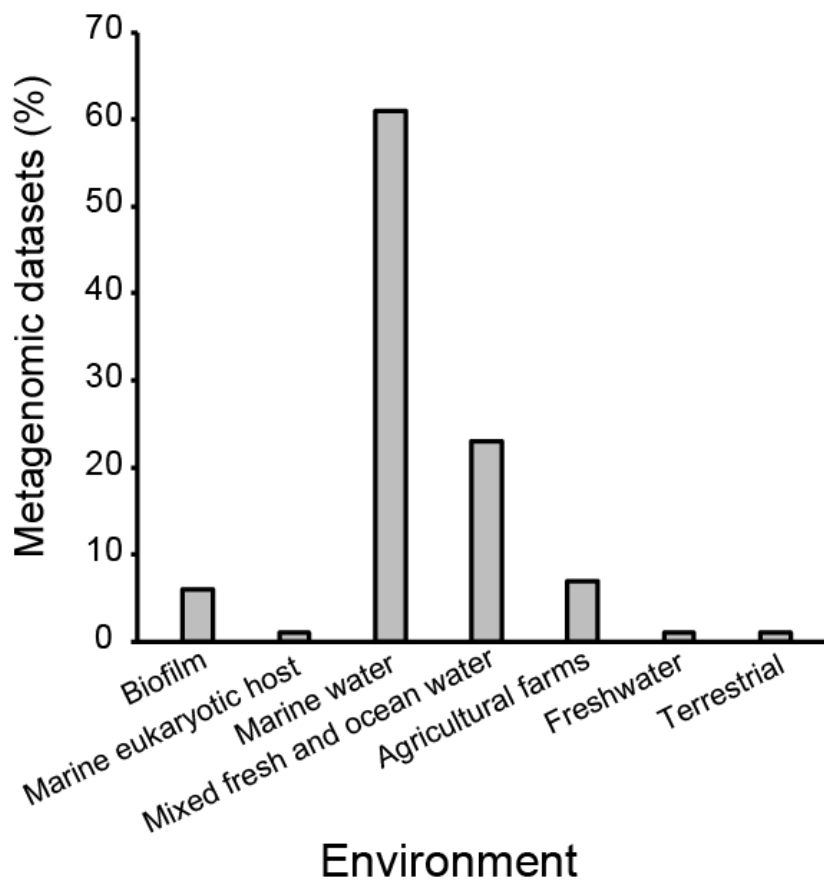


Figure 4.17. Categories of metagenomic datasets containing *Pseudoalteromonas tunicata* BapP genes identified using PebbleScout. The top 100 BapP-containing datasets were retrieved using PebbleScout (Shiryev & Agarwala, 2024) from the NCBI Sequence Read Archive, and summarized based on metadata. The analysis reveals frequent occurrence of *P. tunicata* BapP sequences in marine metagenomes and biofilms.

4.4 Discussion

Biofilm-formation by marine bacteria is critical for marine microbial ecology and also has substantial economic implications (Carvalho, 2018). This study established the role of a

novel protein, EAR30327, identified as the top biofilm-associated protein in *P. tunicata*, a bacterium with ecologically important roles in marine biofilms. In particular, this work identified EAR30327 as novel Ca²⁺-dependent adhesin and related species, which I confirmed experimentally as playing a key role in biofilm formation. I designated this protein *Pseudoalteromonas tunicata* biofilm adhesin protein or BapP.

Sequence and structural analysis of EAR30327 (BapP) predicted it as a putative adhesin protein. Alphafold modeling combined with sequence analysis produced a structural model consisting of a unique N-terminal 5-bladed propeller followed by 12 tandem beta-sandwich repeats similar to those found in other non-fibrillar, bacterial associated protein (bap) adhesins (Berne et al., 2015). The beta-sandwich repeats appear to match previous sequence models of immunoglobulin (BIG) domains as well as cadherin-like (CDHL) domains, which are present in other bacterial adhesins (Cao et al., 2005; Vance et al., 2020). For instance, tandem CDHL domains are found in the giant RTX adhesin, SiiE, from *Salmonella enterica* (Peters et al., 2017), and also the large, secreted proteins (e.g., CabD and CabC) from the marine bacterium, *Saccharophagus degradans*, which mediates Ca²⁺-dependent homophilic and heterophilic interactions (Peters et al., 2017) and has carbohydrate-binding activity (Fraiberg et al., 2011). Despite the similarities of BapP to adhesins such as LapA and CadB, only a portion of the BapP repeats align with other adhesins suggesting that they may have diverged substantially from those in related proteins and undergone independent tandem duplication in a progenitor of the BapP family. In addition, the N-terminal beta-propeller domain appears to be a unique feature of *P. tunicata* BapP and also its close homologs which include BapP-related proteins in other *Pseudoalteromonas* species as well as a divergent paralog identified in the *P. tunicata* genome (EAR26681).

As predicted by my proteomic analysis and the bioinformatic analysis of the BapP sequence and structure, the $\Delta bapP$ knockout mutant was defective in forming robust pellicle biofilms and had a significant reduction in biofilm formation based on crystal violet assays. Biofilm formation in the WT strain was also found to be Ca²⁺-dependent, and this effect was

significantly reduced in $\Delta bapP$. These results suggest that BapP may function like other bacterial Ca^{2+} -dependent adhesins. Given the functional and structural similarity of BapP to Baps, there are several outstanding questions. First, the mechanism for BapP secretion is currently unclear. The LapA adhesin, like other Bap/RTX adhesins that are secreted by the T1SS, requires its own tripartite complex (LapEBC) for secretion but remains tethered to the cell surface through a cleavable N-terminal retention module (Smith et al., 2018). Given that the genomic neighborhood of *P. tunicata* BapP encodes several components of ABC transporters, and that homologs of BapP (e.g., WP_284601796.1) outside of *P. tunicata* are encoded adjacent to the *tolC* gene, it is tempting to speculate that BapP may also be secreted through a T1SS mechanism. However, one feature that favors a different mechanism is the predicted Sec/SPI signal peptide at the N-terminus of BapP. The presence of this Sec signal suggests that BapP is first directed to the periplasm as an intermediate and is then secreted as a passenger through a separate transport mechanism. One possibility is that, after translocation to the periplasm, BapP is secreted extracellularly through a type II secretion system, or through a beta-barrel transporter (e.g., BamA) such as those used by the Type V secretion system. However, unlike adhesins secreted by the type Vb or two-Partner Secretion (TPS) system, it lacks the typical beta-helical or beta-solenoid structure found in TPS secreted adhesins (Kajava & Steven, 2006).

A second outstanding question concerns the molecular mechanism underlying the role of BapP in biofilm formation. The presence of cadherin-like and bacterial immunoglobulin (BIG) domains provide hints given the known mechanism of other bacterial adhesins that possess these domains (Guo et al., 2019). For example, it has been shown that the addition of calcium plays a role in rigidifying the tandem beta-sandwich “extender” regions of RTX adhesins, allowing them to project extracellularly and reach their targets (Vance et al., 2020).

In other cell-surface adhesins such as the CHDL domain-containing *Rhizobium*-adhering protein RapA2, it has been demonstrated that RapA2 acts as a lectin and binds to acidic exopolysaccharides in a calcium-dependent manner (Abdian et al., 2013). Future work is required to determine the nature of BapP calcium-dependent interactions and targets, and

its relative importance in mediating adhesion to biotic surfaces, abiotic surfaces, cell-cell adhesion, EPS and biofilm matrix, or perhaps other adhesive functions that could influence biofilm formation.

There are several limitations of my study that should be addressed by future research on BapP and similar adhesins in related bacterial species. The limitation that is worth mentioning is that my bioinformatic analysis of the BapP protein was complicated by the lack of homologs of known structure of function. This was overcome in part using Alphafold modeling combined with sequence analysis (Jumper et al., 2021), but the true structure of BapP may deviate from the prediction. Although sequence similarities to other proteins were detected in the repetitive regions (e.g., through BLAST), artifactual alignments can occur between repetitive sequences (Pertselidis & Fondon, 2001). Nonetheless, the predicted structural model of BapP, domain composition, and detected relationships to other adhesin proteins (even if distant), provided a functional hypothesis that was confirmed experimentally. Together my data strongly suggests that this protein forms a unique family of adhesins and may also possess unique properties regarding its function in biofilms, interactions, and secretion mechanism.

Chapter 5

Discussions/conclusion

5.1 Summary

Biofilms are complex multicellular communities that are essential to microbial ecology in marine environments (Antunes et al., 2019; Qian et al., 2022). However, the molecular mechanisms that govern their development and resilience remain incompletely understood, especially in lesser studied, non-model organisms. The overarching aim of this thesis has been to elucidate the proteomic determinants of biofilm development in *Pseudoalteromonas tunicata*, with a focus on identification and characterization of proteins of unknown functions that are potentially critical to biofilm formation and maintenance.

Chapter 1 introduced biofilm formation, the ecological significance of *P. tunicata*, and the rationale for studying its proteome in the context of biofilm development.

Chapter 2 presented the results of a proteomic survey, where advanced techniques such as LC-MS/MS shotgun proteomics and bioinformatic analyses were employed to identify key proteins associated with different stages of biofilm development. The use of LC-MS/MS shotgun proteomics had a substantial advantage over traditional methods of protein comparison because it enabled quantification of many proteins within what can be a highly complex and technically challenging mixture of proteins and other compounds – the biofilm matrix. Through LC-MS/MS shotgun proteomics, I identified hundreds of biofilm-associated proteins, revealing temporal patterns of protein expression, including novel proteins with potential roles in biofilm resilience and architecture. Through a comprehensive proteomic analysis, several key proteins associated with biofilm development were identified, including EAR30327 (BapP) and EAR28894 (Slr4). Both of these proteins were selected for further study because: 1) they were hypothetical proteins associated with biofilms; 2) they stood out statistically from all others; EAR30327 was the top biofilm-associated protein by differential

abundance analysis (number 1 ranked in *p*value), and EAR28894 was the most abundant hypothetical protein detected in biofilms.

Chapter 3 then focused on the characterization of EAR28894. This protein was demonstrated to be an S-layer protein (Slr4) providing a protective layer not only around cells but also around biofilm matrix components. Based on this observation, I speculate that Slr4 plays a role in biofilm matrix protection in *P. tunicata* and also in other marine Gammaproteobacteria.

Chapter 4 then detailed the characterization of EAR30327. This protein was demonstrated to be an adhesin protein (BapP), which provides *P. tunicata* with a critical function in surface adhesion. Structural and functional analyses indicated that BapP likely mediates biofilm stability through calcium-dependent mechanisms, potentially involving novel secretion pathways.

Together this thesis integrates findings from studies of biofilm formation in *P. tunicata*, focusing on the roles of key proteins such as BapP and Slr4. These discoveries highlight the adaptive strategies employed by *P. tunicata* to thrive in marine environments through the evolution of unique surface-associated proteins.

5.2 Additional biofilm-associated proteins during biofilm formation in *Pseudoalteromonas tunicata*

Although I focused on two proteins for further characterization in this thesis, below I discuss additional proteins detected among the list of 232 that were significantly biofilm-associated. These proteins provide additional insights into biofilm regulatory pathways in *P. tunicata*, and also provide starting points for future work.

Putative TonB-dependent Receptors (TBDTs): TBDTs are enriched in outer membrane vesicles (OMVs) and the bacterial outer membrane. These OMVs have been shown to exhibit higher spectral counts of TBDTs than cell membranes (Veith et al., 2015). Such proteins, which are beta-barrel proteins, bind to and transport ferric chelates (siderophores), vitamin B12, nickel complexes, and carbohydrates. This process requires energy in the form of a proton motive force and involves a complex of three inner membrane proteins, TonB-ExbB-ExbD (Fujita et al., 2019). Tang et al. (2012) found that members of the Gammaproteobacteria utilize specific TBDTs to hydrolyze polysaccharides in a marine environment, which can enhance biofilm formation. The involvement of the TonB system in the transport of large macromolecules like phage DNA and bacteriocins has been well-documented (Llobès et al., 2001). Specifically, in *Salmonella enterica* serotype Enteritidis, bacteriophage H8 was shown to be TonB-dependent (Rabsch et al., 2007). In the context of *P. tunicata*, TonB-dependent receptors likely play a crucial role in nutrient acquisition during biofilm formation, making this system essential for biofilm development and stability in nutrient-limited marine environments.

The bifunctional enzyme 2',3'-cyclic Nucleotide 2'-phosphodiesterase/3'-nucleotidase Bifunctional Periplasmic Precursor Protein: This protein is responsible for degrading ribonucleic acid by catalyzing the conversion of 2',3'-cyclic nucleotide to a 3'-nucleotide, followed by the conversion of the 3'-nucleotide to the corresponding nucleoside and phosphate (The UniProt Consortium et al., 2023). Synthesized as a precursor protein, it undergoes signal sequence removal upon export to the periplasm (López-Villamizar et al., 2016). The extracellular DNA released during biofilm formation is degraded by this enzyme, which allows *P. tunicata* to utilize nucleotides as a nutrient source (Lennon, 2007). In biofilm environments, the degradation of eDNA stabilizes the biofilm matrix and provides resistance against antibiotics and degrading agents (Allesen-Holm et al., 2006; Jennings et al., 2015). This enzyme's ability to degrade eDNA makes it significant in biofilm

development by maintaining the structural integrity and providing resistance against external stresses, contributing to the robustness of *P. tunicata* biofilms.

Resistance-nodulation-division (RND) transporters: RND transporters, including TriA and TriB fusion proteins, are essential for efflux pump function (Mima et al., 2007). These efflux pumps, which are among the most clinically significant in Gram-negative bacteria, consist of a cytoplasmic membrane pump, a periplasmic adaptor protein, and an outer membrane protein channel (Nikaido & Takatsuka, 2009; Piddock, 2006). In biofilm-forming bacteria, RND efflux pumps play a critical role in exporting extracellular polymeric substances and noxious substances, such as antibiotics, into the external environment. This efflux activity helps biofilms tolerate antibiotics and disinfectants, not through genetic changes but through survival mechanisms in the biofilm lifestyle (Corona & Martinez, 2013). In *P. tunicata*, these efflux pumps may also be involved in quorum sensing, influencing adhesion, quorum quenching, and the efflux of harmful molecules (Alav et al., 2018), all of which contribute to biofilm stability and antibiotic resistance.

ATP-binding cassette (ABC) transporters: ABC transporters are part of a large superfamily that transports substrates across cellular membranes, mediating nutrient uptake using energy derived from ATP hydrolysis (H.-B. Yang et al., 2018). Some ABC transporters have been shown to negatively regulate biofilm formation (Zhu et al., 2008), while ATP-binding proteins (ABPs) provide the energy necessary to drive these transport processes. The loss of an ABC permease results in defective biofilm formation and reduced pathogenicity (Kiran et al., 2009). In the context of *P. tunicata*, ABC transporters likely contribute to the regulation of nutrient acquisition and biofilm architecture, impacting both biofilm integrity and bacterial survival in marine environments.

Among the list of 232 biofilm-associated proteins there are also Ferric Siderophore Receptor proteins, secreted proteases, and PKD-domain containing proteins, all of which have been linked to roles within biofilms. Putative Exogenous Ferric Siderophore Receptors are vital for bacterial iron acquisition, which is essential for metabolism and biofilm development (Zago & Chugani, 2009). In *P. tunicata*, these receptors likely facilitate biofilm formation by promoting siderophore-mediated iron uptake in iron-limited marine environments, enhancing virulence and biofilm growth (Johnson et al., 2005). Secreted serine proteases, such as those in the subtilisin family, affect various host functions and inhibit the biofilm formation of other microorganisms (Vandecandelaere et al., 2014). In *P. tunicata*, serine proteases contribute to bacterial adhesion and are involved in biofilm formation (Klemm et al., 2006). The PKD (Polycystic Kidney Disease) domain, originally identified in the polycystic kidney disease protein (Bycroft et al., 1999), is also found in the extracellular regions of proteins involved in interactions, including S-layer proteins in archaea. In *P. tunicata*, PKD domains likely play a role in protein-protein and protein-carbohydrate interactions, crucial for biofilm stability and structure (Bycroft et al., 1999; Jing et al., 2002).

The identified biofilm-associated proteins in *P. tunicata* play a wide variety of important roles in maintaining biofilm integrity, facilitating nutrient acquisition, and enhancing resistance to environmental stresses. By understanding these mechanisms, I gain valuable insights into the unique biofilm lifestyle of *P. tunicata*, with implications for marine biofilm formation and potential applications in biofilm management strategies.

5.3 BapP: insights and future questions

The discovery of BapP provides new insights into the mechanisms of biofilm adhesion and stability in marine environments. The results from Chapter 4 suggest that BapP likely acts as a Ca²⁺-dependent biofilm adhesin, which is crucial for the early stages of biofilm formation. The knockout of the *bapP* gene resulted in a significant reduction in biofilm formation both on the surface of centrifuge tubes and in pellicles, highlighting its essential role. However, it

is difficult to determine at this point whether BapP plays more of a role in early reversible (transient) adhesion, or the later irreversible adhesion. Given the significant increase in BapP abundance from the planktonic to biofilm stage, I hypothesize that its function is more associated with irreversible binding to the surface and between cells in a Ca^{2+} -dependent manner.

Given that the BapP knockout does not completely lose its ability to form biofilms with increasing Ca^{2+} levels, this suggests that there exist additional Ca-dependent adhesins or mechanisms that may contribute to biofilm formation in *P. tunicata*. Indeed, analysis of the *P. tunicata* proteome revealed numerous candidates, such as another BapP-related protein (EAR26681, PTD2_17117). Future studies that perform multiple knockouts of these adhesins may be helpful in determining their relative contribution to adhesion and biofilm formation.

The structural analysis suggests that BapP shares similarities with other bacterial adhesins. Structural analyses revealed that BapP contains a unique N-terminal beta-propeller domain and multiple beta-sandwich repeats, which resemble bacterial immunoglobulin (BIG) and cadherin-like (CDHL) domains found in other bacterial adhesins. These structural features suggest that BapP facilitates cell-cell and cell-surface adhesion in a calcium-dependent manner, contributing to the formation and maintenance of robust biofilms (P. Tiwari et al., 2018). However, the unique N-terminal beta-propeller domain of BapP in *P. tunicata* suggests a novel mechanism of action or anchoring role for this part of the protein. While the structural analysis provided a model for BapP function, the absence of homologous proteins with known structures limits my ability to predict its precise role within the biofilm matrix. Future research should focus on identifying the secretion pathway of BapP and its interactions with other biofilm components to fully understand its role in biofilm formation.

5.4 Slr4: insights and future questions

Regarding Slr4, the results from this study generate new insights into the function of S-layer proteins in *P. tunicata*, but also more broadly for S-layer proteins in general. In particular,

the observation of Slr4 shedding into the extracellular matrix and detection of increased Slr4 in biofilms implicates S-layer proteins as major components of the biofilm matrix. Since this finding, another study has been published that supports a biofilm matrix role for S-layer proteins (Wong et al., 2023). Wong et al. have shown that an S-layer protein from anammox bacteria are part of the biofilm matrix and act as adhesive structures that help to form the three-dimensional multicellular biofilm lattice. The authors described the S-layer as a “public good” EPS constituent, providing a function to promote the assembly of other bacteria within the biofilm and therefore providing broad benefit to the microbial community.

Building on this idea of S-layer proteins serving as a biofilm structural component, it would be interesting in future work to explore the role of Slr4 in multi-species biofilms. Further investigation of the Slr4 knockout mutant to explore phenotypic and fitness advantages that the WT provides in a biofilm context is also needed. This is a challenging goal as the functions of S-layer proteins are elusive even in the context of planktonic bacteria.

The precise molecular interactions between Slr4 and other biofilm components, such as outer membrane vesicles and filamentous structures, are also not fully understood. Future studies focusing on characterizing the structural dynamics of Slr4 using advanced techniques such as cryo-EM could be helpful to elucidate its structural role in biofilm formation. Lastly, the evolutionary behaviour of Slr4-related proteins among marine Gammaproteobacteria raises questions about the evolutionary pressures that have shaped these proteins' functions, and the reasons for their apparent rapid sequence evolution and divergence.

5.5 Concluding Remarks

This thesis combines three studies to investigate novel molecular determinants of biofilm formation in *Pseudoalteromonas tunicata*. The discovery of BapP and Slr4 highlight the adaptive strategies employed by *P. tunicata* to thrive in marine environments, particularly

through the evolution of unique surface-associated proteins. The identification of BapP and Slr4 as critical components of the biofilm matrix supports the hypothesis that biofilm-associated proteins are essential for biofilm development and stability. Additionally, the studies highlight the dynamic nature of protein expression during different biofilm developmental stages, providing new insights into the temporal regulation of biofilm formation.

Structural and functional analyses indicated that BapP likely mediates biofilm stability through calcium-dependent mechanisms, potentially involving unique secretion pathways. The hypothesis that BapP functions similarly to other bacterial adhesins is strongly supported by the structural and functional analyses. The discovery of calcium-dependent adhesion further validates the proposed mechanism of action.

The hypothesis regarding Slr4's role in biofilm matrix protection is supported by the observed abundance of S-layer material in biofilms and the protective functions associated with S-layer proteins in other bacteria. The discussion highlights the critical roles of BapP and Slr4 in biofilm formation and maintenance, emphasizing their distinct functions and contributions to biofilm resilience in marine environments. The findings advance our understanding of biofilm dynamics and provide a foundation for future research in microbial ecology and biofilm control strategies.

The research in this thesis revealed the complex interplay between different biofilm-associated proteins and their contributions to biofilm stability and adaptation. Unexpected findings, such as the unique structural features of BapP and the abundance of Slr4 in biofilms, have opened new directions for research into biofilm formation and function.

The findings of this thesis research underscore the complexity of biofilm formation in marine environments and highlight the importance of unique surface-associated proteins in mediating biofilm development and resilience. The identification of BapP and Slr4, along with other novel proteins, provides a foundation for future research into the molecular

mechanisms governing biofilm formation and the evolutionary pressures driving these adaptations in marine microbial communities.

References

- Abdian, P. L., Caramelo, J. J., Ausmees, N., & Zorreguieta, A. (2013). RapA2 Is a Calcium-binding Lectin Composed of Two Highly Conserved Cadherin-like Domains That Specifically Recognize *Rhizobium leguminosarum* Acidic Exopolysaccharides. *Journal of Biological Chemistry*, 288(4), 2893–2904. <https://doi.org/10.1074/jbc.M112.411769>
- Agarwal, H., Bajpai, S., Mishra, A., Kohli, I., Varma, A., Fouillaud, M., Dufossé, L., & Joshi, N. C. (2023). Bacterial Pigments and Their Multifaceted Roles in Contemporary Biotechnology and Pharmacological Applications. *Microorganisms*, 11(3), 614. <https://doi.org/10.3390/microorganisms11030614>
- Alav, I., Sutton, J. M., & Rahman, K. M. (2018). Role of bacterial efflux pumps in biofilm formation. *Journal of Antimicrobial Chemotherapy*, 73(8), 2003–2020. <https://doi.org/10.1093/jac/dky042>
- Ali, S., Jenkins, B., Cheng, J., Lobb, B., Wei, X., Egan, S., Charles, T. C., McConkey, B. J., Austin, J., & Doxey, A. C. (2020). Slr4, a newly identified S-layer protein from marine *Gammaproteobacteria*, is a major biofilm matrix component. *Molecular Microbiology*, 114(6), 979–990. <https://doi.org/10.1111/mmi.14588>
- Ali, S., Jenkins, B., & Doxey, A. (2020). Complete proteomics (LC-MS/MS) dataset of *Pseudoalteromonas tunicata* planktonic and biofilm cultures. (p. 193212416 Bytes) [Dataset]. figshare. <https://doi.org/10.6084/M9.FIGSHARE.11993505.V1>
- Allesen-Holm, M., Barken, K. B., Yang, L., Klausen, M., Webb, J. S., Kjelleberg, S., Molin, S., Givskov, M., & Tolker-Nielsen, T. (2006). A characterization of DNA release in *Pseudomonas aeruginosa* cultures and biofilms. *Molecular Microbiology*, 59(4), 1114–1128. <https://doi.org/10.1111/j.1365-2958.2005.05008.x>

- An, S., Wu, J., & Zhang, L.-H. (2010). Modulation of *Pseudomonas aeruginosa* Biofilm Dispersal by a Cyclic-Di-GMP Phosphodiesterase with a Putative Hypoxia-Sensing Domain. *Applied and Environmental Microbiology*, 76(24), 8160–8173. <https://doi.org/10.1128/AEM.01233-10>
- Antunes, J., Leão, P., & Vasconcelos, V. (2019). Marine biofilms: Diversity of communities and of chemical cues. *Environmental Microbiology Reports*, 11(3), 287–305. <https://doi.org/10.1111/1758-2229.12694>
- Arbing, M. A., Chan, S., Shin, A., Phan, T., Ahn, C. J., Rohlin, L., & Gunsalus, R. P. (2012). Structure of the surface layer of the methanogenic archaean *Methanosarcina acetivorans*. *Proceedings of the National Academy of Sciences of the United States of America*, 109(29), 11812–11817. <https://doi.org/10.1073/pnas.1120595109>
- Asma, S. T., Imre, K., Morar, A., Imre, M., Acaroz, U., Shah, S. R. A., Hussain, S. Z., Arslan-Acaroz, D., Istanbulgil, F. R., Madani, K., Athanassiou, C., Atanasoff, A., Morar, D., Herman, V., & Zhu, K. (2022). Natural Strategies as Potential Weapons against Bacterial Biofilms. *Life*, 12(10), Article 10. <https://doi.org/10.3390/life12101618>
- Awram, P., & Smit, J. (1998). The *Caulobacter crescentus* paracrystalline S-layer protein is secreted by an ABC transporter (type I) secretion apparatus. *Journal of Bacteriology*, 180(12), 3062–3069.
- Back, C. R., Sztukowska, M. N., Till, M., Lamont, R. J., Jenkinson, H. F., Nobbs, A. H., & Race, P. R. (2017). The *Streptococcus gordonii* Adhesin CshA Protein Binds Host Fibronectin via a Catch-Clamp Mechanism. *Journal of Biological Chemistry*, 292(5), 1538–1549. <https://doi.org/10.1074/jbc.M116.760975>
- Ballestrero, F., Thomas, T., Burke, C., Egan, S., & Kjelleberg, S. (2010). Identification of compounds with bioactivity against the nematode *Caenorhabditis elegans* by a screen based on the functional genomics of the marine bacterium *Pseudoalteromonas tunicata* D2. *Applied*

- and Environmental Microbiology*, 76(17), 5710–5717. <https://doi.org/10.1128/AEM.00695-10>
- Baranova, E., Fronzes, R., Garcia-Pino, A., Van Gerven, N., Papapostolou, D., Péhau-Arnaudet, G., Pardon, E., Steyaert, J., Howorka, S., & Remaut, H. (2012). SbsB structure and lattice reconstruction unveil Ca²⁺ triggered S-layer assembly. *Nature*, 487(7405), 119–122. <https://doi.org/10.1038/nature11155>
- Baraquet, C., & Harwood, C. S. (2016). FleQ DNA Binding Consensus Sequence Revealed by Studies of FleQ-Dependent Regulation of Biofilm Gene Expression in *Pseudomonas aeruginosa*. *Journal of Bacteriology*, 198(1), 178–186. <https://doi.org/10.1128/JB.00539-15>
- Barken, K. B., Pamp, S. J., Yang, L., Gjermansen, M., Bertrand, J. J., Klausen, M., Givskov, M., Whitchurch, C. B., Engel, J. N., & Tolker-Nielsen, T. (2008). Roles of type IV pili, flagellum-mediated motility and extracellular DNA in the formation of mature multicellular structures in *Pseudomonas aeruginosa* biofilms. *Environmental Microbiology*, 10(9), 2331–2343. <https://doi.org/10.1111/j.1462-2920.2008.01658.x>
- Barnhart, M. M., & Chapman, M. R. (2006). Curli Biogenesis and Function. *Annual Review of Microbiology*, 60(1), 131–147. <https://doi.org/10.1146/annurev.micro.60.080805.142106>
- Beebout, C. J., Eberly, A. R., Werby, S. H., Reasoner, S. A., Brannon, J. R., De, S., Fitzgerald, M. J., Huggins, M. M., Clayton, D. B., Cegelski, L., & Hadjifrangiskou, M. (2019). Respiratory Heterogeneity Shapes Biofilm Formation and Host Colonization in Uropathogenic *Escherichia coli*. *mBio*, 10(2), 10.1128/mbio.02400-18. <https://doi.org/10.1128/mbio.02400-18>
- Belas, R. (2014). Biofilms, flagella, and mechanosensing of surfaces by bacteria. *Trends in Microbiology*, 22(9), 517–527. <https://doi.org/10.1016/j.tim.2014.05.002>

- Benjamini, Y., & Hochberg, Y. (1995). Controlling the False Discovery Rate: A Practical and Powerful Approach to Multiple Testing. *Journal of the Royal Statistical Society. Series B (Methodological)*, 57(1), 289–300.
- Bernbom, N., Ng, Y. Y., Olsen, S. M., & Gram, L. (2013). *Pseudoalteromonas* spp. Serve as Initial Bacterial Attractants in Mesocosms of Coastal Waters but Have Subsequent Antifouling Capacity in Mesocosms and when Embedded in Paint. *Applied and Environmental Microbiology*, 79(22), 6885–6893. <https://doi.org/10.1128/AEM.01987-13>
- Berne, C., Ducret, A., Hardy, G. G., & Brun, Y. V. (2015). Adhesins Involved in Attachment to Abiotic Surfaces by Gram-Negative Bacteria. *Microbiology Spectrum*, 3(4). <https://doi.org/10.1128/microbiolspec.MB-0018-2015>
- Berne, C., Ellison, C. K., Ducret, A., & Brun, Y. V. (2018). Bacterial adhesion at the single-cell level. *Nature Reviews Microbiology*, 16(10), 616–627. <https://doi.org/10.1038/s41579-018-0057-5>
- Beulin, D. S. J., Yamaguchi, M., Kawabata, S., & Ponnuraj, K. (2014). Crystal structure of PfbA, a surface adhesin of *Streptococcus pneumoniae*, provides hints into its interaction with fibronectin. *International Journal of Biological Macromolecules*, 64, 168–173. <https://doi.org/10.1016/j.ijbiomac.2013.11.035>
- Beurmann, S., Ushijima, B., Svoboda, C. M., Videau, P., Smith, A. M., Donachie, S. P., Aeby, G. S., & Callahan, S. M. (2017). *Pseudoalteromonas piratica* sp. Nov., a budding, prosthecate bacterium from diseased *Montipora capitata*, and emended description of the genus *Pseudoalteromonas*. *International Journal of Systematic and Evolutionary Microbiology*, 67(8), 2683–2688. <https://doi.org/10.1099/ijsem.0.001995>
- Beveridge, T. J. (1994). Bacterial S-layers. *Current Opinion in Structural Biology*, 4(2), 204–212. [https://doi.org/10.1016/S0959-440X\(94\)90309-3](https://doi.org/10.1016/S0959-440X(94)90309-3)

- Beveridge, T. J., Pouwels, P. H., Sára, M., Kotiranta, A., Lounatmaa, K., Kari, K., Kerosuo, E., Haapasalo, M., Egelseer, E. M., Schocher, I., Sleytr, U. B., Morelli, L., Callegari, M. L., Nomellini, J. F., Bingle, W. H., Smit, J., Leibovitz, E., Lemaire, M., Miras, I., Koval, S. F. (1997). Functions of S-layers. *FEMS Microbiology Reviews*, *20*(1–2), 99–149. <https://doi.org/10.1111/j.1574-6976.1997.tb00305.x>
- Bharat, T. A. M., Kureisaite-Ciziene, D., Hardy, G. G., Yu, E. W., Devant, J. M., Hagen, W. J. H., Brun, Y. V., Briggs, J. A. G., & Löwe, J. (2017). Structure of the hexagonal surface layer on *Caulobacter crescentus* cells. *Nature Microbiology*, *2*(7), 17059. <https://doi.org/10.1038/nmicrobiol.2017.59>
- Boltz, J. P., Smets, B. F., Rittmann, B. E., Van Loosdrecht, M. C. M., Morgenroth, E., & Daigger, G. T. (2017). From biofilm ecology to reactors: A focused review. *Water Science and Technology*, *75*(8), 1753–1760. <https://doi.org/10.2166/wst.2017.061>
- Boot, H. J., & Pouwels, P. H. (1996). Expression, secretion and antigenic variation of bacterial S-layer proteins. *Molecular Microbiology*, *21*(6), 1117–1123. <https://doi.org/10.1046/j.1365-2958.1996.711442.x>
- Bowman, J. P. (2007). Bioactive Compound Synthetic Capacity and Ecological Significance of Marine Bacterial Genus *Pseudoalteromonas*. *Mar. Drugs*.
- Boyd, C. D., Smith, T. J., El-Kirat-Chatel, S., Newell, P. D., Dufrière, Y. F., & O’Toole, G. A. (2014). Structural Features of the *Pseudomonas fluorescens* Biofilm Adhesin LapA Required for LapG-Dependent Cleavage, Biofilm Formation, and Cell Surface Localization. *Journal of Bacteriology*, *196*(15), 2775–2788. <https://doi.org/10.1128/JB.01629-14>
- Bradford, M. M. (1976). A rapid and sensitive method for the quantitation of microgram quantities of protein utilizing the principle of protein-dye binding. *Analytical Biochemistry*, *72*(1–2), 248–254. [https://doi.org/10.1016/0003-2697\(76\)90527-3](https://doi.org/10.1016/0003-2697(76)90527-3)

- Braithwaite, R. A., & McEvoy, L. A. (2004). Marine Biofouling on Fish Farms and Its Remediation. *Advances in Marine Biology*, 47, 215–252. [https://doi.org/10.1016/S0065-2881\(04\)47003-5](https://doi.org/10.1016/S0065-2881(04)47003-5)
- Burden, D. W. (2008). *Guide to the Homogenization of Biological Samples*. 7.
- Bycroft, M., Bateman, A., Clarke, J., Hamill, S. J., Sandford, R., Thomas, R. L., & Chothia, C. (1999). The structure of a PKD domain from polycystin-1: Implications for polycystic kidney disease. *The EMBO Journal*, 18(2), 297–305. <https://doi.org/10.1093/emboj/18.2.297>
- Cao, B., Shi, L., Brown, R. N., Xiong, Y., Fredrickson, J. K., Romine, M. F., Marshall, M. J., Lipton, M. S., & Beyenal, H. (2011). Extracellular polymeric substances from *Shewanella* sp. HRCR-1 biofilms: Characterization by infrared spectroscopy and proteomics. *Environmental Microbiology*, 13(4), 1018–1031. <https://doi.org/10.1111/j.1462-2920.2010.02407.x>
- Cao, L., Yan, X., Borysenko, C. W., Blair, H. C., Wu, C., & Yu, L. (2005). CHDL: A cadherin-like domain in Proteobacteria and Cyanobacteria. *FEMS Microbiology Letters*, 251(2), 203–209. <https://doi.org/10.1016/j.femsle.2005.08.004>
- Carrier, A., Pessi, G., & Eberl, L. (2015). Microbial Biofilms and Quorum Sensing. In B. Lugtenberg (Ed.), *Principles of Plant-Microbe Interactions*, 45–52. Springer International Publishing. https://doi.org/10.1007/978-3-319-08575-3_7
- Carvalho, C. C. R. de C. (2018). Marine Biofilms: A Successful Microbial Strategy With Economic Implications. *Frontiers in Marine Science*, 5. <https://doi.org/10.3389/fmars.2018.00126>
- Chandramohan, A., Duprat, E., Remusat, L., Severine, Z., Lombard, C., & Kish, A. (2019). *Frontiers / Novel Mechanism for Surface Layer Shedding and Regenerating in Bacteria Exposed to Metal-Contaminated Conditions*. *Frontiers in Microbiology*, 9. <https://doi.org/10.3389/fmicb.2018.03210>

- Chang, C.-Y. (2018). Surface Sensing for Biofilm Formation in *Pseudomonas aeruginosa*. *Frontiers in Microbiology*, 8, 2671. <https://doi.org/10.3389/fmicb.2017.02671>
- Chapman, M. R., Robinson, L. S., Pinkner, J. S., Roth, R., Heuser, J., Hammar, M., Normark, S., & Hultgren, S. J. (2002). Role of *Escherichia coli* Curli Operons in Directing Amyloid Fiber Formation. *Science*, 295(5556), 851–855. <https://doi.org/10.1126/science.1067484>
- Christensen, D. G., Marsden, A. E., Hodge-Hanson, K., Essock-Burns, T., & Visick, K. L. (2020). LapG mediates biofilm dispersal in *Vibrio fischeri* by controlling maintenance of the VCBS-containing adhesin LapV. *Molecular Microbiology*, 114(5), 742–761. <https://doi.org/10.1111/mmi.14573>
- Cooke, A. C., Florez, C., Dunshee, E. B., Lieber, A. D., Terry, M. L., Light, C. J., & Schertzer, J. W. (2020). *Pseudomonas* Quinolone Signal-Induced Outer Membrane Vesicles Enhance Biofilm Dispersion in *Pseudomonas aeruginosa*. *mSphere*, 5(6), e01109-20. <https://doi.org/10.1128/mSphere.01109-20>
- Corona, F., & Martinez, J. (2013). Phenotypic Resistance to Antibiotics. *Antibiotics*, 2(2), 237–255. <https://doi.org/10.3390/antibiotics2020237>
- Dalisay, D. S., Webb, J. S., Scheffel, A., Svenson, C., James, S., Holmström, C., Egan, S., & Kjelleberg, S. (2006). A mannose-sensitive haemagglutinin (MSHA)-like pilus promotes attachment of *Pseudoalteromonas tunicata* cells to the surface of the green alga *Ulva australis*. *Microbiology*, 152(10), 2875–2883. <https://doi.org/10.1099/mic.0.29158-0>
- Dang, H., & Lovell, C. R. (2015). Microbial Surface Colonization and Biofilm Development in Marine Environments. *Microbiology and Molecular Biology Reviews*, 80(1), 91–138. <https://doi.org/10.1128/mnbr.00037-15>
- Đapa, T., Leuzzi, R., Ng, Y. K., Baban, S. T., Adamo, R., Kuehne, S. A., Scarselli, M., Minton, N. P., Serruto, D., & Unnikrishnan, M. (2013). Multiple factors modulate biofilm formation by the

- anaerobic pathogen *Clostridium difficile*. *Journal of Bacteriology*, 195(3), 545–555.
<https://doi.org/10.1128/JB.01980-12>
- Davey, M. E., & O’toole, G. A. (2000). Microbial Biofilms: From Ecology to Molecular Genetics. *Microbiology and Molecular Biology Reviews*, 64(4), 847–867.
<https://doi.org/10.1128/MMBR.64.4.847-867.2000>
- Davies, J. C. (2002). *Pseudomonas aeruginosa* in cystic fibrosis: Pathogenesis and persistence. *Paediatric Respiratory Reviews*, 3(2), 128–134. [https://doi.org/10.1016/S1526-0550\(02\)00003-3](https://doi.org/10.1016/S1526-0550(02)00003-3)
- Deivanayagam, C. C. S., Wann, E. R., Chen, W., Carson, M., Rajashankar, K. R., Höök, M., & Narayana, S. V. L. (2002). A novel variant of the immunoglobulin fold in surface adhesins of *Staphylococcus aureus*: Crystal structure of the fibrinogen-binding MSCRAMM, clumping factor A. *The EMBO Journal*, 21(24), 6660–6672. <https://doi.org/10.1093/emboj/cdf619>
- Del Pozo, J. L., Rouse, M. S., & Patel, R. (2008). Bioelectric Effect and Bacterial Biofilms. A Systematic Review. *The International Journal of Artificial Organs*, 31(9), 786–795.
<https://doi.org/10.1177/039139880803100906>
- Dergham, Y., Le Coq, D., Nicolas, P., Bidnenko, E., Dérozier, S., Deforet, M., Huillet, E., Sanchez-Vizueté, P., Deschamps, J., Hamze, K., & Briandet, R. (2023). Direct comparison of spatial transcriptional heterogeneity across diverse *Bacillus subtilis* biofilm communities. *Nature Communications*, 14(1), 7546. <https://doi.org/10.1038/s41467-023-43386-w>
- Di Biase, A., Kowalski, M. S., Devlin, T. R., & Oleszkiewicz, J. A. (2019). Moving bed biofilm reactor technology in municipal wastewater treatment: A review. *Journal of Environmental Management*, 247, 849–866. <https://doi.org/10.1016/j.jenvman.2019.06.053>
- Dickschat, J. S. (2010). Quorum sensing and bacterial biofilms. *Natural Product Reports*, 27(3), 343.
<https://doi.org/10.1039/b804469b>

- Dunne, W. M. (2002). Bacterial Adhesion: Seen Any Good Biofilms Lately? *Clinical Microbiology Reviews*, 15(2), 155–166. <https://doi.org/10.1128/CMR.15.2.155-166.2002>
- Dupree, E. J., Jayathirtha, M., Yorkey, H., Mihasan, M., Petre, B. A., & Darie, C. C. (2020). A Critical Review of Bottom-Up Proteomics: The Good, the Bad, and the Future of this Field. *Proteomes*, 8(3), 14. <https://doi.org/10.3390/proteomes8030014>
- Eckhard, U., Bandukwala, H., Mansfield, M. J., Marino, G., Cheng, J., Wallace, I., Holyoak, T., Charles, T. C., Austin, J., Overall, C. M., & Doxey, A. C. (2017). Discovery of a proteolytic flagellin family in diverse bacterial phyla that assembles enzymatically active flagella. *Nature Communications*, 8(1), 521. <https://doi.org/10.1038/s41467-017-00599-0>
- Eckhard, U., Blöchl, C., Jenkins, B. G. L., Mansfield, M. J., Huber, C. G., Doxey, A. C., & Brandstetter, H. (2020). Identification and characterization of the proteolytic flagellin from the common freshwater bacterium *Hylemonella gracilis*. *Scientific Reports*, 10(1), 19052. <https://doi.org/10.1038/s41598-020-76010-8>
- Edgar, R. C. (2004). MUSCLE: Multiple sequence alignment with high accuracy and high throughput. *Nucleic Acids Research*, 32(5), 1792–1797. <https://doi.org/10.1093/nar/gkh340>
- Edwards, P., & Smit, J. (1991). A transducing bacteriophage for *Caulobacter crescentus* uses the paracrystalline surface layer protein as a receptor. *Journal of Bacteriology*, 173(17), 5568–5572. <https://doi.org/10.1128/jb.173.17.5568-5572.1991>
- Egan, S., Holmström, C., & Kjelleberg, S. (2001). *Pseudoalteromonas ulvae* sp. Nov., a bacterium with antifouling activities isolated from the surface of a marine alga. *International Journal of Systematic and Evolutionary Microbiology*, 51(Pt 4), 1499–1504. <https://doi.org/10.1099/00207713-51-4-1499>

- Egan, S., James, S., Holmström, C., & Kjelleberg, S. (2001). Inhibition of algal spore germination by the marine bacterium *Pseudoalteromonas tunicata*. *FEMS Microbiology Ecology*, 35(1), 67–73. <https://doi.org/10.1111/j.1574-6941.2001.tb00789.x>
- Egan, S., James, S., Holmström, C., & Kjelleberg, S. (2002). Correlation between pigmentation and antifouling compounds produced by *Pseudoalteromonas tunicata*. *Environmental Microbiology*, 4(8), 433–442. <https://doi.org/10.1046/j.1462-2920.2002.00322.x>
- Ellison, C. K., Whitfield, G. B., & Brun, Y. V. (2022). Type IV Pili: Dynamic bacterial nanomachines. *FEMS Microbiology Reviews*, 46(2), fuab053. <https://doi.org/10.1093/femsre/fuab053>
- Erskine, E., MacPhee, C. E., & Stanley-Wall, N. R. (2018). Functional Amyloid and Other Protein Fibers in the Biofilm Matrix. *Journal of Molecular Biology*, 430(20), 3642–3656. <https://doi.org/10.1016/j.jmb.2018.07.026>
- Evans, F. F., Egan, S., & Kjelleberg, S. (2008). Ecology of type II secretion in marine *gammaproteobacteria*. *Environmental Microbiology*, 10(5), 1101–1107. <https://doi.org/10.1111/j.1462-2920.2007.01545.x>
- Fagan, R. P., & Fairweather, N. F. (2014). Biogenesis and functions of bacterial S-layers. *Nature Reviews Microbiology*, 12(3), 211–222. <https://doi.org/10.1038/nrmicro3213>
- Faria, S. I., Teixeira-Santos, R., Gomes, L. C., Silva, E. R., Morais, J., Vasconcelos, V., & Mergulhão, F. J. M. (2020). Experimental Assessment of the Performance of Two Marine Coatings to Curb Biofilm Formation of Microfoulers. *Coatings*, 10(9), Article 9. <https://doi.org/10.3390/coatings10090893>
- Fazli, M., Almlad, H., Rybtke, M. L., Givskov, M., Eberl, L., & Tolker-Nielsen, T. (2014). Regulation of biofilm formation in *Pseudomonas* and *Burkholderia* species. *Environmental Microbiology*, 16(7), 1961–1981. <https://doi.org/10.1111/1462-2920.12448>

- Finan, T. M., Hartweig, E., LeMieux, K., Bergman, K., Walker, G. C., & Signer, E. R. (1984). General transduction in *Rhizobium meliloti*. *Journal of Bacteriology*, *159*(1), 120–124.
- Finan, T. M., Kunkel, B., De Vos, G. F., & Signer, E. R. (1986). Second symbiotic megaplasmid in *Rhizobium meliloti* carrying exopolysaccharide and thiamine synthesis genes. *Journal of Bacteriology*, *167*(1), 66–72. <https://doi.org/10.1128/jb.167.1.66-72.1986>
- Finn, R. D., Bateman, A., Clements, J., Coghill, P., Eberhardt, R. Y., Eddy, S. R., Heger, A., Hetherington, K., Holm, L., Mistry, J., Sonnhammer, E. L. L., Tate, J., & Punta, M. (2014). Pfam: The protein families database. *Nucleic Acids Research*, *42*(D1), D222–D230. <https://doi.org/10.1093/nar/gkt1223>
- Fleming, D., Niese, B., Redman, W., Vanderpool, E., Gordon, V., & Rumbaugh, K. P. (2022). Contribution of *Pseudomonas aeruginosa* Exopolysaccharides Pel and Psl to Wound Infections. *Frontiers in Cellular and Infection Microbiology*, *12*, 835754. <https://doi.org/10.3389/fcimb.2022.835754>
- Flemming, H.-C., Wingender, J., Szewzyk, U., Steinberg, P., Rice, S. A., & Kjelleberg, S. (2016). Biofilms: An emergent form of bacterial life. *Nature Reviews Microbiology*, *14*(9), 563–575. <https://doi.org/10.1038/nrmicro.2016.94>
- Flemming, H.-C., & Wuertz, S. (2019). Bacteria and archaea on Earth and their abundance in biofilms. *Nature Reviews Microbiology*, *17*(4), 247–260. <https://doi.org/10.1038/s41579-019-0158-9>
- Fong, J. N. C., & Yildiz, F. H. (2015). Biofilm Matrix Proteins. *Microbiology Spectrum*, *3*(2), 3.2.28. <https://doi.org/10.1128/microbiolspec.MB-0004-2014>
- Fraiberg, M., Borovok, I., Bayer, E. A., Weiner, R. M., & Lamed, R. (2011). Cadherin Domains in the Polysaccharide-Degrading Marine Bacterium *Saccharophagus degradans* 2-40 Are

- Carbohydrate-Binding Modules. *Journal of Bacteriology*, 193(1), 283–285.
<https://doi.org/10.1128/JB.00842-10>
- Franks, A., Egan, S., Holmström, C., James, S., Lappin-Scott, H., & Kjelleberg, S. (2006). Inhibition of Fungal Colonization by *Pseudoalteromonas tunicata* Provides a Competitive Advantage during Surface Colonization. *Applied and Environmental Microbiology*, 72(9), 6079–6087.
<https://doi.org/10.1128/AEM.00559-06>
- Friedman, L., & Kolter, R. (2004). Genes involved in matrix formation in *Pseudomonas aeruginosa* PA14 biofilms. *Molecular Microbiology*, 51(3), 675–690. <https://doi.org/10.1046/j.1365-2958.2003.03877.x>
- Fujita, M., Mori, K., Hara, H., Hishiyama, S., Kamimura, N., & Masai, E. (2019). A TonB-dependent receptor constitutes the outer membrane transport system for a lignin-derived aromatic compound. *Communications Biology*, 2(1), 432. <https://doi.org/10.1038/s42003-019-0676-z>
- Gardiner, M., Hoke, D. E., & Egan, S. (2014). An ortholog of the *Leptospira interrogans* lipoprotein LipL32 aids in the colonization of *Pseudoalteromonas tunicata* to host surfaces. *Frontiers in Microbiology*, 5. <https://doi.org/10.3389/fmicb.2014.00323>
- Ge, X., Shi, X., Shi, L., Liu, J., Stone, V., Kong, F., Kitten, T., & Xu, P. (2016). Involvement of NADH Oxidase in Biofilm Formation in *Streptococcus sanguinis*. *PLOS ONE*, 11(3), e0151142. <https://doi.org/10.1371/journal.pone.0151142>
- Geoghegan, J. A., Corrigan, R. M., Gruszka, D. T., Speziale, P., O’Gara, J. P., Potts, J. R., & Foster, T. J. (2010). Role of Surface Protein SasG in Biofilm Formation by *Staphylococcus aureus*. *Journal of Bacteriology*, 192(21), 5663–5673. <https://doi.org/10.1128/jb.00628-10>
- Gerbino, E., Carasi, P., Mobili, P., Serradell, M. A., & Gómez-Zavaglia, A. (2015). Role of S-layer proteins in bacteria. *World Journal of Microbiology and Biotechnology*, 31(12), 1877–1887.
<https://doi.org/10.1007/s11274-015-1952-9>

- Gouy, M., Guindon, S., & Gascuel, O. (2010). SeaView Version 4: A Multiplatform Graphical User Interface for Sequence Alignment and Phylogenetic Tree Building. *Molecular Biology and Evolution*, 27(2), 221–224. <https://doi.org/10.1093/molbev/msp259>
- Goyal, P., Krasteva, P. V., Van Gerven, N., Gubellini, F., Van Den Broeck, I., Troupiotis-Tsailaki, A., Jonckheere, W., Péhau-Arnaudet, G., Pinkner, J. S., Chapman, M. R., Hultgren, S. J., Howorka, S., Fronzes, R., & Remaut, H. (2014). Structural and mechanistic insights into the bacterial amyloid secretion channel CsgG. *Nature*, 516(7530), 250–253. <https://doi.org/10.1038/nature13768>
- Grudniak, A. M., Włodkowska, J., & Wolska, K. I. (2015). Chaperone DnaJ Influences the Formation of Biofilm by Escherichia coli. *Polish Journal of Microbiology*, 64(3), 279–283.
- Guindon, S., & Gascuel, O. (2003). A simple, fast, and accurate algorithm to estimate large phylogenies by maximum likelihood. *Systematic Biology*, 52(5), 696–704. <https://doi.org/10.1080/10635150390235520>
- Guo, S., Vance, T. D. R., Stevens, C. A., Voets, I., & Davies, P. L. (2019). RTX Adhesins are Key Bacterial Surface Megaproteins in the Formation of Biofilms. *Trends in Microbiology*, 27(5), 453–467. <https://doi.org/10.1016/j.tim.2018.12.003>
- Hall-Stoodley, L., Costerton, J. W., & Stoodley, P. (2004). Bacterial biofilms: From the Natural environment to infectious diseases. *Nature Reviews Microbiology*, 2(2), 95–108. <https://doi.org/10.1038/nrmicro821>
- Harris, J. R., & De Carlo, S. (2014). Negative staining and cryo-negative staining: Applications in biology and medicine. *Methods in Molecular Biology (Clifton, N.J.)*, 1117, 215–258. https://doi.org/10.1007/978-1-62703-776-1_11

- Hickman, J. W., & Harwood, C. S. (2008). Identification of FleQ from *Pseudomonas aeruginosa* as a c-di-GMP-responsive transcription factor. *Molecular Microbiology*, *69*(2), 376–389.
<https://doi.org/10.1111/j.1365-2958.2008.06281.x>
- Hinsa, S. M., Espinosa-Urgel, M., Ramos, J. L., & O’Toole, G. A. (2003). Transition from reversible to irreversible attachment during biofilm formation by *Pseudomonas fluorescens* WCS365 requires an ABC transporter and a large secreted protein. *Molecular Microbiology*, *49*(4), 905–918. <https://doi.org/10.1046/j.1365-2958.2003.03615.x>
- Hobley, L., Harkins, C., MacPhee, C. E., & Stanley-Wall, N. R. (2015). Giving structure to the biofilm matrix: An overview of individual strategies and emerging common themes. *FEMS Microbiology Reviews*, *39*(5), 649–669. <https://doi.org/10.1093/femsre/fuv015>
- Hobley, L., Ostrowski, A., Rao, F. V., Bromley, K. M., Porter, M., Prescott, A. R., MacPhee, C. E., van Aalten, D. M. F., & Stanley-Wall, N. R. (2013). BslA is a self-assembling bacterial hydrophobin that coats the *Bacillus subtilis* biofilm. *Proceedings of the National Academy of Sciences of the United States of America*, *110*(33), 13600–13605.
<https://doi.org/10.1073/pnas.1306390110>
- Hoke, D. E., Zhang, K., Egan, S., Hatfaludi, T., Buckle, A. M., & Adler, B. (2011). Membrane proteins of *Pseudoalteromonas tunicata* during the transition from planktonic to extracellular matrix-adherent state. *Environmental Microbiology Reports*, *3*(3), 405–413.
<https://doi.org/10.1111/j.1758-2229.2011.00246.x>
- Holmström, C., Egan, S., Franks, A., McCloy, S., & Kjelleberg, S. (2002). Antifouling activities expressed by marine surface associated *Pseudoalteromonas* species. *FEMS Microbiology Ecology*, *41*(1), 47–58. <https://doi.org/10.1111/j.1574-6941.2002.tb00965.x>

- Holmström, C., James, S., Egan, S., & Kjelleberg, S. (1996). Inhibition of common fouling organisms by marine bacterial isolates with special reference to the role of pigmented bacteria. *Biofouling*, 10(1–3), 251–259. <https://doi.org/10.1080/08927019609386284>
- Holmstrom, C., James, S., Neilan, B. A., White, D. C., & Kjelleberg, S. (1998). *Pseudoalteromonas tunicata* sp. Nov., a bacterium that produces antifouling agents. *International Journal of Systematic Bacteriology*, 48(4), 1205–1212. <https://doi.org/10.1099/00207713-48-4-1205>
- Holmström, H., & Kjelleberg, K. (1999). Marine *Pseudoalteromonas* species are associated with higher organisms and produce biologically active extracellular agents. *FEMS Microbiology Ecology*, 30(4), 285–293. <https://doi.org/10.1111/j.1574-6941.1999.tb00656.x>
- Horinouchi, S., Ueda, K., Nakayama, J., & Ikeda, T. (2010). Cell-to-cell communications among microorganisms. *Comprehensive Natural Products II: Chemistry and Biology*, 4, 283–337. <https://doi.org/10.1016/B978-008045382-8.00098-8>
- Hug, I., Deshpande, S., Sprecher, K. S., Pfohl, T., & Jenal, U. (2017). Second messenger-mediated tactile response by a bacterial rotary motor. *Science*, 358(6362), 531–534. <https://doi.org/10.1126/science.aan5353>
- Huxley - Jones, J., Robertson, D. L., & Boot-Handford, R. P. (2007). On the origins of the extracellular matrix in vertebrates. *Matrix Biology*, 26(1), 2–11. <https://doi.org/10.1016/j.matbio.2006.09.008>
- Huxley-Jones, J., Foord, S. M., & Barnes, M. R. (2008). Drug discovery in the extracellular matrix. *Drug Discovery Today*, 13(15), 685–694. <https://doi.org/10.1016/j.drudis.2008.05.005>
- Jackson, K. D., Starkey, M., Kremer, S., Parsek, M. R., & Wozniak, D. J. (2004). Identification of *psl*, a Locus Encoding a Potential Exopolysaccharide That Is Essential for *Pseudomonas aeruginosa* PAO1 Biofilm Formation. *Journal of Bacteriology*, 186(14), 4466–4475. <https://doi.org/10.1128/JB.186.14.4466-4475.2004>

- Jain, A., Gupta, Y., Agrawal, R., Jain, S., & Khare, P. (2007). Biofilms A Microbial Life Perspective: A Critical Review. *Critical Reviews in Therapeutic Drug Carrier Systems*, 24(5), 393–443. <https://doi.org/10.1615/CritRevTherDrugCarrierSyst.v24.i5.10>
- James, P., Halladay, J., & Craig, E. A. (1996). Genomic Libraries and a Host Strain Designed for Highly Efficient Two-Hybrid Selection in Yeast. *Genetics*, 144(4), 1425–1436. <https://doi.org/10.1093/genetics/144.4.1425>
- Janesch, B., Koerdt, A., Messner, P., & Schäffer, C. (2013). The S-Layer Homology Domain-Containing Protein SlhA from *Paenibacillus alvei* CCM 2051T Is Important for Swarming and Biofilm Formation. *PLoS ONE*, 8(9), e76566. <https://doi.org/10.1371/journal.pone.0076566>
- Jennings, L. K., Storek, K. M., Ledvina, H. E., Coulon, C., Marmont, L. S., Sadovskaya, I., Secor, P. R., Tseng, B. S., Scian, M., Filloux, A., Wozniak, D. J., Howell, P. L., & Parsek, M. R. (2015). Pel is a cationic exopolysaccharide that cross-links extracellular DNA in the *Pseudomonas aeruginosa* biofilm matrix. *Proceedings of the National Academy of Sciences of the United States of America*, 112(36), 11353–11358. <https://doi.org/10.1073/pnas.1503058112>
- Jing, H., Takagi, J., Liu, J., Lindgren, S., Zhang, R., Joachimiak, A., Wang, J., & Springer, T. A. (2002). Archaeal Surface Layer Proteins Contain β Propeller, PKD, and β Helix Domains and Are Related to Metazoan Cell Surface Proteins. *Structure*, 10(10), 1453–1464. [https://doi.org/10.1016/S0969-2126\(02\)00840-7](https://doi.org/10.1016/S0969-2126(02)00840-7)
- Joh, D., Wann, E. R., Kreikemeyer, B., Speziale, P., & Höök, M. (1999). Role of fibronectin-binding MSCRAMMs in bacterial adherence and entry into mammalian cells. *Matrix Biology*, 18(3), 211–223. [https://doi.org/10.1016/S0945-053X\(99\)00025-6](https://doi.org/10.1016/S0945-053X(99)00025-6)

Johnson, J. R., Jelacic, S., Schoening, L. M., Clabots, C., Shaikh, N., Mobley, H. L. T., & Tarr, P. I.

(2005). The IrgA Homologue Adhesin Iha Is an *Escherichia coli* Virulence Factor in Murine Urinary Tract Infection. *Infection and Immunity*, 73(2), 965–971.

<https://doi.org/10.1128/iai.73.2.965-971.2005>

Jumper, J., Evans, R., Pritzel, A., Green, T., Figurnov, M., Ronneberger, O., Tunyasuvunakool, K.,

Bates, R., Židek, A., Potapenko, A., Bridgland, A., Meyer, C., Kohl, S. A. A., Ballard, A. J.,

Cowie, A., Romera-Paredes, B., Nikolov, S., Jain, R., Adler, J., Hassabis, D. (2021). Highly accurate protein structure prediction with AlphaFold. *Nature*, 596(7873), 583–589.

<https://doi.org/10.1038/s41586-021-03819-2>

Kajava, A. V., & Steven, A. C. (2006). The turn of the screw: Variations of the abundant beta-

solenoid motif in passenger domains of Type V secretory proteins. *Journal of Structural*

Biology, 155(2), 306–315. <https://doi.org/10.1016/j.jsb.2006.01.015>

Kaplan, J. B. (2010). Biofilm dispersal: Mechanisms, clinical implications, and potential therapeutic

uses. *Journal of Dental Research*, 89(3), 205–218.

<https://doi.org/10.1177/0022034509359403>

Kehoe, M. A. (1994). Chapter 11 Cell-wall-associated proteins in Gram-positive bacteria. *New*

Comprehensive Biochemistry, 217–261. [https://doi.org/10.1016/s0167-7306\(08\)60414-7](https://doi.org/10.1016/s0167-7306(08)60414-7)

Kim, Y. W., Subramanian, S., Gerasopoulos, K., Ben-Yoav, H., Wu, H.-C., Quan, D., Carter, K.,

Meyer, M. T., Bentley, W. E., & Ghodssi, R. (2015). Effect of electrical energy on the

efficacy of biofilm treatment using the bioelectric effect. *Npj Biofilms and Microbiomes*, 1(1),

15016. <https://doi.org/10.1038/npjbiofilms.2015.16>

Kiran, M. D., Akiyoshi, D. E., Giacometti, A., Cirioni, O., Scalise, G., & Balaban, N. (2009). OpuC –

an ABC Transporter that is Associated with *Staphylococcus Aureus* Pathogenesis. *The*

- International Journal of Artificial Organs*, 32(9), 600–610.
<https://doi.org/10.1177/039139880903200909>
- Klemm, P., Vejborg, R. M., & Sherlock, O. (2006). Self-associating autotransporters, SAATs: Functional and structural similarities. *International Journal of Medical Microbiology*, 296(4), 187–195. <https://doi.org/10.1016/j.ijmm.2005.10.002>
- Kobayashi, K., & Iwano, M. (2012). BslA(YuaB) forms a hydrophobic layer on the surface of *Bacillus subtilis* biofilms. *Molecular Microbiology*, 85(1), 51–66.
<https://doi.org/10.1111/j.1365-2958.2012.08094.x>
- Koutsoudis, M. D., Tsaltas, D., Minogue, T. D., & Von Bodman, S. B. (2006). Quorum-sensing regulation governs bacterial adhesion, biofilm development, and host colonization in *Pantoea stewartii* subspecies *stewartii*. *Proceedings of the National Academy of Sciences of the United States of America*, 103(15), 5983–5988. <https://doi.org/10.1073/pnas.0509860103>
- Koval, S. F., & Hynes, S. H. (1991). Effect of paracrystalline protein surface layers on predation by *Bdellovibrio bacteriovorus*. *Journal of Bacteriology*, 173(7), 2244–2249.
<https://doi.org/10.1128/jb.173.7.2244-2249.1991>
- Kumar, A., Alam, A., Grover, S., Pandey, S., Tripathi, D., Kumari, M., Rani, M., Singh, A., Akhter, Y., Ehtesham, N. Z., & Hasnain, S. E. (2019). Peptidyl-prolyl isomerase-B is involved in *Mycobacterium tuberculosis* biofilm formation and a generic target for drug repurposing-based intervention. *Npj Biofilms and Microbiomes*, 5(1), 1–11.
<https://doi.org/10.1038/s41522-018-0075-0>
- Larsson, A. (2014). AliView: A fast and lightweight alignment viewer and editor for large datasets. *Bioinformatics (Oxford, England)*, 30(22), 3276–3278.
<https://doi.org/10.1093/bioinformatics/btu531>

- Lasa, I., & Penadés, J. R. (2006). Bap: A family of surface proteins involved in biofilm formation. *Research in Microbiology*, 157(2), 99–107. <https://doi.org/10.1016/j.resmic.2005.11.003>
- Latasa, C., Solano, C., Penadés, J. R., & Lasa, I. (2006). Biofilm-associated proteins. *Comptes Rendus. Biologies*, 329(11), 849–857. <https://doi.org/10.1016/j.crv.2006.07.008>
- Lazar, V. (2011). Quorum sensing in biofilms – How to destroy the bacterial citadels or their cohesion/power? *Anaerobe*, 17(6), 280–285. <https://doi.org/10.1016/j.anaerobe.2011.03.023>
- Lennon, J. T. (2007). Diversity and Metabolism of Marine Bacteria Cultivated on Dissolved DNA. *Applied and Environmental Microbiology*, 73(9), 2799–2805. <https://doi.org/10.1128/AEM.02674-06>
- Leo, J. C., Oberhettinger, P., Schütz, M., & Linke, D. (2015). The inverse autotransporter family: Intimin, invasins and related proteins. *International Journal of Medical Microbiology: IJMM*, 305(2), 276–282. <https://doi.org/10.1016/j.ijmm.2014.12.011>
- Letunic, I., & Bork, P. (2019). Interactive Tree Of Life (iTOL) v4: Recent updates and new developments. *Nucleic Acids Research*, 47(W1), W256–W259.
- Lister, J. L., & Horswill, A. R. (2014). *Staphylococcus aureus* biofilms: Recent developments in biofilm dispersal. *Frontiers in Cellular and Infection Microbiology*, 4, 178. <https://doi.org/10.3389/fcimb.2014.00178>
- Liu, W., Li, S., Wang, Z., Yan, E. C. Y., & Leblanc, R. M. (2017). Characterization of Surface-Active Biofilm Protein BslA in Self-Assembling Langmuir Monolayer at the Air–Water Interface. *Langmuir*, 33(30), 7548–7555. <https://doi.org/10.1021/acs.langmuir.7b01739>
- Lloubès, R., Cascales, E., Walburger, A., Bouveret, E., Lazdunski, C., Bernadac, A., & Journet, L. (2001). The Tol-Pal proteins of the *Escherichia coli* cell envelope: An energized system required for outer membrane integrity? *Research in Microbiology*, 152(6), 523–529. [https://doi.org/10.1016/S0923-2508\(01\)01226-8](https://doi.org/10.1016/S0923-2508(01)01226-8)

- Longford, S., Tujula, N., Crocetti, G., Holmes, A., Holmström, C., Kjelleberg, S., Steinberg, P., & Taylor, M. (2007). Comparisons of diversity of bacterial communities associated with three sessile marine eukaryotes. *Aquatic Microbial Ecology*, *48*, 217–229.
<https://doi.org/10.3354/ame048217>
- López-Villamizar, I., Cabezas, A., Pinto, R. M., Canales, J., Ribeiro, J. M., Cameselle, J. C., & Costas, M. J. (2016). The Characterization of Escherichia coli CpdB as a Recombinant Protein Reveals that, besides Having the Expected 3'-Nucleotidase and 2',3'-Cyclic Mononucleotide Phosphodiesterase Activities, It Is Also Active as Cyclic Dinucleotide Phosphodiesterase. *PLOS ONE*, *11*(6), e0157308.
<https://doi.org/10.1371/journal.pone.0157308>
- Lovejoy, C., Bowman, J. P., & Hallegraeff, G. M. (1998). Algicidal Effects of a Novel Marine *Pseudoalteromonas* Isolate (Class *Proteobacteria*, Gamma Subdivision) on Harmful Algal Bloom Species of the Genera *Chattonella*, *Gymnodinium*, and *Heterosigma*. *Applied and Environmental Microbiology*, *64*(8), 2806–2813. <https://doi.org/10.1128/AEM.64.8.2806-2813.1998>
- Luo, Y., Zhao, K., Baker, A. E., Kuchma, S. L., Coggan, K. A., Wolfgang, M. C., Wong, G. C. L., & O'Toole, G. A. (2015). A Hierarchical Cascade of Second Messengers Regulates *Pseudomonas aeruginosa* Surface Behaviors. *mBio*, *6*(1), e02456-14.
<https://doi.org/10.1128/mBio.02456-14>
- Mai-Prochnow, A., Evans, F., Dalisay-Saludes, D., Stelzer, S., Egan, S., James, S., Webb, J. S., & Kjelleberg, S. (2004). Biofilm Development and Cell Death in the Marine Bacterium *Pseudoalteromonas tunicata*. *Applied and Environmental Microbiology*, *70*(6), 3232–3238.
<https://doi.org/10.1128/AEM.70.6.3232-3238.2004>

- Mai-Prochnow, A., Lucas-Elio, P., Egan, S., Thomas, T., Webb, J. S., Sanchez-Amat, A., & Kjelleberg, S. (2008). Hydrogen Peroxide Linked to Lysine Oxidase Activity Facilitates Biofilm Differentiation and Dispersal in Several Gram-Negative Bacteria. *Journal of Bacteriology*, *190*(15), 5493–5501. <https://doi.org/10.1128/jb.00549-08>
- Majdura, J., Jankiewicz, U., Gałazka, A., & Orzechowski, S. (2023). The Role of Quorum Sensing Molecules in Bacterial–Plant Interactions. *Metabolites*, *13*(1), 114. <https://doi.org/10.3390/metabo13010114>
- Mann, E. E., & Wozniak, D. J. (2012). *Pseudomonas* biofilm matrix composition and niche biology. *FEMS Microbiology Reviews*, *36*(4), 893–916. <https://doi.org/10.1111/j.1574-6976.2011.00322.x>
- Marchler-Bauer, A., Derbyshire, M. K., Gonzales, N. R., Lu, S., Chitsaz, F., Geer, L. Y., Geer, R. C., He, J., Gwadz, M., Hurwitz, D. I., Lanczycki, C. J., Lu, F., Marchler, G. H., Song, J. S., Thanki, N., Wang, Z., Yamashita, R. A., Zhang, D., Zheng, C., & Bryant, S. H. (2015). CDD: NCBI’s conserved domain database. *Nucleic Acids Research*, *43*(D1), D222–D226. <https://doi.org/10.1093/nar/gku1221>
- Marguet, E., Gaudin, M., Gaudiard, E., Fourquaux, I., Le Blond Du Plouy, S., Matsui, I., & Forterre, P. (2013). Membrane vesicles, nanpods and/or nanotubes produced by hyperthermophilic archaea of the genus *Thermococcus*. *Biochemical Society Transactions*, *41*(1), 436–442. <https://doi.org/10.1042/BST20120293>
- McLean, R. J. C., Whiteley, M., Stickler, D. J., & Fuqua, W. C. (2006). Evidence of autoinducer activity in naturally occurring biofilms. *FEMS Microbiology Letters*, *154*(2), 259–263. <https://doi.org/10.1111/j.1574-6968.1997.tb12653.x>
- McNab, R., Forbes, H., Handley, P. S., Loach, D. M., Tannock, G. W., & Jenkinson, H. F. (1999). Cell Wall-Anchored CshA Polypeptide (259 Kilodaltons) in *Streptococcus gordonii* Forms

- Surface Fibrils That Confer Hydrophobic and Adhesive Properties. *Journal of Bacteriology*, *181*(10), 3087–3095. <https://doi.org/10.1128/JB.181.10.3087-3095.1999>
- McNab, R., Holmes, A. R., & Jenkinson, H. F. (1995). Cell-surface polypeptides as determinants of hydrophobicity in *Streptococcus gordonii* and *Streptococcus sanguis*. *Colloids and Surfaces B: Biointerfaces*, *5*(3–4), 135–142. [https://doi.org/10.1016/0927-7765\(95\)01213-3](https://doi.org/10.1016/0927-7765(95)01213-3)
- McNab, R., & Jenkinson, H. F. (1998). Altered adherence properties of a *Streptococcus gordonii* hppA (oligopeptide permease) mutant result from transcriptional effects on cshA adhesin gene expression. *Microbiology (Reading, England)*, *144* (Pt 1), 127–136. <https://doi.org/10.1099/00221287-144-1-127>
- McNab, R., Jenkinson, H. F., Loach, D. M., & Tannock, G. W. (1994). Cell-surface-associated polypeptides CshA and CshB of high molecular mass are colonization determinants in the oral bacterium *Streptococcus gordonii*. *Molecular Microbiology*, *14*(4), 743–754. <https://doi.org/10.1111/j.1365-2958.1994.tb01311.x>
- McPhee, J. B., Tamber, S., Bains, M., Maier, E., Gellatly, S., Lo, A., Benz, R., & Hancock, R. E. W. (2009). The major outer membrane protein OprG of *Pseudomonas aeruginosa* contributes to cytotoxicity and forms an anaerobically regulated, cation-selective channel. *FEMS Microbiology Letters*, *296*(2), 241–247. <https://doi.org/10.1111/j.1574-6968.2009.01651.x>
- Mendler, K., Chen, H., Parks, D. H., Lobb, B., Hug, L. A., & Doxey, A. C. (2019). AnnoTree: Visualization and exploration of a functionally annotated microbial tree of life. *Nucleic Acids Research*, *47*(9), 4442–4448. <https://doi.org/10.1093/nar/gkz246>
- Mesnage, S., Fontaine, T., Mignot, T., Delepierre, M., Mock, M., & Fouet, A. (2000). Bacterial SLH domain proteins are non-covalently anchored to the cell surface via a conserved mechanism involving wall polysaccharide pyruvylation. *The EMBO Journal*, *19*(17), 4473–4484. <https://doi.org/10.1093/emboj/19.17.4473>

- Mesnage, S., Tosi-Couture, E., Gounon, P., Mock, M., & Fouet, A. (1998). The Capsule and S-Layer: Two Independent and Yet Compatible Macromolecular Structures in *Bacillus anthracis*. *Journal of Bacteriology*, *180*(1), 52–58. <https://doi.org/10.1128/JB.180.1.52-58.1998>
- Messner, P., & Sleytr, U. B. (1988). *Separation and purification of S-layers from Gram-positive and Gram-negative bacteria* (illustrated ed.). Wiley & Sons, Chichester.
- Mima, T., Joshi, S., Gomez-Escalada, M., & Schweizer, H. P. (2007). Identification and Characterization of TriABC-OpmH, a Triclosan Efflux Pump of *Pseudomonas aeruginosa* Requiring Two Membrane Fusion Proteins. *Journal of Bacteriology*, *189*(21), 7600–7609. <https://doi.org/10.1128/jb.00850-07>
- Mirdita, M., Schütze, K., Moriwaki, Y., Heo, L., Ovchinnikov, S., & Steinegger, M. (2022). ColabFold: Making protein folding accessible to all. *Nature Methods*, *19*(6), 679–682. <https://doi.org/10.1038/s41592-022-01488-1>
- Mirzaei, R., Mohammadzadeh, R., Alikhani, M. Y., Shokri Moghadam, M., Karampoor, S., Kazemi, S., Barfipoursalar, A., & Yousefimashouf, R. (2020). The biofilm-associated bacterial infections unrelated to indwelling devices. *IUBMB Life*, *72*(7), 1271–1285. <https://doi.org/10.1002/iub.2266>
- Mitchell, A. L., Almeida, A., Beracochea, M., Boland, M., Burgin, J., Cochrane, G., Crusoe, M. R., Kale, V., Potter, S. C., Richardson, L. J., Sakharova, E., Scheremetjew, M., Korobeynikov, A., Shlemov, A., Kunyavskaya, O., Lapidus, A., & Finn, R. D. (2020). MGnify: The microbiome analysis resource in 2020. *Nucleic Acids Research*, *48*(D1), D570–D578. <https://doi.org/10.1093/nar/gkz1035>
- Monroe, D. (2007). Looking for Chinks in the Armor of Bacterial Biofilms. *PLoS Biology*, *5*(11), e307. <https://doi.org/10.1371/journal.pbio.0050307>

- Monzon, V., & Bateman, A. (2022). Large-Scale Discovery of Microbial Fibrillar Adhesins and Identification of Novel Members of Adhesive Domain Families. *Journal of Bacteriology*, 204(6), e00107-22. <https://doi.org/10.1128/jb.00107-22>
- Munoz-Lopez, M., & Garcia-Perez, J. (2010). DNA Transposons: Nature and Applications in Genomics. *Current Genomics*, 11(2), 115–128. <https://doi.org/10.2174/138920210790886871>
- Nadell, C. D., Drescher, K., & Foster, K. R. (2016). Spatial structure, cooperation and competition in biofilms. *Nature Reviews Microbiology*, 14(9), 589–600. <https://doi.org/10.1038/nrmicro.2016.84>
- Nesvizhskii, A. I., & Aebersold, R. (2005). Interpretation of shotgun proteomic data: The protein inference problem. *Molecular & Cellular Proteomics: MCP*, 4(10), 1419–1440. <https://doi.org/10.1074/mcp.R500012-MCP200>
- Nikaido, H., & Takatsuka, Y. (2009). Mechanisms of RND multidrug efflux pumps. *Biochimica et Biophysica Acta (BBA) - Proteins and Proteomics*, 1794(5), 769–781. <https://doi.org/10.1016/j.bbapap.2008.10.004>
- O’Neill, M. A., Morris, V. J., Selvendran, R. R., Sutherland, I. W., & Taylor, I. T. (1986). Structure of the extracellular gelling polysaccharide produced by *Enterobacter* (NCIB 11870) species. *Carbohydrate Research*, 148(1), 63–69. [https://doi.org/10.1016/0008-6215\(86\)80037-4](https://doi.org/10.1016/0008-6215(86)80037-4)
- O’Toole, G. A. (2011). Microtiter Dish Biofilm Formation Assay. *Journal of Visualized Experiments*, 47, 2437. <https://doi.org/10.3791/2437>
- O’Toole, G. A., & Wong, G. C. (2016). Sensational biofilms: Surface sensing in bacteria. *Current Opinion in Microbiology*, 30, 139–146. <https://doi.org/10.1016/j.mib.2016.02.004>
- Park, A. J., Murphy, K., Krieger, J. R., Brewer, D., Taylor, P., Habash, M., & Khursigara, C. M. (2014). A Temporal Examination of the Planktonic and Biofilm Proteome of Whole Cell

- Pseudomonas aeruginosa* PAO1 Using Quantitative Mass Spectrometry. *Molecular & Cellular Proteomics*, 13(4), 1095–1105. <https://doi.org/10.1074/mcp.M113.033985>
- Park, S., & Sauer, K. (2022). Controlling Biofilm Development Through Cyclic di-GMP Signaling. *Advances in Experimental Medicine and Biology*, 1386, 69–94. https://doi.org/10.1007/978-3-031-08491-1_3
- Patti, J. M., Jonsson, H., Guss, B., Switalski, L. M., Wiberg, K., Lindberg, M., & Höök, M. (1992). Molecular characterization and expression of a gene encoding a *Staphylococcus aureus* collagen adhesin. *Journal of Biological Chemistry*, 267(7), 4766–4772. [https://doi.org/10.1016/S0021-9258\(18\)42898-0](https://doi.org/10.1016/S0021-9258(18)42898-0)
- Persat, A., Inclan, Y. F., Engel, J. N., Stone, H. A., & Gitai, Z. (2015). Type IV pili mechanochemically regulate virulence factors in *Pseudomonas aeruginosa*. *Proceedings of the National Academy of Sciences of the United States of America*, 112(24), 7563–7568. <https://doi.org/10.1073/pnas.1502025112>
- Pertsemlidis, A., & Fondon, J. W. (2001). Having a BLAST with bioinformatics (and avoiding BLASTphemy). *Genome Biology*, 2(10). <https://doi.org/10.1186/gb-2001-2-10-reviews2002>
- Peters, B., Stein, J., Klingl, S., Sander, N., Sandmann, A., Taccardi, N., Sticht, H., Gerlach, R. G., Muller, Y. A., & Hensel, M. (2017). Structural and functional dissection reveals distinct roles of Ca²⁺-binding sites in the giant adhesin SiiE of *Salmonella enterica*. *PLoS Pathogens*, 13(5), e1006418. <https://doi.org/10.1371/journal.ppat.1006418>
- Pheatmap* [Computer software]. <https://github.com/raivokolde/pheatmap>
- Piddock, L. J. V. (2006). Multidrug-resistance efflux pumps - not just for resistance. *Nature Reviews Microbiology*, 4(8), 629–636. <https://doi.org/10.1038/nrmicro1464>

- Poppinga, L., Janesch, B., Fünfhaus, A., Sekot, G., Garcia-Gonzalez, E., Hertlein, G., Hedtke, K., Schäffer, C., & Genersch, E. (2012). Identification and functional analysis of the S-layer protein SplA of *Paenibacillus larvae*, the causative agent of American Foulbrood of honey bees. *PLoS Pathogens*, 8(5), e1002716. <https://doi.org/10.1371/journal.ppat.1002716>
- Qian, P.-Y., Cheng, A., Wang, R., & Zhang, R. (2022). Marine biofilms: Diversity, interactions and biofouling. *Nature Reviews. Microbiology*, 20(11), 671–684. <https://doi.org/10.1038/s41579-022-00744-7>
- Qing, R. (2017). Self-Assembling 2D Nano-Crystalline of Recombinant Surface Layer Proteins (S-Layer) on Solid Substrates and Electrical Responses. *MRS Advances*, 2(6), 349–355. <https://doi.org/10.1557/adv.2017.36>
- Rabsch, W., Ma, L., Wiley, G., Najjar, F. Z., Kaserer, W., Schuerch, D. W., Klebba, J. E., Roe, B. A., Gomez, J. A. L., Schallmey, M., Newton, S. M. C., & Klebba, P. E. (2007). FepA- and TonB-Dependent Bacteriophage H8: Receptor Binding and Genomic Sequence. *Journal of Bacteriology*, 189(15), 5658–5674. <https://doi.org/10.1128/JB.00437-07>
- Rao, D., Skovhus, T., Tujula, N., Holmström, C., Dahllöf, I., Webb, J. S., & Kjelleberg, S. (2010). Ability of *Pseudoalteromonas tunicata* to colonize natural biofilms and its effect on microbial community structure. *FEMS Microbiology Ecology*, 73, 450–457. <https://doi.org/10.1111/j.1574-6941.2010.00917.x>
- Rao, D., Webb, J. S., & Kjelleberg, S. (2005). Competitive Interactions in Mixed-Species Biofilms Containing the Marine Bacterium *Pseudoalteromonas tunicata*. *Applied and Environmental Microbiology*, 71(4), 1729–1736. <https://doi.org/10.1128/AEM.71.4.1729-1736.2005>
- Rao, R. S., Karthika, R. U., Singh, S., Shashikala, P., Kanungo, R., Jayachandran, S., & Prashanth, K. (2008). Correlation between biofilm production and multiple drug resistance in imipenem

- resistant clinical isolates of *acinetobacter baumannii*. *Indian Journal of Medical Microbiology*, 26(4), 333–337. [https://doi.org/10.1016/S0255-0857\(21\)01809-0](https://doi.org/10.1016/S0255-0857(21)01809-0)
- Ritter, A., Com, E., Bazire, A., Goncalves, M. D. S., Delage, L., Pennec, G. L., Pineau, C., Dreanno, C., Compère, C., & Dufour, A. (2012). Proteomic studies highlight outer-membrane proteins related to biofilm development in the marine bacterium *Pseudoalteromonas* sp. D41. *PROTEOMICS*, 12(21), 3180–3192. <https://doi.org/10.1002/pmic.201100644>
- Rodrigues-Oliveira, T., Belmok, A., Vasconcellos, D., Schuster, B., & Kyaw, C. M. (2017). Archaeal S-Layers: Overview and Current State of the Art. *Frontiers in Microbiology*, 8, 2597. <https://doi.org/10.3389/fmicb.2017.02597>
- Römling, U. (2012). Cyclic di-GMP, an established secondary messenger still speeding up. *Environmental Microbiology*, 14(8), 1817–1829. <https://doi.org/10.1111/j.1462-2920.2011.02617.x>
- Römling, U., Galperin, M. Y., & Gomelsky, M. (2013). Cyclic di-GMP: The First 25 Years of a Universal Bacterial Second Messenger. *Microbiology and Molecular Biology Reviews*, 77(1), 1–52. <https://doi.org/10.1128/MMBR.00043-12>
- Rumbaugh, K. P., & Sauer, K. (2020). Biofilm dispersion. *Nature Reviews Microbiology*, 18(10), 571–586. <https://doi.org/10.1038/s41579-020-0385-0>
- Sára, M. (2001). Conserved anchoring mechanisms between crystalline cell surface S-layer proteins and secondary cell wall polymers in Gram-positive bacteria? *Trends in Microbiology*, 9(2), 47–49; discussion 49-50. [https://doi.org/10.1016/s0966-842x\(00\)01905-3](https://doi.org/10.1016/s0966-842x(00)01905-3)
- Sára, M., & Sleytr, U. B. (2000). S-layer proteins. *Journal of Bacteriology*, 182(4), 859–868. <https://doi.org/10.1128/JB.182.4.859-868.2000>

- Saravanan, P., Nancharaiah, Y. V., Venugopalan, V. P., Rao, T. S., & Jayachandran, S. (2006). Biofilm formation by *Pseudoalteromonas ruthenica* and its removal by chlorine. *Biofouling*, 22(6), 371–381. <https://doi.org/10.1080/08927010601029103>
- Sauer, K., Camper, A. K., Ehrlich, G. D., Costerton, J. W., & Davies, D. G. (2002). *Pseudomonas aeruginosa* Displays Multiple Phenotypes during Development as a Biofilm. *Journal of Bacteriology*, 184(4), 1140–1154. <https://doi.org/10.1128/jb.184.4.1140-1154.2002>
- Schäfer, A., Tauch, A., Jäger, W., Kalinowski, J., Thierbach, G., & Pühler, A. (1994). Small mobilizable multi-purpose cloning vectors derived from the *Escherichia coli* plasmids pK18 and pK19: Selection of defined deletions in the chromosome of *Corynebacterium glutamicum*. *Gene*, 145(1), 69–73. [https://doi.org/10.1016/0378-1119\(94\)90324-7](https://doi.org/10.1016/0378-1119(94)90324-7)
- Schembri, M. A., Kjærgaard, K., & Klemm, P. (2003). Global gene expression in *Escherichia coli* biofilms. *Molecular Microbiology*, 48(1), 253–267. <https://doi.org/10.1046/j.1365-2958.2003.03432.x>
- Schneider, G., Guttman, P., Rehbein, S., Werner, S., & Follath, R. (2012). Cryo X-ray microscope with flat sample geometry for correlative fluorescence and nanoscale tomographic imaging. *Journal of Structural Biology*, 177(2), 212–223. <https://doi.org/10.1016/j.jsb.2011.12.023>
- Schrödinger. (2024). *BioLuminate*, Schrödinger. <https://pymol.org/>
- Schultze-Lam, S., Harauz, G., & Beveridge, T. J. (1992). Participation of a cyanobacterial S layer in fine-grain mineral formation. *Journal of Bacteriology*, 174(24), 7971–7981. <https://doi.org/10.1128/jb.174.24.7971-7981.1992>
- Schuster, B., & Sleytr, U. B. (2014). Biomimetic interfaces based on S-layer proteins, lipid membranes and functional biomolecules. *Journal of the Royal Society, Interface*, 11(96), 20140232. <https://doi.org/10.1098/rsif.2014.0232>

- Serra, D. O., Klauck, G., & Hengge, R. (2015). Vertical stratification of matrix production is essential for physical integrity and architecture of macrocolony biofilms of *Escherichia coli*. *Environmental Microbiology*, *17*(12), 5073–5088. <https://doi.org/10.1111/1462-2920.12991>
- Serra, D. O., Richter, A. M., & Hengge, R. (2013). Cellulose as an architectural element in spatially structured *Escherichia coli* biofilms. *Journal of Bacteriology*, *195*(24), 5540–5554. <https://doi.org/10.1128/JB.00946-13>
- Serra, D. O., Richter, A. M., Klauck, G., Mika, F., & Hengge, R. (2013). Microanatomy at Cellular Resolution and Spatial Order of Physiological Differentiation in a Bacterial Biofilm. *mBio*, *4*(2), e00103-13. <https://doi.org/10.1128/mBio.00103-13>
- Shinde, A., Illath, K., Gupta, P., Shinde, P., Lim, K.-T., Nagai, M., & Santra, T. S. (2021). A Review of Single-Cell Adhesion Force Kinetics and Applications. *Cells*, *10*(3), 577. <https://doi.org/10.3390/cells10030577>
- Shiryev, S. A., & Agarwala, R. (2024). Indexing and searching petabase-scale nucleotide resources. *Nature Methods*, *21*(6), 994–1002. <https://doi.org/10.1038/s41592-024-02280-z>
- Sidhu, M. S., & Olsen, I. (1997). S-layers of *Bacillus* species. *Microbiology*, *143*(4), 1039–1052. <https://doi.org/10.1099/00221287-143-4-1039>
- Sleytr, U. B., Schuster, B., Egelseer, E.-M., & Pum, D. (2014). S-layers: Principles and applications. *FEMS Microbiology Reviews*, *38*(5), 823–864. <https://doi.org/10.1111/1574-6976.12063>
- Smith, T. J., Font, M. E., Kelly, C. M., Sondermann, H., & O’Toole, G. A. (2018). An N-Terminal Retention Module Anchors the Giant Adhesin LapA of *Pseudomonas fluorescens* at the Cell Surface: A Novel Subfamily of Type I Secretion Systems. *Journal of Bacteriology*, *200*(8), e00734-17. <https://doi.org/10.1128/JB.00734-17>

- Solanki, V., Tiwari, M., & Tiwari, V. (2023). Investigation of Peptidoglycan-Associated Lipoprotein of *Acinetobacter baumannii* and Its Interaction with Fibronectin To Find Its Therapeutic Potential. *Infection and Immunity*, *91*(5). <https://doi.org/10.1128/iai.00023-23>
- Srey, S., Jahid, I. K., & Ha, S.-D. (2013). Biofilm formation in food industries: A food safety concern. *Food Control*, *31*(2), 572–585. <https://doi.org/10.1016/j.foodcont.2012.12.001>
- Stelzer, S., Egan, S., Larsen, M. R., Bartlett, D. H., & Kjelleberg, S. (2006). Unravelling the role of the ToxR-like transcriptional regulator WmpR in the marine antifouling bacterium *Pseudoalteromonas tunicata*. *Microbiology*, *152*(5), 1385–1394. <https://doi.org/10.1099/mic.0.28740-0>
- Szczepaniak, J., Press, C., & Kleanthous, C. (2020). The multifarious roles of Tol-Pal in Gram-negative bacteria. *FEMS Microbiology Reviews*, *44*(4), 490–506. <https://doi.org/10.1093/femsre/fuaa018>
- T. Ibrahim, H., Qiang, H., S. Al-Reka, W., & Qiqi, Y. (2012). Improvements in Biofilm Processes for Wastewater Treatment. *Pakistan Journal of Nutrition*, *11*(8), 708–734. <https://doi.org/10.3923/pjn.2012.708.734>
- Tang, K., Jiao, N., Liu, K., Zhang, Y., & Li, S. (2012). Distribution and Functions of TonB-Dependent Transporters in Marine Bacteria and Environments: Implications for Dissolved Organic Matter Utilization. *PLoS ONE*, *7*(7). <https://doi.org/10.1371/journal.pone.0041204>
- Tayeb-Fligelman, E., Tabachnikov, O., Moshe, A., Goldshmidt-Tran, O., Sawaya, M. R., Coquelle, N., Colletier, J.-P., & Landau, M. (2017). The cytotoxic *Staphylococcus aureus* PSM α 3 reveals a cross- α amyloid-like fibril. *Science*, *355*(6327), 831–833. <https://doi.org/10.1126/science.aaf4901>
- The UniProt Consortium, Bateman, A., Martin, M.-J., Orchard, S., Magrane, M., Ahmad, S., Alpi, E., Bowler-Barnett, E. H., Britto, R., Bye-A-Jee, H., Cukura, A., Denny, P., Dogan, T.,

- Ebenezer, T., Fan, J., Garmiri, P., Da Costa Gonzales, L. J., Hatton-Ellis, E., Hussein, A., Zhang, J. (2023). UniProt: The Universal Protein Knowledgebase in 2023. *Nucleic Acids Research*, 51(D1), D523–D531. <https://doi.org/10.1093/nar/gkac1052>
- Thomas, R. W. S. P., & Allsopp, D. (1983). *The effects of certain periphytic marine bacteria upon the settlement and growth of Enteromorpha, a fouling alga*. 5, 348–357.
- Thomas, T., Evans, F. F., Schleheck, D., Mai-Prochnow, A., Burke, C., Penesyan, A., Dalisay, D. S., Stelzer-Braid, S., Saunders, N., Johnson, J., Ferriera, S., Kjelleberg, S., & Egan, S. (2008). Analysis of the *Pseudoalteromonas tunicata* Genome Reveals Properties of a Surface-Associated Life Style in the Marine Environment. *PLoS ONE*, 3(9). <https://doi.org/10.1371/journal.pone.0003252>
- Thomas, W. E., Trintchina, E., Forero, M., Vogel, V., & Sokurenko, E. V. (2002). Bacterial Adhesion to Target Cells Enhanced by Shear Force. *Cell*, 109(7), 913–923. [https://doi.org/10.1016/S0092-8674\(02\)00796-1](https://doi.org/10.1016/S0092-8674(02)00796-1)
- Tiwari, M. K., & Kepp, K. P. (2015). Modeling the Aggregation Propensity and Toxicity of Amyloid- β Variants. *Journal of Alzheimer's Disease: JAD*, 47(1), 215–229. <https://doi.org/10.3233/JAD-150046>
- Tiwari, P., Mrigwani, A., Kaur, H., Kaila, P., Kumar, R., & Guptasarma, P. (2018). Structural-Mechanical and Biochemical Functions of Classical Cadherins at Cellular Junctions: A Review and Some Hypotheses. *Advances in Experimental Medicine and Biology*, 107–138. https://doi.org/10.1007/978-981-13-3065-0_9
- Tolker-Nielsen, T. (2015). Biofilm Development. *Microbiology Spectrum*, 3(2), 3.2.21. <https://doi.org/10.1128/microbiolspec.MB-0001-2014>

- Tomás, J. M. (2012). The Main *Aeromonas* Pathogenic Factors. *ISRN Microbiology*, 2012, 1–22.
<https://doi.org/10.5402/2012/256261>
- Toyofuku, M., Roschitzki, B., Riedel, K., & Eberl, L. (2012). Identification of Proteins Associated with the *Pseudomonas aeruginosa* Biofilm Extracellular Matrix. *Journal of Proteome Research*, 11(10), 4906–4915. <https://doi.org/10.1021/pr300395j>
- Tremblay, B. J.-M., Lobb, B., & Doxey, A. C. (2021). PhyloCorrelate: Inferring bacterial gene–gene functional associations through large-scale phylogenetic profiling. *Bioinformatics*, 37(1), 17–22. <https://doi.org/10.1093/bioinformatics/btaa1105>
- Van Gerven, N., Klein, R. D., Hultgren, S. J., & Remaut, H. (2015). Bacterial Amyloid Formation: Structural Insights into Curli Biogenesis. *Trends in Microbiology*, 23(11), 693–706.
<https://doi.org/10.1016/j.tim.2015.07.010>
- Vance, T. D. R., Ye, Q., Conroy, B., & Davies, P. L. (2020). Essential role of calcium in extending RTX adhesins to their target. *Journal of Structural Biology: X*, 4, 100036.
<https://doi.org/10.1016/j.yjsbx.2020.100036>
- Vandecandelaere, I., Depuydt, P., Nelis, H. J., & Coenye, T. (2014). Protease production by *Staphylococcus epidermidis* and its effect on *Staphylococcus aureus* biofilms. *Pathogens and Disease*, 70(3), 321–331. <https://doi.org/10.1111/2049-632X.12133>
- Veith, P. D., Chen, Y.-Y., Chen, D., O'Brien-Simpson, N. M., Cecil, J. D., Holden, J. A., Lenzo, J. C., & Reynolds, E. C. (2015). *Tannerella forsythia* Outer Membrane Vesicles Are Enriched with Substrates of the Type IX Secretion System and TonB-Dependent Receptors. *Journal of Proteome Research*, 14(12), 5355–5366. <https://doi.org/10.1021/acs.jproteome.5b00878>
- von Kügelgen, A., Tang, H., Hardy, G. G., Kureisaite-Ciziene, D., Brun, Y. V., Stansfeld, P. J., Robinson, C. V., & Bharat, T. A. M. (2020). In Situ Structure of an Intact

- Lipopolysaccharide-Bound Bacterial Surface Layer. *Cell*, 180(2), 348-358.
<https://doi.org/10.1016/j.cell.2019.12.006>
- Wai, S. N., Mizunoe, Y., Takade, A., Kawabata, S.-I., & Yoshida, S.-I. (1998). *Vibrio cholerae* O1 Strain TSI-4 Produces the Exopolysaccharide Materials That Determine Colony Morphology, Stress Resistance, and Biofilm Formation. *Applied and Environmental Microbiology*, 64(10), 3648–3655. <https://doi.org/10.1128/AEM.64.10.3648-3655.1998>
- Wang, S., Zhao, Y., Breslawec, A. P., Liang, T., Deng, Z., Kuperman, L. L., & Yu, Q. (2023). Strategy to combat biofilms: A focus on biofilm dispersal enzymes. *NPJ Biofilms and Microbiomes*, 9, 63. <https://doi.org/10.1038/s41522-023-00427-y>
- Wei, X., Tan, H., Lobb, B., Zhen, W., Wu, Z., Parks, D. H., Neufeld, J. D., Moreno-Hagelsieb, G., & Doxey, A. C. (2024). AnnoView enables large-scale analysis, comparison, and visualization of microbial gene neighborhoods. *Briefings in Bioinformatics*, 25(3), bbae229.
<https://doi.org/10.1093/bib/bbae229>
- Willing, S. E., Candela, T., Shaw, H. A., Seager, Z., Mesnage, S., Fagan, R. P., & Fairweather, N. F. (2015). *Clostridium difficile* surface proteins are anchored to the cell wall using CWB2 motifs that recognise the anionic polymer PSII. *Molecular Microbiology*, 96(3), 596–608.
<https://doi.org/10.1111/mmi.12958>
- Wong, L. L., Lu, Y., Ho, J. C. S., Mugunthan, S., Law, Y., Conway, P., Kjelleberg, S., & Seviour, T. (2023). Surface-layer protein is a public-good matrix exopolymer for microbial community organisation in environmental anammox biofilms. *The ISME Journal*, 17(6), 803–812.
<https://doi.org/10.1038/s41396-023-01388-y>
- Xu, Y., Liang, X., Chen, Y., Koehler, T. M., & Höök, M. (2004). Identification and biochemical characterization of two novel collagen binding MSCRAMMs of *Bacillus anthracis*. *The*

- Journal of Biological Chemistry*, 279(50), 51760–51768.
<https://doi.org/10.1074/jbc.M406417200>
- Yachdav, G., Kloppmann, E., Kajan, L., Hecht, M., Goldberg, T., Hamp, T., Hönigschmid, P., Schafferhans, A., Roos, M., Bernhofer, M., Richter, L., Ashkenazy, H., Punta, M., Schlessinger, A., Bromberg, Y., Schneider, R., Vriend, G., Sander, C., Ben-Tal, N., & Rost, B. (2014). PredictProtein—An open resource for online prediction of protein structural and functional features. *Nucleic Acids Research*, 42(Web Server issue), W337-343.
<https://doi.org/10.1093/nar/gku366>
- Yang, D. C., Blair, K. M., & Salama, N. R. (2016). Staying in Shape: The Impact of Cell Shape on Bacterial Survival in Diverse Environments. *Microbiology and Molecular Biology Reviews*, 80(1), 187–203. <https://doi.org/10.1128/MMBR.00031-15>
- Yang, H.-B., Hou, W.-T., Cheng, M.-T., Jiang, Y.-L., Chen, Y., & Zhou, C.-Z. (2018). Structure of a MacAB-like efflux pump from *Streptococcus pneumoniae*. *Nature Communications*, 9(1), 196. <https://doi.org/10.1038/s41467-017-02741-4>
- Yang, S., Zhang, J. J., & Huang, X.-Y. (2009). Orai1 and STIM1 Are Critical for Breast Tumor Cell Migration and Metastasis. *Cancer Cell*, 15(2), 124–134.
<https://doi.org/10.1016/j.ccr.2008.12.019>
- You, Y., Ye, F., Mao, W., Yang, H., Lai, J., & Deng, S. (2023). An overview of the structure and function of the flagellar hook FlgE protein. *World Journal of Microbiology & Biotechnology*, 39(5), 126. <https://doi.org/10.1007/s11274-023-03568-6>
- Zago, A., & Chugani, S. (2009). *Encyclopedia of Microbiology*. Academic Press.
- Zeng, Z., Zhan, W., Wang, W., Wang, P., Tang, K., & Wang, X. (2019). Biofilm formation in *Pseudoalteromonas lipolytica* is related to IS5-like insertions in the capsular polysaccharide operon. *FEMS Microbiology Ecology*, 95(6). <https://doi.org/10.1093/femsec/fiz065>

- Zhang, J., Wang, C., Han, J.-R., Chen, G.-J., & Du, Z.-J. (2019). *Alteromonas flava* sp. Nov. And *Alteromonas facilis* sp. Nov., two novel copper tolerating bacteria isolated from a sea cucumber culture pond in China. *Systematic and Applied Microbiology*, 42(2), 217–222. <https://doi.org/10.1016/j.syapm.2018.11.006>
- Zhao, A., Sun, J., & Liu, Y. (2023). Understanding bacterial biofilms: From definition to treatment strategies. *Frontiers in Cellular and Infection Microbiology*, 13. <https://doi.org/10.3389/fcimb.2023.1137947>
- Zhou, L., Zhang, Y., Ge, Y., Zhu, X., & Pan, J. (2020). Regulatory Mechanisms and Promising Applications of Quorum Sensing-Inhibiting Agents in Control of Bacterial Biofilm Formation. *Frontiers in Microbiology*, 11. <https://doi.org/10.3389/fmicb.2020.589640>
- Zhu, X., Long, F., Chen, Y., Knøchel, S., She, Q., & Shi, X. (2008). A Putative ABC Transporter Is Involved in Negative Regulation of Biofilm Formation by *Listeria monocytogenes*. *Applied and Environmental Microbiology*, 74(24), 7675–7683. <https://doi.org/10.1128/AEM.01229-08>

Appendix A

Protein Sequences

>EAR28894.1 hypothetical protein PTD2_07619

MEIMFKKTLALAITGVSVAANA AVVKTSVTATTA VLQQTAIGTAKAHAKGTALGASGVFG
TAADATNSANCKALAA YGVSLTKADGTA AHAVAADGSGGDVATFADGSGRELTTVHTTA
ATVKPVLSTTAAKDGLEYTQATALEIKPVIVAGIGGYKAEDTLTFQFSGAKLDLTKTTAPSIT
VAAAGQAGAGVTFDILDITDSQIRFTVKATTPANDFVRGNGILELSNIFLDSTGLAATTSVMV
NSFGTNTSGTKFDESTAATIVSLLPQYTTTEVTLLDADIDVGKDRQQFANNLTADVLA VKHT
KNPTSANVLPANTTYVVTGDFSWAYAPSVDTNKDGLSSAELMAANVA VLAGGDDTVKS
LALNATNTELTIVTNIVGAALDATNTITFNVPGYDSGKGTNPMISVQDFTVKVDTMSDKSVG
SKAVNMPSLAKTAAGTWKLN GSVVVVPYV PFGPATQPILRHTNAGTQTGDITVRYMVEGV
HTAWQSLAAAGIKDAKPGVRDMLGLVTDALKGEGYDSTTTGFKVALEVVTNVPSKDV FVY
GGAKITAEGQDRIHLGTFKTNVN

>PTD2_07619 (EAR28894) deletion/replacement

PstI (ATGCTGCAGTAA)

>EAR30327.1 hypothetical protein PTD2_02121

MKLKRLTCGVLLALGGQVQANEVCSSEVYGVNLTNAGSSIVKITPTTGQFALHSSVLQYSDAL
AYQESTDRLYYVTKPVNGKPRLVYVDMATEQHVDVAATTGTYRLAFSPDGQTLWGSS EDT
VFNINTNDGTVSNKVTLTG FATDADKLWGDIVFINDTLHIVTNKKLFAVDLAAGTVREVGM
HNLSVTGSTIDSLGQLLVSSNAGNNKTDLYTLDPATAKPSLLSSINYRINDLATRTYVQPACT
QLQDNVSSVEAIKNNSVEGQVLHARVHFEQPISTDTVTYLNENASDAQKNADFDRFVELSFD
NGMTWTSVKNISTIATTD AFKGLSHFDVRIHSFKDGDIEGNENFVLEAWNEGQADKKSRI FTI
VDQDSSSPDVTSVTLTSENVPEGVFMVADV VLSQATTSEFDHYIQLVTNSENPAYSALNEDF
TGQLEISFNRGISWQSIGLVGELIKARIYEGVSEYKLR AKVYSDGVTEGAETA AISISASSDGLF
AIERPFTINDAVK SCLPKVMYTIALPNPFS EDGYMDFEVGYRSEAKCDGQYKFELVETSISYV
DKAKKGVDFSTLVDIKDINSREFEQFAVDASGVVTIDVPKGSAGFVVRVY GKPDDIIEGPEEF
SINAWASPDQSDLFFKDITILDGDNITPSTSPNV SLLSINPNAAEQ TARITVSLEKATTVIDSV
LNVKFN DVEAISTEDYNNIAAVSFDV GATWQSVDLKSQAALLLP IGTQTVLIDVATKTDDEF
ETSESTMFSAWGQDDQSDFKTRKLTITDMTTASISLSSVTGNVVEGQQVELLLRLNQALNED
ATIYFAPYDGTAKVGGQDFSA NYTITL EAGKTDYSIFINTDDDL DLEDIEYFDVQVTGLVNV S
GSQTLRV FINDNEQTPTMDQVRALATSVKEGDEASFAVSLTHALNAPTLVSLSLTDDSAKAG
DDFASIVNV SFDNGVTWSSTLLPNTVEVPAQVSEFIVKVT TIRDTERESTE EFSLKAWTTSNAS
DIAQASGTITDNGAPIATDDSAE VNEDSLANNIDVLGNDS DPENDKLTVASATSNEGVVQINI
NGTLNFQPD TNFNGIATITYVVVDEFGGEDTAYVSVNVIPVNDAPIARPD LAKVSEDSQDNII
VVLSNDEDIDKDTLSVTSASANNGTVIINIDGT VTYTPNANFTGTD TISYSVSDGKGG SAS
STVTVTVDNQNDAPTAAPFTAIVDEDSLNNVIDVSAYLADNDNDTLTLSSPAANNGVVTVV
DNGKLTYPKPGFVGS DTITYTVSDGKGGTAQGVITMTVKNVNDAPVAKPKAVEVNENSQN
NIITLADVLEDADNDVLTVTNISAQHGT VTLQNGQLVYTPQASYS GADEITYTVSDGKGGSA
QGYVEVTIKPVNATISLIAVNGASREEGQTATYRIVLNQAISNDATIEVQVTNGTAFKGSDFSF
TNTTMTVPAGQTSVEFN VVTIEDSTHEELEDY NVKIIAKSNATGT AQLKAVIVDDDCLPAEY
TRINYRFISESAGWDNDWG IKVVDGKYTKLLDERGASGSFDVPLGKNITYVLARDGKSNDLTT
DFKWNGTDQRWEDTYRGDADYND FVVNVTTAKVSYGCK

> PTD2_02121 (EAR30327) deletion/replacement

MSR (ATGGGATCCTAA)

Appendix B

Media composition

Complex media (CM1)

Tryptone	10 g
Yeast Extract	5 g
NaCl	10 g
CaCl ₂	2.5 mM
MgSO ₄	2.5 mM
Agar	15 g
dH ₂ O	1L

Difco Marine agar 2216

Peptone	5g/L
Yeast extract	1g/L
Ferric Citrate	0.1g/L
Sodium Chloride	19.45g/L
Magnesium Chloride	8.8g/L
Sodium Sulfate	3.24g/L
Calcium Chloride	1.8g/L
Potassium Chloride	0.55g/L
Sodium Bicarbonate	0.16g/L
Potassium Bromide	0.08g/L
Strontium Chloride	34mg/L
Boric Acid	22mg/L
Sodium Silicate	4mg/L
Sodium Fluoride	2.4mg/L
Ammonium Nitrate	1.6mg/L
Disodium Phosphate	8mg/L
Agar	15g/L

Difco Marine broth 2216

Ammonium nitrate	1.6 mg/L
boric acid	22.0 mg/L
calcium chloride,	1.8 g/L
disodium phosphate	8.0 mg/L
ferric citrate	0.1 g/L
magnesium chloride	5.9 g/L
magnesium sulfate	3.24 g/L
peptone	5.0 g/L
potassium bromide	0.08 g/L
potassium chloride	0.55 g/L
sodium bicarbonate	0.16 g/L
sodium chloride	19.45 g/L
sodium fluoride	2.4 mg/L
sodium silicate	4.0 mg/L
strontium chloride	34.0 mg/L
yeast extract	1.0 g/L

Appendix C

Proteomics LC-MS/MS protein

C.1. Proteomics LC-MS/MS protein abundance across all samples data. All detected *P. tunicata* proteins and supplementary information are included in the following link:

https://drive.google.com/drive/folders/1PiRzz4wc_cgmEdbOyhkCZafkn8eXYJyW?usp=drive_link

C.2. The supplementary material and data that supports the findings of Ali et al., (2020) article) are available in:

The NCBI GenBank database (<https://www.ncbi.nlm.nih.gov/protein/EAR28894>), as well as in “figshare” at <https://doi.org/10.6084/m9.figshare.11993505.v1>

Appendix D

D.1. The top thirty supporting peptides for EAR28894 identification by LC-MS/MS.

The full list is available online (Ali, Jenkins, & Doxey, 2020).

Peptide	-10lgP	Mass	Length	ppm	m/z	z	RT	Fract ion	Scan	Number Spec	Start	End	PTM
R.YMVEGVHTAWQS LAAAGIK.D	119.18	2031.02	19	-7.4	1016.51	2	20.76	2	3156	9	491	509	
K.DGLEYTQATALEIK PVIVAGIGGYK.A	117.52	2605.40	25	-8.2	1303.70	2	22.33	2	3432	45	140	164	
R.YM(+15.99)VEGVH TAWQSLAAAGIK.D	111.23	2047.02	19	-5.9	683.34	3	20.02	2	3018	5	491	509	Oxidation (M)
R.DMLGLVTDALKGE GYDSTTTGFK.V	107.36	2418.16	23	-4.7	1210.08	2	24.78	2	3863	13	517	539	
R.HTNAGTQTGDITV R.Y	104.91	1469.72	14	-6.2	735.86	2	11.4	2	1422	4	477	490	
K.GTNPMSVQDFTV K.V	100.89	1535.77	14	-4.9	768.89	2	20.01	2	3017	4	413	426	
K.ADGTAAHAVAAD GSGGDVATFADGSG R.E	97.12	2403.07	27	-7.9	802.02	3	14.93	2	2057	9	86	112	
R.DM(+15.99)LGLVTD ALKGEGYDSTTTGFK .V	92.65	2434.16	23	-6.5	1218.08	2	20.99	2	3197	6	517	539	Oxidation (M)
R.QQFAN(+.98)NLTA DVLAVK.H	91.34	1631.85	15	-6.5	816.93	2	19.91	2	Ta	3	298	312	Deamidation (NQ)
K.VALEVVTNVPSKD VIFYGGAK.I	90.54	2191.19	21	-7.8	1096.59	2	19.65	2	2941	18	540	560	
K.GTNP(+15.99)ISV QDFTVK.V	88.79	1551.76	14	-6.3	776.88	2	18.42	2	2717	3	413	426	Oxidation (M)
A.TALEIKPVIVAGIG GYK.A	88.03	1728.02	17	-8.1	865.01	2	19.96	2	3005	2	148	164	
R.YMVEGVHTAWQ(+ .98)SLAAAGIK.D	88	2032.01	19	-3.6	1017.01	2	21.43	2	3275	3	491	509	Deamidation (NQ)
K.LSSAELMAANVAV LAGGDDTVK.S	87.8	2131.08	22	-5.6	1066.54	2	22.34	2	3433	4	352	373	
K.DGLEYTQ(+.98)AT ALEIKPVIVAGIGGYK .A	87.28	2606.38	25	10.3	652.61	4	22.38	2	3441	12	140	164	Deamidation (NQ)
R.QQFANLTDVLA VK.H	84.32	1630.87	15	-3.8	816.44	2	20.18	2	3053	4	298	312	
K.TSVTATTAVLQQT AIGTAK.A	83.11	1861.02	19	-7.8	931.51	2	18.03	2	2646	3	28	46	
R.DMLGLVTDALK.G	83.06	1174.63	11	-5.3	588.32	2	23.81	2	3689	7	517	527	
K.AEDTLTFQFSGAK. L	82.59	1413.68	13	-4.9	707.84	2	19.86	2	2984	31	165	177	
K.ALAIFYGVSLTK.A	82.53	1239.69	12	-6.6	620.85	2	19.91	2	2993	2	74	85	
K.LSSAELM(+15.99)A ANVAVLAGGDDTVK .S	81.88	2147.08	22	0.2	1074.55	2	19.61	2	2933	4	352	373	Oxidation (M)
R.ELTTVHTTAANAC(+57.02)LATVKPVLST TAAK.D	81.48	2768.47	27	-5.8	693.12	4	16.99	2	2429	5	113	139	Carbamidom ethylation
R.Q(+.98)QFANLTA DVLAVK.H	81.46	1631.85	15	-6.5	816.93	2	20.55	2	3119	2	298	312	Deamidation (NQ)
K.DRQQFANLTDV LAVK.H	80.18	1902.00	17	-4.4	952.00	2	19.83	2	2976	4	296	312	
K.LNGSVVVVPYVPF GPATQPILR.H	79.7	2322.31	22	3.3	775.11	3	23.76	2	3680	3	455	476	
K.LN(+.98)GSVVVVP YVFPATQPILR.H	79.29	2323.29	22	-4.5	775.44	3	24.08	2	3738	7	455	476	Deamidation (NQ)
K.VALEVVTNVPSK.D	78.86	1254.72	12	-3.7	419.25	3	16.45	2	2334	13	540	551	
T.ALEIKPVIVAGIGG YK.A	77.2	1626.97	16	-5.8	543.33	3	19.84	2	2979	4	149	164	

K.GTALGASGVFGTA ADATNSANCKA.L	76.07	2154.00	24	-5.8	719.00	3	17.55	2	2553	4	51	74
Y.MVEGVHTAWQSL AAAGIK.D	75.15	1867.96	18	-2.8	934.99	2	20.84	2	3171	2	492	509

Frac* Fraction

D.2. Niche analysis of Slr4-containing species. Sources supporting habitat definitions in this table are available online in the Supplementary Material of (Ali, Jenkins, & Doxey, 2020).

Protein sequences	Species	Marine	Host-associated	Freshwater	Habitat description
WP_055732151.1	<i>Agarivorans gilvus</i>	Yes	Yes		Seaweed
WP_026972292.1	<i>Aliagarivorans marinus</i>	Yes			Seawater
WP_026957844.1	<i>Aliagarivorans taiwanensis</i>	Yes			Seawater
WP_091340846.1	<i>Alkalimonas amylolytica</i>	No		Yes	Lake Chahannor in China Isolated from a sea cucumber culture pond in China
WP_124748942.1	<i>Alteromonas facilis</i>	Yes	Yes		Isolated from the alkaline, low-saline ikaite columns in the Ikka Fjord, SW Greenland
WP_046556214.1	<i>Arsukibacterium ikkense</i>	Yes			Isolated from seawater samples from the Chukchi Sea in the Arctic Ocean
WP_085282491.1	<i>Colwellia chukchiensis</i>	Yes			Isolated from the mussel <i>Mytilus edulis</i> from the South Sea in Korea
WP_085298075.1	<i>Colwellia mytili</i>	Yes	Yes		Seawater
WP_118961217.1	<i>Colwellia sp. RSH04</i>	Yes			Marine sediment, Pacific Ocean: the Tonga Trench
WP_057830656.1	<i>Colwellia sp. TT2012</i>	Yes			marine sediment metagenome; deep-sea hydrothermal vent sediments from dive 4571_4 depth 0-3 cm
RLB69876.1	<i>Deltaproteobacteria bacterium</i>	Yes			mediterranean seawater-France
PCH94196.1, PCI59289.1	<i>Gammaproteobacteria bacterium</i>	Yes			

WP_040521162.1, WP_070111740.1	<i>Glaciecola punicea</i> <i>Glaciecola punicea</i> ACAM 611	Yes		isolated from sea-ice cores collected from coastal areas of eastern Antarctica
GAB56998.1 PTB83247.1, PTB83248.1, PTB84530.1, PTB85125.1, PTB85126.1, RUO41646.1, RUO41647.1, RUO41648.1		Yes		Antarctic sea ice
	<i>Idiomarina aestuarii</i>	Yes		isolation of the type strain from shallow coastal seawater.
WP_133538702.1	<i>Idiomarina aquatica</i>	Yes		Isolated from salterns isolated from the reef-building coral <i>Isopora palifera</i>
WP_126834469.1	<i>Idiomarina aquimaris</i>	Yes	Yes	
KFZ29179.1, WP_034731676.1 RUO53158.1, WP_126763865.1, WP_126763868.1, WP_126763869.1	<i>Idiomarina atlantica</i>	Yes		isolated from the deep sea sediment of the North Atlantic Ocean
RUO56263.1, WP_126771356.1, WP_126771358.1, WP_126771362.1	<i>Idiomarina halophila</i>	Yes		isolated from the sediment of the solar saltern pond located in Gomso, Republic of Korea
	<i>Idiomarina homiensis</i>	Yes		isolated from seashore sand in Korea
RUO62606.1, WP_126753970.1	<i>Idiomarina insulisalae</i>	Yes		isolated from a sea salt evaporation pond on the Island of Sal in the Cape Verde Archipelago
WP_026861598.1, WP_126775152.1	<i>Idiomarina sediminum</i>	Yes		isolated from the soil of a sea salt evaporation pond
HAD47721.1	<i>Idiomarina sp.</i>	Yes		marine metagenome
MBG23301.1	<i>Idiomarinaceae bacterium</i>	Yes		marine metagenome from a Mediterranean Sea water sample
WP_088331539.1	<i>Lacimicrobium sp. SS2-24</i>	Yes	Yes	sediment from sea cucumber culture
WP_031571199.1	<i>Pararheinheimera texasensis</i>	No	Yes	USA: Spring Lake; San Marcos; Texas
MBU77382.1	<i>Pseudoalteromonadaceae bacterium</i>	Yes		marine metagenome from a South Atlantic Ocean water sample
WP_077536094.1	<i>Pseudoalteromonas aliena</i>	Yes		Sea of Japan, Pacific Ocean
WP_010361438.1	<i>Pseudoalteromonas citrea</i>	Yes		Marine
WP_091983032.1	<i>Pseudoalteromonas denitrificans</i>	Yes		Marine
SFC52264.1	<i>Pseudoalteromonas denitrificans DSM 6059</i>	Yes		Marine

KID36130.1	<i>Pseudoalteromonas elyakovii</i>	Yes		isolated from marine environments
CCQ10312.1	<i>Pseudoalteromonas luteoviolacea</i> B = ATCC 29581	Yes		Marine
WP_010368594.1, WP_045962959.1, WP_045987911.1, WP_088531627.1, WP_117332793.1	<i>Pseudoalteromonas piscicida</i>	Yes		found in the marine environment
WP_119852593.1	<i>Pseudoalteromonas profundii</i>	Yes		isolated from a deep-sea seamount
WP_022946007.1	<i>Pseudoalteromonas ruthenica</i>	Yes	Yes	isolated from marine invertebrates
WP_130050461.1	<i>Pseudoalteromonas shioyasakiensis</i>	Yes		isolated from Pacific Ocean sediment
MAD02172.1	<i>Pseudoalteromonas</i> sp.	Yes		marine metagenome from a Pacific Ocean water sample
MBD58444.1	<i>Pseudoalteromonas</i> sp.	Yes		marine metagenome from an Indian Ocean water sample
WP_042150686.1	<i>Pseudoalteromonas</i> sp. '520P1 No. 412'	Yes		Marine
WP_042150686.1	<i>Pseudoalteromonas</i> sp. '520P1 No. 423'	Yes		Marine
WP_069020791.1	<i>Pseudoalteromonas</i> sp. BMB	Yes	Yes	Isolated from gut of comb jelly
WP_130151616.1	<i>Pseudoalteromonas</i> sp. CO133X	Yes	Yes	Octocoral
WP_130151616.1	<i>Pseudoalteromonas</i> sp. CO302Y	Yes	Yes	Octocoral
WP_130126916.1	<i>Pseudoalteromonas</i> sp. CO342X	Yes		host-associated (Muricea sp.), Panama: Coiba National Park
WP_099029058.1	<i>Pseudoalteromonas</i> sp. GCY	Yes		Isolated from Northern Yellow Sea
WP_095726933.1	<i>Pseudoalteromonas</i> sp. HM-SA03	Yes	Yes	Source (marine), Host (Hapalochlaena), Location (Australia: Moreton Bay)
WP_125251093.1	<i>Pseudoalteromonas</i> sp. J010	Yes	Yes	Isolated from surface of crustose coralline alga
WP_086997608.1	<i>Pseudoalteromonas</i> sp. JB197	No		Isolated from cheese rind
WP_119861005.1	<i>Pseudoalteromonas</i> sp. MSK9-3	Yes		Isolated from surface saline water
WP_017217139.1	<i>Pseudoalteromonas</i> sp. NJ631	Yes	Yes	Isolation source (ocean), host - Hymeniacidon perleve (marine sponge)
WP_128731076.1	<i>Pseudoalteromonas</i> sp. PS5	Yes	Yes	Isolated from (host: Neogoniolithon solubile), USA: reef near Looe Key
WP_053910113.1	<i>Pseudoalteromonas</i> sp. SW0106-04	Yes		Seawater (Indian Ocean)
WP_105171055.1	<i>Pseudoalteromonas</i> sp. T1lg24	Yes		Isolated from sea water (sediment depth)

WP_024611180.1	<i>Pseudoalteromonas sp. TB64</i>	Yes	Yes		Isolated from a sponge, Antarctica isolated from the surface of the sponge <i>Mycale adhaerens</i> in Hong Kong waters
WP_010561144.1, WP_100912554.1	<i>Pseudoalteromonas spongiae</i>	No	Yes	Yes	
WP_009838156.1, WP_119081635.1	<i>Pseudoalteromonas tunicata</i>	Yes			Marine organism originally isolated from tunicates
WP_086744222.1	<i>Pseudoalteromonas ulvae</i>	Yes	Yes		Isolated from surface of marine alga
WP_134053939.1	<i>Rheinheimera aquimaris</i>	Yes			isolated from seawater of the East Sea in Korea
WP_019674711.1	<i>Rheinheimera perlucida</i>	Yes			Isolated from surface water from Baltic Sea
WP_132584183.1	<i>Rheinheimera sp. D18</i>	Yes			Isolated from yellow sea (China)
WP_127697655.1	<i>Rheinheimera sp. KYPC3</i>	No		Yes	Isolated from freshwater stream
WP_068063761.1	<i>Rheinheimera sp. SA_1</i>	No		Yes	isolated from "iron backwash sludge of a waterworks in Germany"
PHS21107.1	<i>Robiginitomaculum sp.</i>	Yes			from Antarctic seawater
WP_109338879.1	<i>Salinimonas sp. HMF8227</i>	Yes			Isolated from saltern in South Korea
WP_119977519.1	<i>Shewanella algidipiscicola</i>	Yes	Yes		isolated from marine fish of the Danish Baltic Sea
WP_059744161.1	<i>Shewanella frigidimarina</i>	Yes			Isolated from Antarctic coastal areas
WP_108947122.1	<i>Shewanella halifaxensis</i>	Yes			Isolated from marine sediment
WP_115405978.1	<i>Shewanella putrefaciens</i>	Yes	Yes		Associated with spoiled fish Isolated from marine sediment
WP_012143353.1	<i>Shewanella sediminis</i>	Yes			
WP_076411007.1	<i>Shewanella sp. UCD-KL12</i>	Yes	Yes		Isolated from seagrass
WP_028771745.1	<i>Shewanella waksmanii</i>	Yes	Yes		Marine strain isolated from sipuncula
WP_044830703.1	<i>Thalassomonas actiniarum</i>	Yes	Yes		Isolated from marine animals
WP_044836570.1	<i>Thalassomonas viridans</i>	Yes			isolated from oysters off the Mediterranean coast
WP_115999569.1, WP_116007234.1, WP_116007235.1, WP_116014431.1	<i>Thalassotalea euphylliae</i>	Yes	Yes		Isolated from coral
WP_074500610.1	<i>Thalassotalea sp. PP2-459</i>	Yes	Yes		Isolated from clam larvae in shellfish hatchery in Spain
WP_074191941.1	<i>Vibrio antiquarius</i>	Yes			Isolated from deep sea hydrothermal vent

WP_104968991.1	<i>Vibrio diabolicus</i>	Yes	Yes	Isolated from a deep-sea hydrothermal vent annelid worm
WP_005434363.1	<i>Vibrio harveyi</i>	Yes	Yes	Pathogen of marine vertebrates and invertebrates
WP_038864853.1, WP_045422135.1	<i>Vibrio jasicida</i>	Yes	Yes	Isolated from marine vertebrates and invertebrates
WP_088881413.1	<i>Vibrio rotiferianus</i>	Yes	Yes	Marine pathogen
WP_095760150.1	<i>Vibrio sp. VIB</i>	Yes	Yes	Isolated from gut of saltwater clam
